

***SECTION 6***

**6**

***Detailed Report, related to overall project  
duration***

Both the numbers and names of the contractors that contributed to this work-package are listed as follows:

1. Norwegian Institute for Air Research (Coordinator).
2. Institute for Environmental Physics (IUP), University of Heidelberg.
3. Institute for Atmospheric Environmental Research, Research Centre Karlsruhe (IMK-IFU).
4. Institute for Environmental Physics, University of Bremen.
7. Dept. of Analytical and Marine Chemistry, Chalmers University of Technology.
8. Environmental Institute, EC Joint Research Centre (JRC).

## 6.1 Background (description of the problem to be solved)

Formaldehyde plays an important role in atmospheric chemistry and is a good tracer of photooxidation and thereby of pollution from fossil fuel combustion and biomass burning.

Air pollution remains a significant source of health problems and WHO thresholds are frequently exceeded. In addition, populations in urban areas are expected to increase by more than 4% between 1995 and 2010. Photochemical smog from burning of fossil fuel is one of the major air pollution problems. Reducing the air pollution in urban areas of Europe constitutes a major challenge, and scientists, bureaucrats and politicians have to collaborate in order to solve the problems. Unabated, the air pollution caused by burning of fossil fuels will lead to a higher incidence of respiratory disease and damage on vegetation and materials.

Formaldehyde (HCHO or H<sub>2</sub>C=O) is the most abundant of the carbonyl compounds in the atmosphere. It is also the smallest member of the aldehyde family. Formaldehyde is found both in the remote background atmosphere and in polluted urban atmospheres. The photooxidation of hydrocarbons invariably generates HCHO in the atmosphere (Finlayson-Pitts and Pitts, 1986; Atkinson, 1994). In the background troposphere, where methane concentration is considerably higher than that of non-methane hydrocarbons (NMHC), methane is the dominant formaldehyde precursor. Close to the surface, local sources of NMHC also become important in producing HCHO. In processes similar to that for methane, formaldehyde is generated from the oxidation of biogenic hydrocarbons, such as isoprene and terpenes (Levine, 1984) and from the oxidation of anthropogenic hydrocarbons. Formaldehyde is also anthropogenically generated directly from incomplete combustion processes, both from biomass burning (Holzinger et al., 1999) and from internal combustion engines. Accurate HCHO measurements are thus important in constraining and validating photochemical models of the troposphere, in understanding the budgets and cycling among various reactive species and the global budget of CO. Despite this importance and the relatively large number of techniques employed, there is still considerable uncertainty in ambient measurements of HCHO. In various intercomparison campaigns, the level of agreement varies from good to quite poor (Cárdenas et al. 2000; Gilpin, 1997, and references cited therein). It is therefore

## Section 6: Detailed report related to overall project duration

of importance to obtain a better understanding of the differences between the various measurement techniques and try to reduce the disagreement between these various techniques. This will be of great value both to validate atmospheric chemistry models and to validate satellite measurements of HCHO. Photochemical smog is one of the most, if not the most, serious air pollution problem in Europe today. Episodes with high concentrations of ozone and NO<sub>x</sub> cause harm to human health and to vegetation. Abatement of such pollution is one of the biggest challenges to environmental authorities, both nationally and at the Community level. There is a clear need for better scientific tools to understand the mechanisms behind the formation of photochemical smog. Better tools are also needed to predict and warn the population against such pollution.

## 6.2 Scientific/technological and socio-economic objectives

Formaldehyde is a good indicator for photochemical smog. It is therefore important that we are able to measure this compound in an accurate way. The single most important objective of the format project is to improve the measurement techniques that are used to measure this compound. More specifically the objectives are:

1. To intercompare the various techniques for measurement of atmospheric formaldehyde,
2. To obtain a better knowledge of the concentrations and distribution of formaldehyde in the troposphere over Europe and globally,
3. To validate satellite measurements (GOME, SCIAMACHY) of formaldehyde,
4. To compare measured and modelled formaldehyde,
5. To use this improved knowledge to strengthen the capability of atmospheric chemistry models to calculate formaldehyde and thereby predict smog episodes in Europe,
6. To use global models together with satellite measurements to obtain a better knowledge of the global distribution and role of HCHO as a tracer of fossil fuel and biomass burning,
7. To assess the socio-economic impact of knowledge gained through the project.

The project will lead to a better overview of the formaldehyde distribution both regionally in the Po valley (chosen as a typical polluted area) and on a global scale through analysis of satellite data. This will again give us better insight in the extent of fossil fuel and biomass burning, both in Europe and globally. The various methods for measuring formaldehyde will be intercompared, and it is the aim to arrive at a better agreement between the various techniques. Atmospheric chemistry models will be compared to field measurements. It is the aim that the tools used to warn authorities and the public in the case of smog episodes will be improved.

In other words, the main objective of FORMAT is to obtain a better knowledge of the regional and global distribution of formaldehyde, an important intermediate in the oxidation of hydrocarbons to CO and a source of oxidative radicals. This can lead to better prediction of smog episodes and to better quantification of emissions from biomass burning. A socioeconomic workpackage will quantify the benefits from the project.

In order to achieve these overall and general objectives the following specific objectives have been defined for the FORMAT project:

1. To put several new measurement techniques to use for the measurement of formaldehyde,
2. To carry out intercomparisons of several different measurement techniques for formaldehyde on the ground,
3. To carry out intercomparisons of some of these techniques from aircraft in order to compare how the vertical profiles obtained by these measurements compare with column measurements,
4. To use these measurements in order to get a best possible picture of the horizontal, vertical and temporal distribution of formaldehyde in the planetary boundary layer in a photochemically polluted area, the Italian the Po Valley,
5. To improve the algorithms for obtaining HCHO from satellite measurements by GOME and SCIAMACHY,

6. To compare the ground based airborne and spaceborne measurements and thereby validate satellite measurements of formaldehyde,
7. To compare measured and modelled formaldehyde and thereby improve and validate the models capability to calculate and predict the occurrence of photochemical smog episodes,
8. To calculate the occurrence of formaldehyde during smog episodes in Europe and use this to aid in the flight planning during the measurement campaigns,
9. To calculate the global distribution of formaldehyde and compare this to satellite measurements,
10. To define recommendations for measurements, modelling and satellite data retrieval of formaldehyde,
11. To inform end users of the results of the FORMAT project,
12. To assess the socio-economic benefits of the increased knowledge gained in the FORMAT project.

## 6.3 Applied methodology, scientific achievements and main deliverables

### WP 1000 Ground-based measurements of formaldehyde and intercomparison

Ground based measurements and a thorough intercomparison must complement airborne measurements as only few measurement techniques for formaldehyde may be used on aircraft. Airborne measurements typically cover short time periods only and might not be representative for the diurnal variation if not accompanied by concurrent continuous ground based monitoring. The methodology of the FORMAT project covers as a first step an intercomparison of all available techniques for measurements of gaseous formaldehyde followed by two campaigns in different seasons with wide spatial spread of instruments in typical Po-Valley landscapes from rural to metropolitan areas. The choice of the Po-Valley for these investigations was due to the expected mid to high concentrations of formaldehyde and the high concentrations of possibly interfering substances that allow a statistically significant comparison of instruments over a wide range of conditions. Satellite derived HCHO concentrations from GOME that can be compared to ground based in situ and remote sensing data are available for the whole of Europe. However, only two areas, Belgium and the Italian Po-Valley show high values and a reasonable variability. In contrast to the original planning, the research area was shifted from the central Po-valley further to the west to Milano to include also one of the biggest city complexes in the area. Also north and south of Milano the population, vegetation and traffic densities vary significantly while the central Po-valley is more homogeneous in land use. Thus higher concentrations and a higher variability of HCHO were expected.

From the logistical point the area around Milano offered some other advantages. Especially the long path DOAS measurements require towers or high buildings for the retroreflectors. The hilly terrain at Alzate and setup already used in the PIPAPO campaign in Bresso (Alicke et al, 2002) facilitated the implantation of DOAS instrumentation in the area. In the 2003 campaign additionally the southern site in Spessa facilitated for a multibeam DOAS system.

Within the course of the summer campaign atypical conditions occurred during the latter part of the campaign due to the Italian holiday season. Taking into account the experience from the first

campaign and the typical conditions in winter it was decided in agreement with the EC to shift the winter campaign into September to take advantage of the still high photochemical activity but already increased stability of the atmosphere. In winter conditions in the Po-Valley the visibility often gets as low that the applicability of the long path measurements cannot be guaranteed.

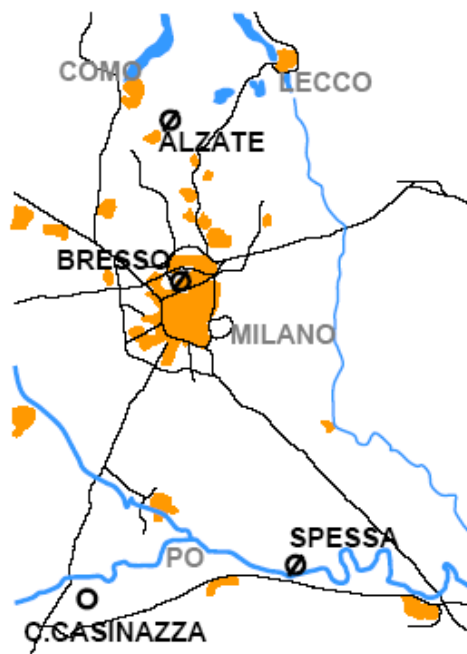


*Fig 6.1100.1: Sites for ground based HCHO measurements during FORMAT 2002 and 2003. Blue lines indicate water, black lines motorways, and the yellow area is settlements (city area of Milano, Como, Lecco, Pavia etc.) Due to logistical problems at C. Cascinone (C. Casinazza) in 2002 the southern site was moved to Spessa in 2003. Spessa, Bresso and Alzate are sites at small airfields*



*Fig 6.1100.2: Typical terrain north and south of Milano. In the north larger patches of forest and agricultural areas with scattered settlements, in the south mainly rice fields. The arrow marks the site of Alzate*

## Section 6: Detailed report related to overall project duration

The individual setups of instruments, the data gathered in the two campaigns and the deliverables of the project are described in the following subsections.

*Table 6.1100.1 summarises the ground-based HCHO measurements performed at the different sites during the two FORMAT campaigns. Most of the processed data have been averaged in 30 minute intervals and uploaded to the ftp site <ftp://zardoz.nilu.no/nadir/projects/other/format/>*

*Table 6.1100.1: ground based HCHO measurements during FORMAT 2002 and 2003. The field no in the tables refers to the contractor number of the institution that performed each measurement.*

No.	Instrument	Location
1, 2	Longpath-DOAS	Bresso, Alzate, Spessa (2003)
3	Hantzsch Analyzer	Bresso, Alzate, Cascina Casc. (2002)/ Spessa (2003)
2, 4	Max-DOAS	Bresso, Alzate
7	SOF, FTIR White cell	Mobile, (Bresso)
8	DNPH cartridges	Bresso, Alzate, Cascina Casc. (2002)/ Spessa (2003)

### **WP 1110 Summer Campaign**

After the intercomparison (WP 1400) in Bresso during the first five days of the campaign (July 24 to July 31), the individual mobile instruments were installed in the different sites, on July 29 and July 30. The long path systems, which are more difficult to move and to install at a new location, were already at the final location. The intercomparison in this case was performed with additional instruments. One Hantzsch analyzer was moved to Alzate to a container, another one to the Cascina Cascinone in the south into an empty room in the second floor of a farm building. The instruments were operated continuously until August 17. The installations always included a refrigerator for the liquids and standards, a data acquisition computer and a maximum 10 m PFA inlet line protected by an inline filter. Once a day the instruments were calibrated with a travelling liquid standard, the inline filters were replaced and data were collected and transferred back to an office in Alzate. The instruments used were basically identical with the commercial version of the Hantzsch analyzer (AL 4001, Aero-Laser, Garmisch-Partenkirchen, Germany) with slight modifications. The technique of the latest version and the instrument used on the microlight aircraft during the campaign is described in Junkermann and Burger, (2005).



*Fig. 6.1000.3: Instrument setup for Hantzsch in situ monitors at Alzate and Bresso. Three containers plus the mobile NILU DOAS were used for DOAS, Hantzsch in situ and VOC measurements. Air sampling for Hantzsch and DNPH cartridges were done half a meter above the roof of the left container. In Bresso the instrument was placed in the old hangar, the inlet was about 6 m from the building.*

DNPH cartridges were installed side by side to the inlet lines of the Hantzsch instruments in autosamplers sampling at two-hour time intervals. Problems with water vapour that led to clogging of the cartridges prohibited sampling during the night. All cartridges were collected once per day and immediately transferred to the laboratory of the JRC in Ispra where they were analyzed the next day.

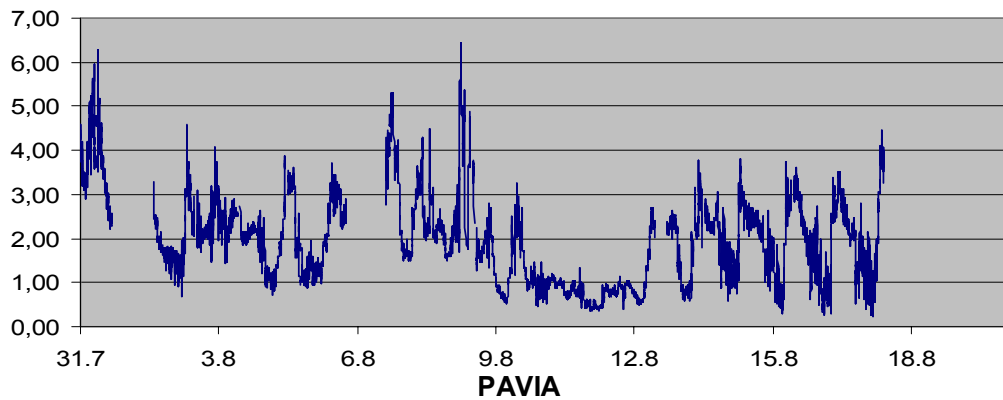


*Fig. 6.1100.4: The farm buildings and hangars of Spessa in 2003. In the front are the DOAS container and the mirrors for four different viewing directions. The Hantzsch inlet was situated in 2.5 m above ground and 80 cm from the building. Sampling position from DNPH cartridges was on the southern side of the farm buildings in 2.5 m above ground on top of a container.*

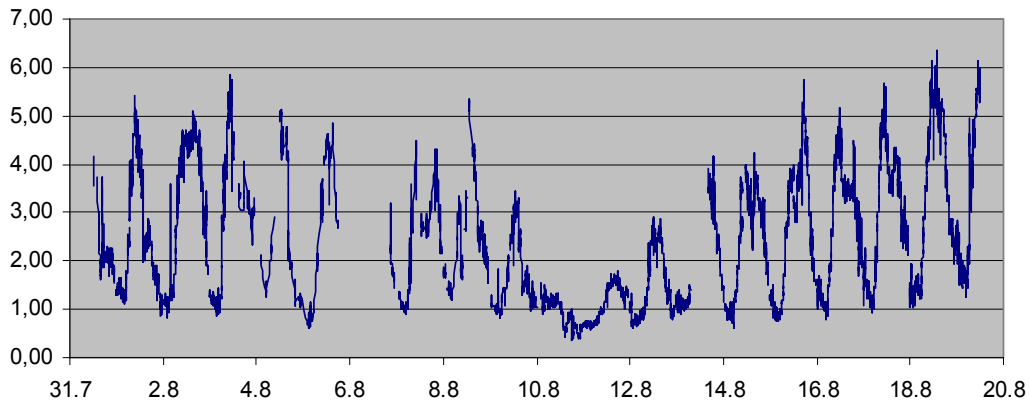
### Spatial distribution of HCHO from the summer campaign

As an example for the mixing ratios found during the summer campaign the data of the Hantzsch instruments are shown in Figures 6.1100.5.a-c. The Hantzsch instruments were operated in the summer campaign continuously on all sites and were operated by the same operator, Partner 3, with a standard set of a travelling calibration standards. Thus it is expected that there are no significant differences between the individual instruments and differences in the data are real local effects. Long Path instruments were available from Bresso and Alzate while in the Cascina Cascinone the guest from Korea were running an additional long path DOAS system. Severe problems with the system and damage to the roof of the building and rainwater on the instrument during a thunderstorm prevented a continuous operation. Thus nearly no DOAS data are available from the southern site. Additional available from the Cascina Cascinone are for the whole period the DNPH cartridge data.

**BRESSO**



**PAVIA**



**ALZATE**

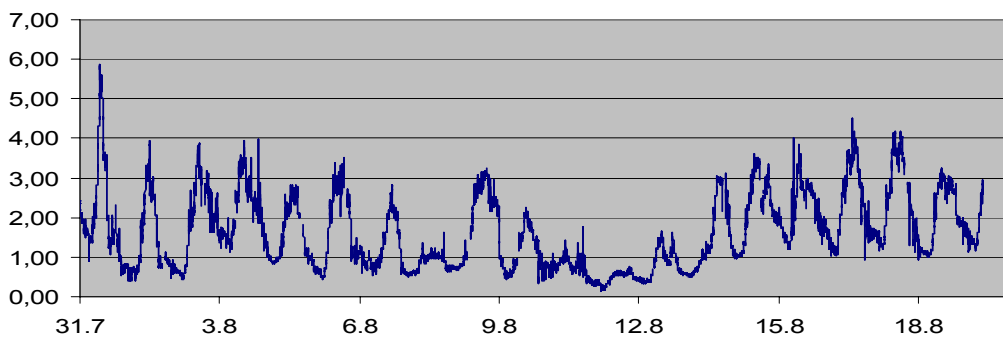


Fig.: 6.1100.5. a-c gives the mixing ratios of HCHO in ppb in Bresso, Pavia (Cascina Cascinone) and Alzate during August 2002 measured by Hantzsch instruments

The mixing ratios observed during August 2002 do not differ significantly between the three sites although the local sources are different. All stations depicted pronounced diurnal variations in agreement with model calculations. Maxima were found at 10:00 and 12:00 UTC. In the afternoon slightly lower (~ 20%) values were found. In the evening the mixing ratio dropped rapidly within a few hours to ~ 1 ppb. The station with the highest mixing ratios was the rural site in the south. The two stations north and south did not show significant differences in the diurnal variations, only Bresso with main urban character had a higher variability in the data. The low mixing ratios compared to the very high values measured at this site during the previous PIPAPO campaign (Alicke et al, 2002) are related to the holiday season in Italy. Factories and smaller businesses are closing down during the first two weeks of August and the main emission sources are substantially reduced. This is also the case for the Alzate site, where small industry and other antropogeneous activities in the densely populated triangle between Lecco, Como and Milano are a significant source for primary emissions of HCHO. South of Milano the main emission sources are agriculture (biogeneous emissions) and possibly motorway traffic that is still running during the holiday season although generally reduced.

## WP 1120 Winter campaign

To investigate the conditions with higher pollutant concentrations a second campaign was performed in September 2003, the original winter campaign. The holiday season ends in the last week of August and September was selected due to the high probability to find stable high pressure situations with still high photochemical conversion rates. Although very high pollution levels are reported from the area for December through February the experience during the first campaign showed that several of the instruments are not suitable for these conditions. Very humid (fog) conditions are critical for automated DNPH sampling and the build-up of ground inversions with visibilities of less than 100 m prevents very often for whole morning hours the use of long path optical techniques.

The sites were identical with the first campaign, only in the south the site was shifted further to the east to the airfield of Spessa (Speziana) directly south of Milano at the Po-river. The old site at the Cascina Cascinone was no longer available after the damage by a thunderstorm in 2002 and the collocation with the operational base of the microlight aircraft provided a better logistical basis. Also in Spessa a good location for multipath DOAS measurements was found.

Point monitoring with the continuously running Hantzsch instruments was performed during the

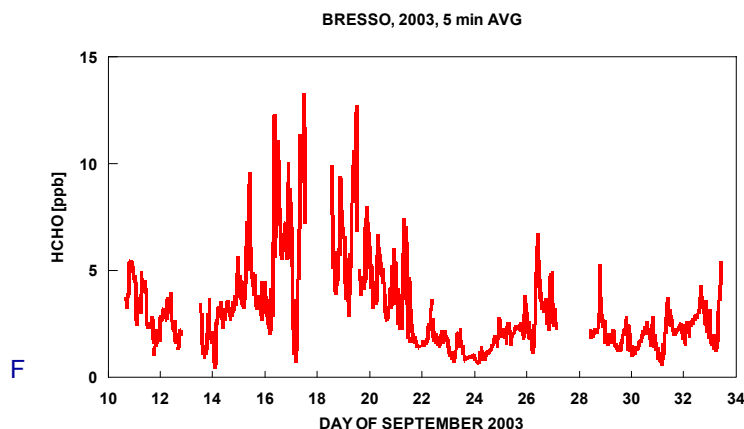


Fig. 6.1100.6, HCHO mixing ratios measured with the Hantzsch instrument at Bresso

whole campaign at all locations with instruments from IMK-IFU (Partner 3). The instruments have a time resolution of ninety seconds and five-minute averages are available for the whole campaign with the exception of the 19th of September when the instrument in Bresso was down for about eight hours.

The mixing ratios found in the different locations were less homogeneous than in the previous campaign. Highest values were observed in Bresso during the first smog episode due to intense traffic and industrial activity in that city. Although all conditions were met to reach high mixing ratios the values were about half of what was reported from the previous PIPAPO campaign, (Alicke et al, 2002). The mixing ratios in the southern station were strongly influenced by the frequent biomass burning in that area. No significant differences were observed between the sites north and south of Milano, Alzate and Spessa with the exception of some biomass burning events. Contrary to the 2002 campaign now Alzate had slightly higher diurnal maxima than Spessa.

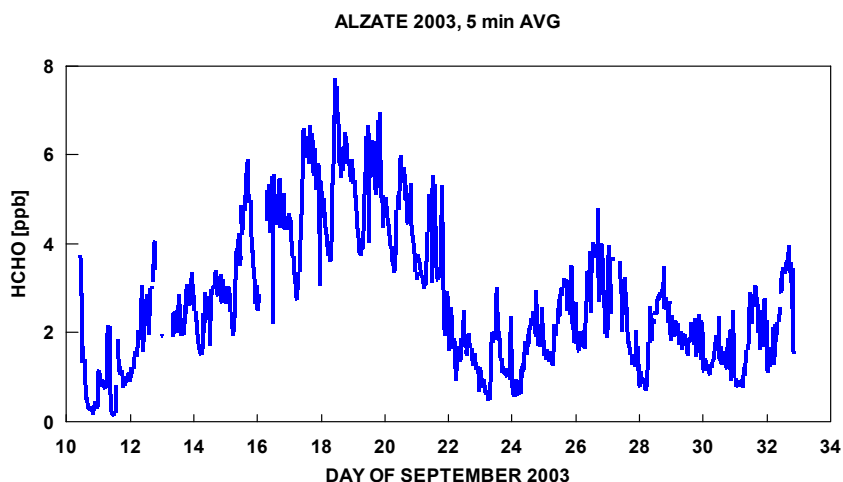


Fig. 6.1100.7: Hantzsch measurements at Alzate during the 2003 campaign.

It is interesting to note that during the high pollution episode in the second week of the campaign the nocturnal minima of HCHO increased from day to day, feature that was not observed in 2002. During the stable high pressure situation nocturnal continuous emissions of HCHO are required to explain this behaviour. In the agricultural area of Spessa, where most of the direct emissions (biogenic or antropogenic) have a diurnal cycle, this night enhancement of the minima has not been observed. Like in the 2002 campaign the nocturnal minima were always close to  $1 \pm 0.5$  ppb HCHO.

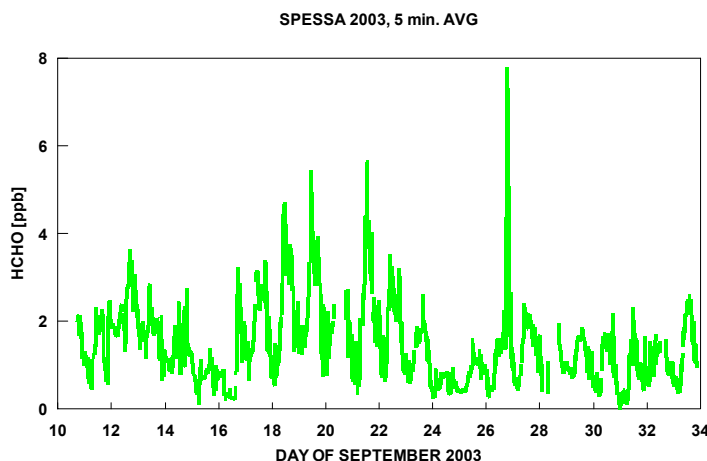


Fig. 6.1100.8, Hantzsch measurements at Spessa during the 2003 campaign. The highest peaks occurred during a period when nearby rice fields were burnt.

The spatial distribution of HCHO at ground level in the Po-Valley during summer and early fall conditions is clearly dominated by local emissions. Although the vegetation and land use patterns between north and south differ significantly the diurnal variability of the HCHO mixing ratios was unexpectedly very similar. The mixing ratios outside of the direct area of the city were found to be in a similar range of up to 5 ppb as the diurnal maximum and ~ 1 ppb as the nocturnal minimum. While we found low emissions during the holiday season in the north, the agricultural areas in the south had a 20% increase in HCHO. This pattern changed with increasing antropogeneous activity after the end of the holidays, causing a 20 % increase in the north. During stable high pressure conditions the northern rural site and the site in the city of Milano showed elevated nighttime mixing ratios that would require a continuous sources of HCHO also during the night. This maybe due to the significant changes in the emission patterns, increase in car traffic and 24 hours operation of chemical and other industry in the north. In the south one of the main emission sources, the biomass burning, is restricted to daylight hours only.

Additional information about the spatial variability was obtained from aircraft measurements during both campaigns (see WP 2110/2120).

Discontinuous grab sampling with DNPH cartridges was performed by the JRC ISPRA (Partner 8). JRC's role in this campaign was primarily carrying out the ground-based measurements of HCHO, CH<sub>3</sub>CHO and CH<sub>3</sub>COCH<sub>3</sub> in Spessa PO (Pa) and Alzate Brianza (Co) Bresso (Mi) as well as VOC ozone precursors in Bresso (Mi). VOCs were continuously monitored day and night. These measurements are described under WP 3100.

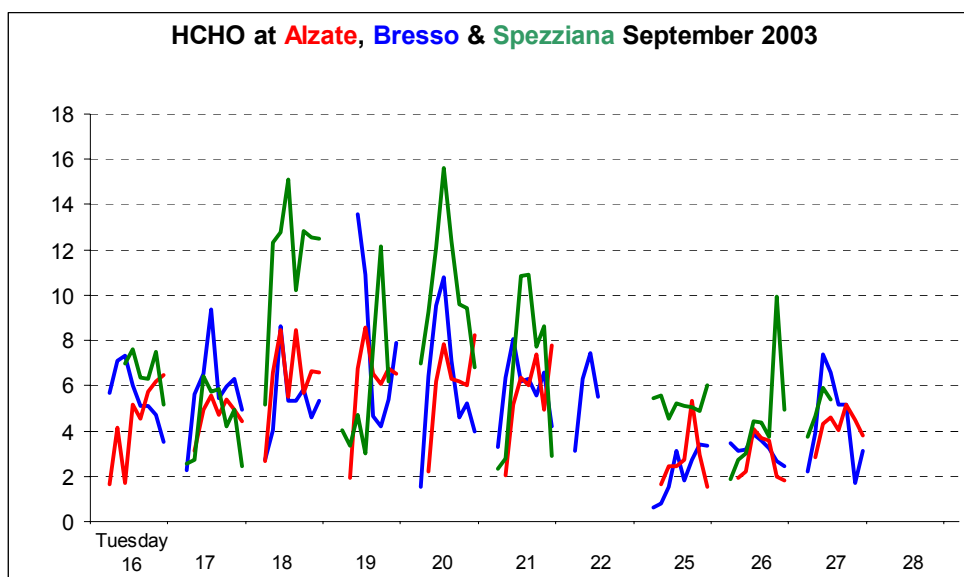


Fig.: 6.1100.9. Measurements of HCHO at the three sites during the second campaign in 2003.

In contrast to the Hantzsch measurements and the good agreement between Hantzsch and DNPH in all other locations and within the 2002 campaign the DNPH technique showed very high values in Spessa. The sampling location was about 100 m south of the sampling location for Hantzsch at

## Section 6: Detailed report related to overall project duration

another area of the farm. As the farm mainly cultivated rice, there is no cattle or any other specific emissions. The source of this discrepancy is still unknown.

Data gathered from the microlight aircraft measurements indicate that in the second campaign the mixing ratios at Spessa were lower than in the other locations.

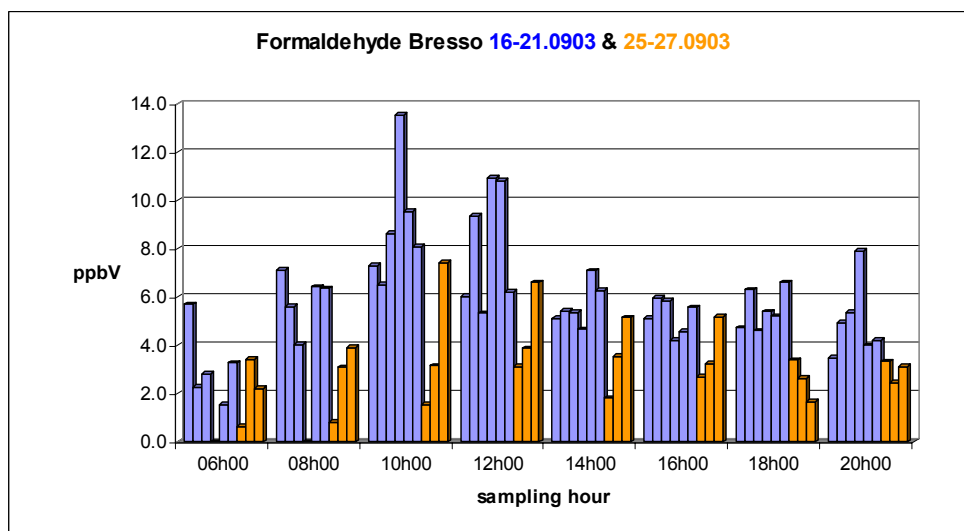


Fig. 6.1100.10: Diurnal pattern of the DNP-HCHO measurements at Bresso. Typical is the maximum in the morning between 10 and 12:00 UTC followed by a fairly stable mixing ratio during the afternoon.

In Bresso and Spessa a new longpath DOAS system of the University of Heidelberg, the Multibeam Longpath DOAS (MB-LP-DOAS), came into operation. It has the advantage of measuring with up to four light beams along different light paths simultaneously. At both sites three different light paths were measured by each instrument. HCHO data for the Bresso site are shown below. A sketch of the setup of light beams in Bresso can be found in WP 3000.

In Spessa another MB-LP-DOAS was used, measuring with three light beams.

MB-LP-DOAS measurements, both in Spessa and Bresso, were often impossible due to fog during the night and morning hours. In addition, strong winds, especially during the last week of the campaign, made accurate measurements difficult.

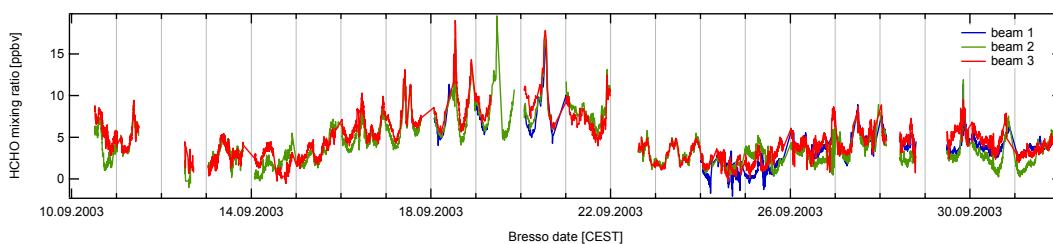


Figure 6.1100.11: Time series of the HCHO mixing ratio in Bresso measured by MB-LP-DOAS (IUP Heidelberg). The system operated with three light beams simultaneously. For details about the setup of the light beams see WP 3000.

## Section 6: Detailed report related to overall project duration

One week of clear weather was terminated at 22.09.2003 due to a decrease of atmospheric pressure, which brought lower temperatures and radiation with it. During this week the formaldehyde mixing ratio reached top values of 18 ppb in Bresso, averaged along the light path.

### **References:**

Alicke, B., U. Platt, and J. Stutz, Impact of nitrous acid photolysis on the total hydroxyl radical budget during the Limitation of Oxidant Production/Pianura Padana Produzione di Ozono study in Milano, J. Geophys. Res., 107(D22), 8196, doi:10.1029/2000JD000075, 2002.

Junkermann W., and Burger, J.M., A new portable instrument for continuous measurement of formaldehyde in ambient air, JOAT, in print July 5. 2005

**WP 1200: MAXDOAS from the ground****MAX-DOAS measurements by IUP HD**

The instrument used during the second campaign in Bresso was formerly installed on board of RS 'Polarstern'. It consists of three telescopes, which were pointing horizontally into different directions (north, west, south), each one oriented at five vertical angles (3°, 6°, 10°, 18°, zenith).

MAX-DOAS measurements were performed between 03.09.2003 and 02.10.2003 in Bresso. Details of the spectral DOAS analysis are presented in Table 6.1200.1 and Fig. 6.1200.1.

*Table 6.1200.1 Trace gas cross sections used for the MAX-DOAS O<sub>4</sub> analysis.*

<b>Molecule</b>	<b>Data source</b>	<b>Adaptation to our instrument</b>
O <sub>4</sub> (296K)	Greenblatt et al., 1990	Interpolation <sup>1</sup>
BrO (228 K)	Wilmouth et al., 1999	Convolution <sup>2</sup>
NO <sub>2</sub> (273K)	Vandaele et al., 1997	I <sub>0</sub> -correction <sup>3</sup>
O <sub>3</sub> (221 K)	Bogumil et al., 2003	I <sub>0</sub> -correction <sup>3</sup>
O <sub>3</sub> (293 K)	Bogumil et al., 2003	I <sub>0</sub> -correction <sup>3</sup>
HCHO (298 K)	Meller and Moortgat, 2000	Convolution <sup>2</sup>

<sup>1</sup>the cross section is interpolated to the wavelength grid of our instrument.

<sup>2</sup>the cross section is convoluted by the instrument function and interpolated to the wavelength grid of our instrument.

<sup>3</sup>the cross section is convoluted by the instrument function and interpolated to the wavelength grid of our instrument. In addition a so-called I<sub>0</sub> correction is applied.

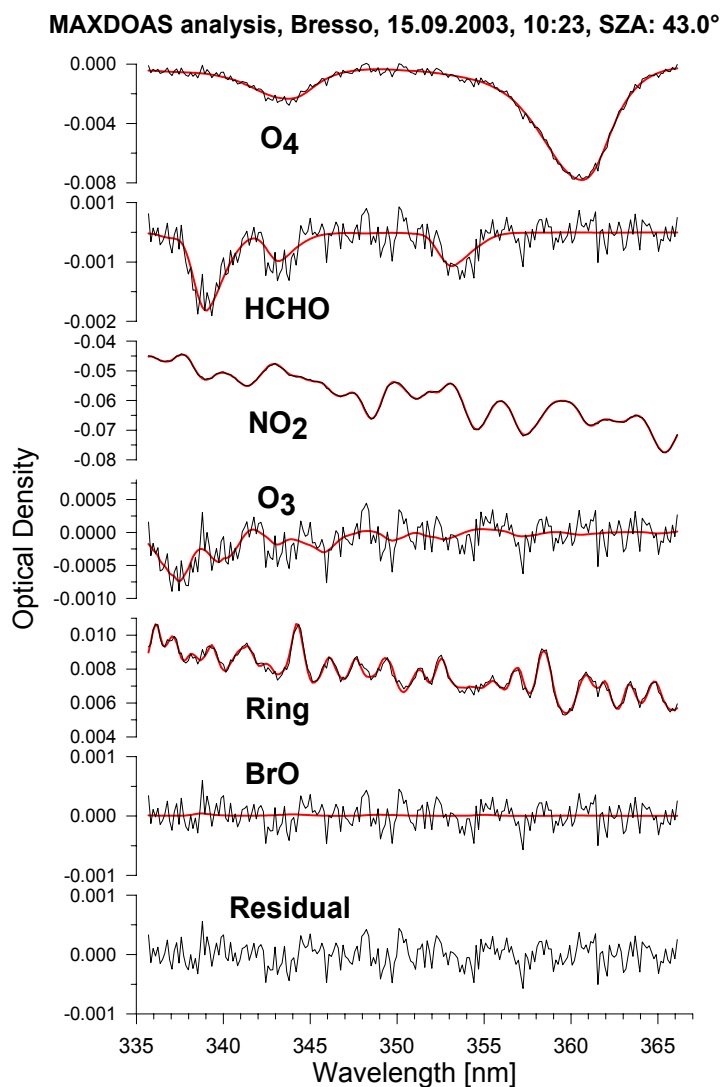


Fig. 6.1200.1 Example of a spectral DOAS analysis. The thick lines show the trace gas cross sections scaled to the respective absorptions detected in the measured spectrum (thin lines). The mainly stratospheric trace gases O<sub>3</sub> and BrO show only a very weak absorption, because both the measured spectrum and the Fraunhofer reference spectrum contain nearly the same stratospheric absorption. In contrast, the trace gases with enhanced tropospheric concentrations show a large absorption (difference) [Wagner et al., 2004].

In general, the telescopes at the different azimuth directions observed almost similar HCHO columns (here a plot is shown for the four elevations of the northward looking telescope). These findings indicate that in general only small horizontal gradients of HCHO appeared over the measurement site. Nevertheless, on some days, systematic gradients could also be observed (see Fig. 6.1200.3).

## Section 6: Detailed report related to overall project duration

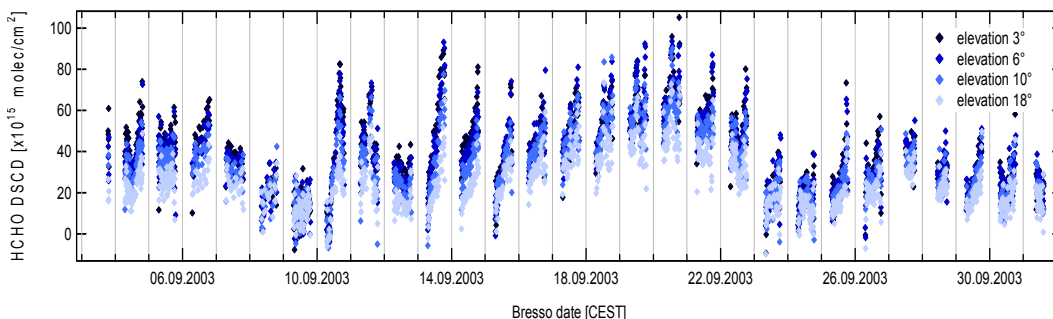


Figure 6.1200.2: Time series of the HCHO differential slant column densities in Bresso measured by MAX-DOAS (IUP Heidelberg). The system measured with three telescopes pointing to the north, west and south, respectively. Each telescope stepped between the elevation angles 3°, 6°, 10°, 18° and zenith.

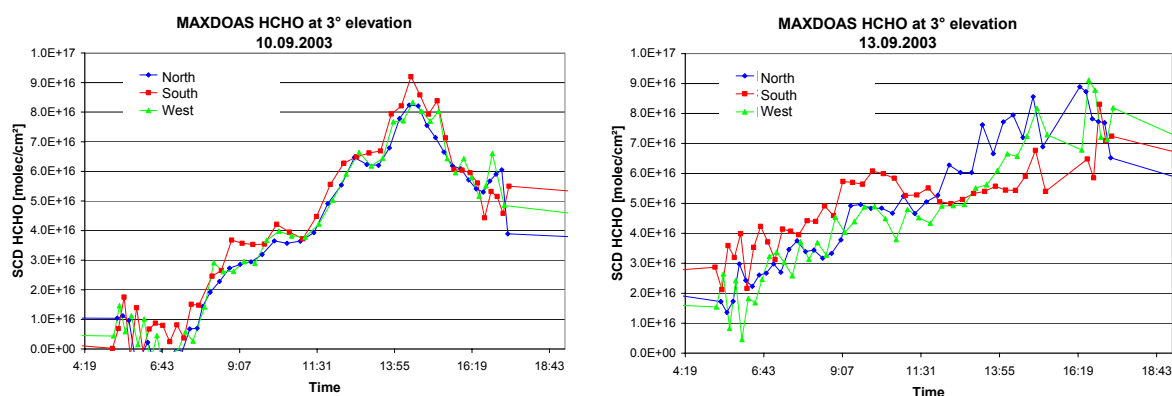


Fig. 6.1200.3 Examples of days with and without horizontal gradients of formaldehyde. Left: on September 10. 2003, the telescopes at all azimuth angles measured almost the same HCHO DSCD throughout the day. This indicates that the HCHO concentration field had no strong horizontal gradients. Right: on September 13. 2003, the telescopes at the different azimuth angles measured systematically different HCHO DSCD. In the morning higher values were found in southern directions, during the evening higher values appeared in northern and western directions.

Besides the analysis of HCHO and NO<sub>2</sub>, also the absorptions of the oxygen dimer O<sub>4</sub> were analysed in detail. From these measurements, it is in particular possible to infer information of the atmospheric aerosol properties [Wagner et al., 2002; 2004]. One example of the influence of an increasing aerosol load on the MAXDOAS O<sub>4</sub> observations is shown in Fig. 6.1200.4. During a period of four days the aerosol load increased strongly leading to significantly reduced O<sub>4</sub> absorptions [Wagner et al., 2004].

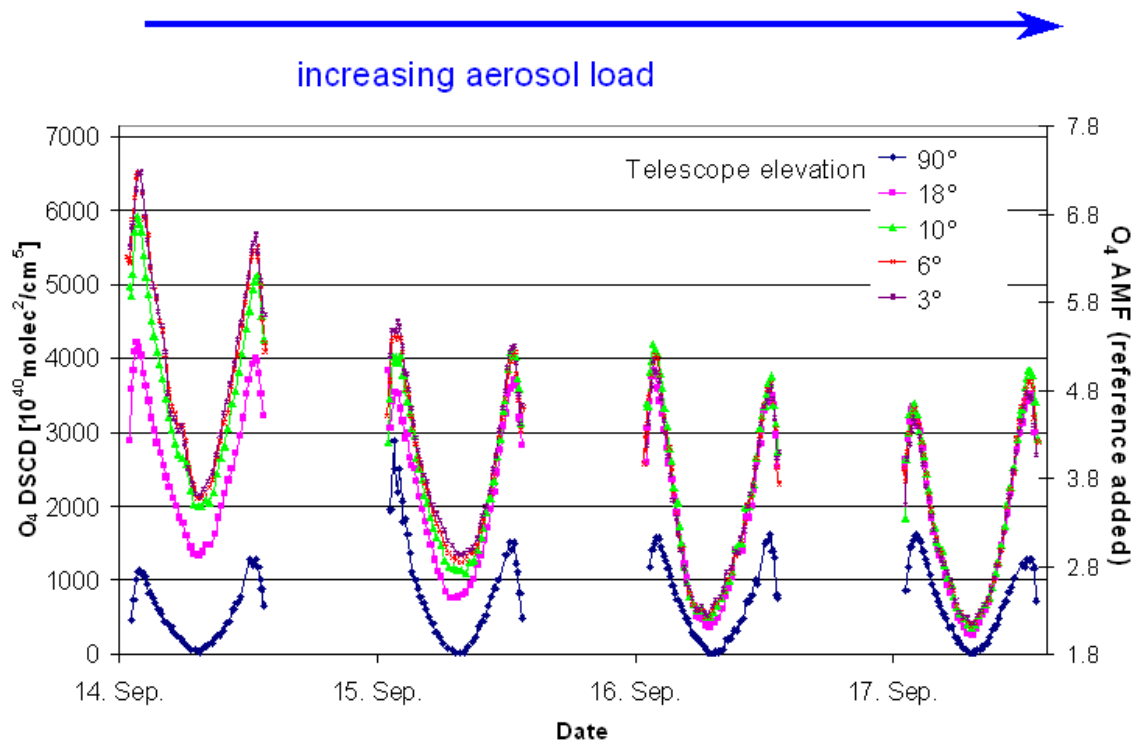


Fig. 6.1200.4:  $O_4$  DSCDs measured for different elevation angles of the southern telescope during four mostly clear days (September, 14 – 17, 2003) at Milano, Italy. Because of the changing sun position during the day the relative azimuth angles of the telescopes with respect to the sun are  $\sim 90^\circ$  during sunrise,  $\sim 0^\circ$  during noon and  $\sim -90^\circ$  during sunset. The main effects are the general reduction of the observed  $O_4$  absorption and the decreasing difference between the low elevation telescopes ( $3^\circ$ ,  $6^\circ$ ,  $10^\circ$ ,  $18^\circ$ ). These effects can be related to the increased aerosol load during the selected period (see text). The zenith observations during the morning of September 15 were affected by sporadic clouds and should not be taken into account for the detailed interpretation of the time series.

#### References

Wagner, T., C.v.Friedeburg, M. Wenig, C.Otten and U. Platt, “UV-visible observations of atmospheric  $O_4$  absorptions using direct moonlight and zenith-scattered sunlight for clear-sky and cloudy sky conditions”, *Journal of Geophysical Research*, Vol. 107, No. D20, pp 4424, 2002

Wagner, T., B. Dix, C.v. Friedeburg, U. Frieß, S. Sanghavi, R. Sinreich, and U. Platt MAX-DOAS  $O_4$  measurements – a new technique to derive information on atmospheric aerosols. (I) Principles and information content, *J. Geophys. Res.*, 109, D22205, doi:10.1029/2004JD004904, 2004

#### MAX-DOAS measurements by IUP Bremen

The Bremen MAX-DOAS instrument was operated at the measurement site Alzate from 20 July to 18 August 2002 (1<sup>st</sup> or *summer* campaign) and from 10 September to 5 October 2003 (2<sup>nd</sup> or *winter* campaign). There were a few interruptions in the measurements during this time period due to power failure. The instrument measured formaldehyde but also  $NO_2$ ,  $O_4$  and the AOD.

Details on the instrumental setup and the standard evaluation procedures were given in the first annual report and in Heckel et al., 2005. An overview on the standard DOAS analysis is given in table 6.1200.1 (*Deliverable 1210.3*).

Table 6.1200.1 DOAS settings for the HCHO analysis.

Molecule	Temperature [K]	Reference
HCHO	298	Meller and Moortgat [2000]
NO <sub>2</sub>	220	Vandaele et al. [1997]
O <sub>3</sub>	241	Burrows et al. [1999]
O <sub>3</sub>	221	Burrows et al. [1999]
O <sub>4</sub>	296	Greenblatt et al. [1990]
BrO	228	Wahner et al. [1988]
Ring	-	Heidelberg: Bussemer [1993] Bremen: Vountas et al. [1997]
Wavelength range	-	Heidelberg: 337 - 358 nm Bremen: 335.0 to 357.0 nm

The following figure shows the vertical columns of HCHO above Alzate for both campaigns (Deliverables 1210.1 and 1220.1).

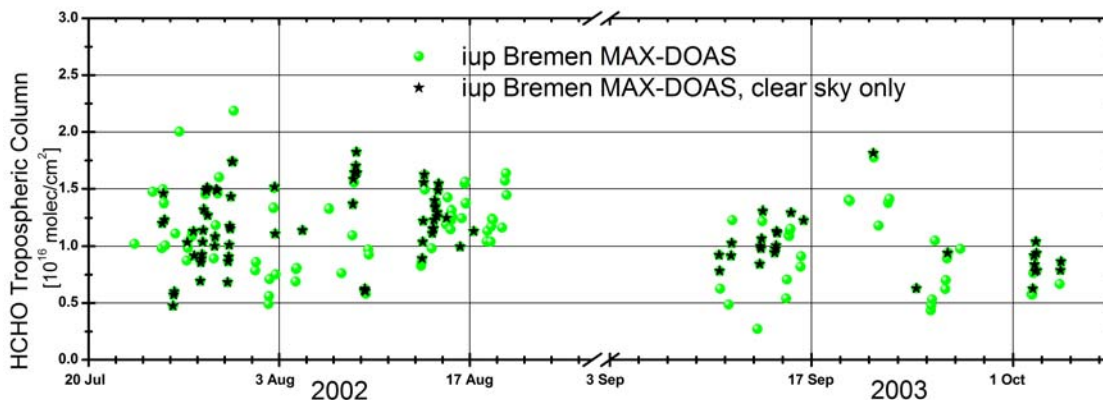


Figure 6.1200.5 Tropospheric HCHO columns measured by the Bremen MAX-DOAS instrument during the field campaigns FORMAT 2002 and FORMAT 2003. The values have been derived using the Bremian advanced MAX-DOAS retrieval algorithm (BREAM) described below (*Deliverable 1220.3*).

As a major outcome of this project a new algorithm for the analysis of MAX-DOAS measurements has been developed (D1220.3): BREAM – **B**remian **A**dvanced **M**AX-DOAS **R**etrieval **A**lgorithm. The following section describes briefly the mode of operation as well as the possibilities and limitations of the new retrieval. Also some applications to data collected within this project will be shown.

Recent studies (e.g. Wagner et al., 2002; Wittrock et al., 2004) have shown that the measured slant column of the oxygen dimer O<sub>4</sub> (O<sub>2</sub>-O<sub>2</sub>) can be used to derive aerosol information, i.e. the extinction profile and to some extent also the aerosol type in the atmosphere. The knowledge is essential to retrieve the correct amount of the chosen absorber (e.g. HCHO). Already a relatively small error in the aerosol extinction can lead to error larger than 100 per cent (Oetjen 2002; Wittrock et al. 2004; Heckel et al., 2005).

In a first step the algorithm uses the radiation transport model SCIATRAN (Rozanov et al., 2001) to calculate  $O_4$  slant columns which are compared to the measured ones in order to reduce uncertainties due to aerosols. The extinction profile in its total quantity as well as in its structure (i.e. the height of the boundary layer) is scaled in an iterative process and therewith the slant columns of  $O_4$  are calculated. The quality of the agreement is evaluated by applying two parameters: The correlation between the measurement and the modelled columns (which is mainly influenced by the height of the boundary layer) and the mean deviation of those (mainly modulated by the extinction). In general, for cloud free scenarios a correlation better than 0.9 and a deviation smaller than 10 per cent between model and measurement can be obtained.

Figure 6.1200.6 illustrates the quality of the retrieved aerosol data. A comparison for the aerosol optical density for three different instruments during the first FORMAT-campaign in 2002 is shown: measurements with a sun photometer as well as with a MICROTOPS-instrument together with the aerosol optical density retrieved from the  $O_4$  measurements with a MAX-DOAS instrument.

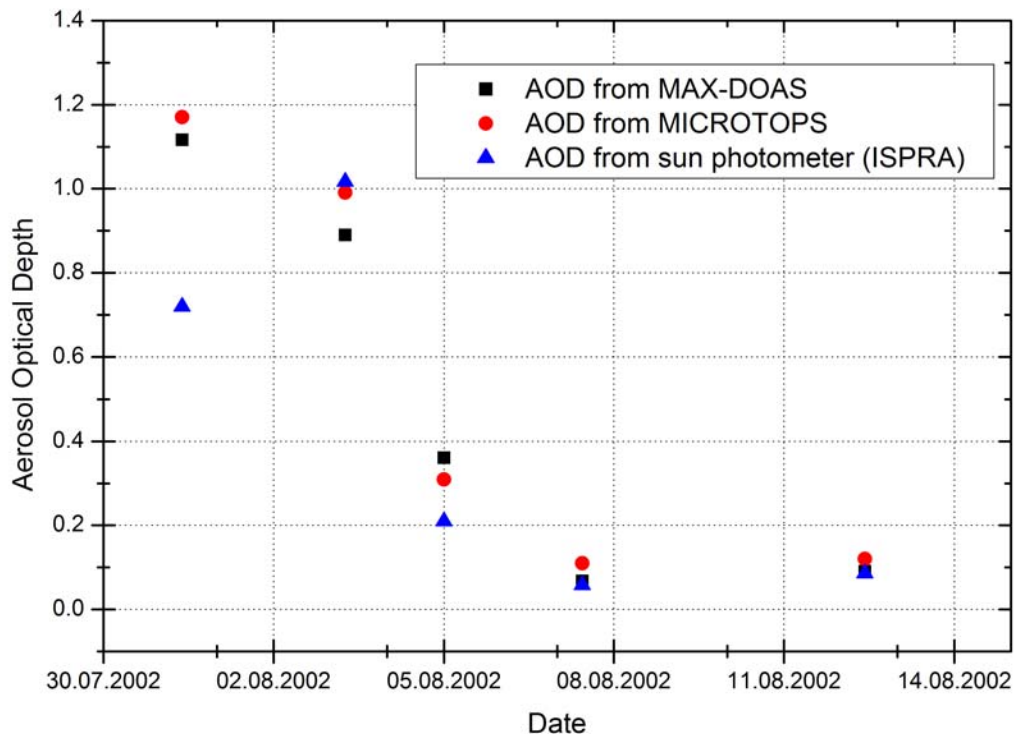


Figure 6.1200.5 Comparison of different aerosol measurements at Alzate, Italy. The MAX-DOAS results have been retrieved using BREAM.

The second step comprises calculation of so called block air mass factors with respect to the chosen absorber using the prior obtained aerosol information. Again SCIATRAN in its full-spherical mode is operated. Block air mass factors are air mass factors which depend on the layer height of the absorber. The overall air mass factor is simply the average of the block air mass factors weighted by the distribution of the trace gas. This concept allows us to describe the relation between the measurement (i.e. the set of slant columns under different elevation angles of the absorber) and the absorber's profile in the atmosphere as a linear system:

$$y = K \cdot x$$

with  $y$  as the measurement vector,  $x$  the wanted profile and  $K$  as the weighting function matrix depending on the block air mass factors.

To solve such a linear system the well known and in atmospheric chemistry long-established method of Optimal Estimation by Rodgers (1976, 1990) seems to be appropriate. With this the profile  $x$  is determined by:

$$x = x_a + (K^T S_e^{-1} K + S_a^{-1})^{-1} K^T S_e^{-1} (y - K x_a)$$

$y$  measurement (differential slant column)

$x_a$  a priori profile

$S_e$  and  $S_a$  error covariance matrices for a priori and measurement

$K$  weighting function matrix

$$K(i,j) = \frac{\text{BDAMF}(i,j) \cdot p(j) \cdot R \cdot N_A \cdot \Delta h}{T(j)}$$

BDAMF block air mass factor relative to the reference

$p$  pressure,  $T$  temperature and  $\Delta h$  layer height

This method can only be applied for an optically thin atmosphere: Extinction of light is mainly caused by scattering and consequently the radiative transfer independent from the concentration of the absorber. This constraint is valid for virtually all absorbers that can be retrieved via the DOAS method:  $\text{NO}_2$ , all halogen oxides and formaldehyde, but fails for ozone in the ultraviolet spectral range or for line absorbers as  $\text{H}_2\text{O}$ .

Various sensitivity studies about information content and stability of the profile retrieval have been performed in this work package. In general, it is an advantage to use several wavelength regions simultaneously. This is possible for e.g.  $\text{NO}_2$  but unfortunately not for  $\text{HCHO}$ .

The averaging kernel matrix is a measure for the quality of the retrieval. The trace of the matrix determines the number of pieces of independent information with respect to the height layers, i.e. the degrees of freedom of this measurement. Typical integration times (20 minutes to one hour) together with a moderate aerosol content yields a number of about two to three. The whole range includes results from about 1.5 for low visibility up to about five considering also large solar zenith angles ( $\text{SZA} > 75^\circ$ ).

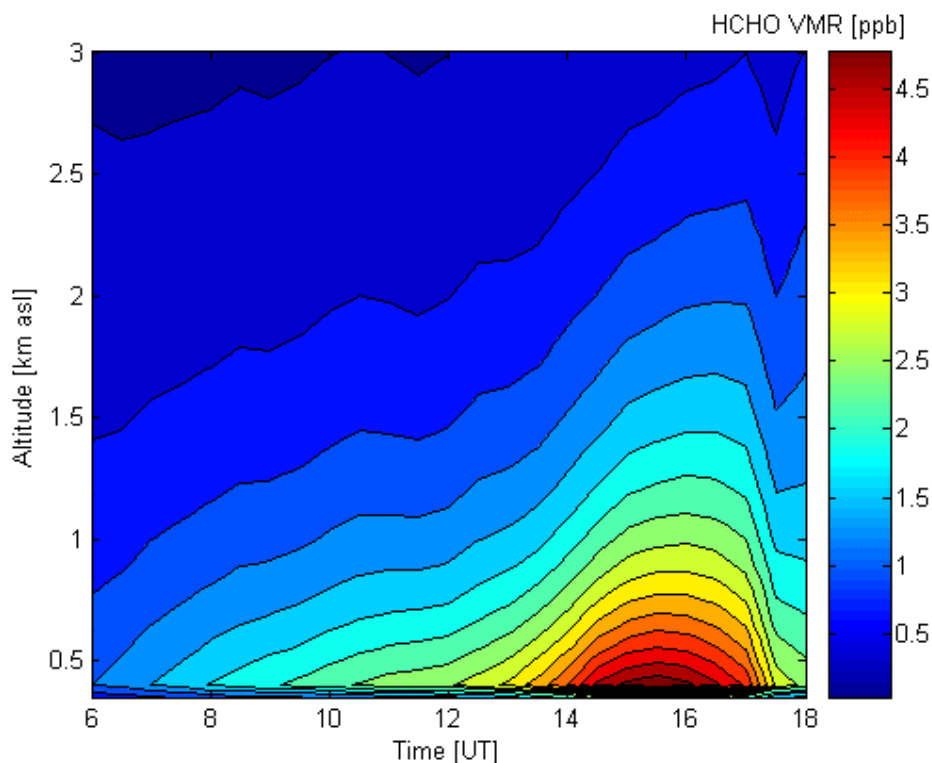


Figure 6.1200.7: Diurnal variation of the HCHO profile above Alzate on August 13, 2002 retrieved from IUP Bremen MAX-DOAS observations.

Exemplarily, Figure 6.1200.7 is showing the profiles for HCHO retrieved from measurements in Alzate on one selected day. The height resolution is decreasing with increasing (vertical) distance to the instrument as expected: it is about 100 m close to the telescope but above 2 to 3 km, i.e. in the free troposphere there can be only one layer distinguished. In contrast to NO<sub>2</sub> Formaldehyde profiles have usually highest values in the second or third layer. An example for the validation of the profile retrieval is shown in Figure 6.1400.2, WP 1400: Good agreement can be found with *in situ* and long-path DOAS observations. Another validation of the method is shown in WP 2300, Figure 6.1400.2, by comparing measurements from the microlight with profiles retrieved by BREAM.

Recapitulating it can be said that profiles from MAX-DOAS measurements are suitable to study tropospheric pollutants. Unlike active systems (e.g. Long-Path DOAS) an automatic operation is possible. At this point the only imposed constraint to the retrieval is the necessity of more or less cloud free scenarios.

#### References:

- Heckel, A., A. Richter, T. Tarsu, F. Wittrock, C. Hak, I. Pundt, W. Junkermann, and J. P. Burrows, MAX-DOAS measurements of formaldehyde in the Po-Valley, *Atmos. Chem. Phys.*, 5, 909–918, 2005
- Rodgers, C. D. "Characterization and error analysis of profiles retrieved from remote sounding measurements", *J. Geophys. Res.*, 95, D5, 5587-5595, (1990)
- Rozanov, A., Rozanov, V. V., and Burrows, J. P.: A numerical radiative transfer model for a spherical planetary atmosphere: combined differential-integral approach involving the Picard iterative approximation, *Journal of Quantitative Spectroscopy and Radiative Transfer*, 69, 491, 2001

## Section 6: Detailed report related to overall project duration

Wagner, T., C.v.Friedeburg, M. Wenig, C.Otten and U. Platt, “UV-visible observations of atmospheric O<sub>4</sub> absorptions using direct moonlight and zenith-scattered sunlight for clear-sky and cloudy sky conditions”, *Journal of Geophysical Research*, Vol. 107, No. D20, pp 4424, 2002

Wittrock, F., H. Oetjen, A. Richter, S. Fietkau, T. Medeke, A. Rozanov, and J. P. Burrows, MAX-DOAS measurements of atmospheric trace gases in Ny-Ålesund, *Atmos. Chem. Phys.*, 4, 955-966, 2004

Wittrock, F. et al., Retrieval of trace gas profiles from MAX-DOAS observations, manuscript in preparation for *ACPD*, 2005.

**Method and data for the whitecell HCHO**

An open path White cell system was operated by Chalmers at the Bresso airport between July 22 to August 18, 2002 and September 11 to October 3, 2003. The instrument measured formaldehyde but also CO, CO<sub>2</sub>, VOC, NO, H<sub>2</sub>CO, N<sub>2</sub>O and CH<sub>4</sub>. The system consisted of a 1 cm<sup>-1</sup> Bomem FTIR spectrometer, connected to a 1 km open path White cell with a base path of 25 m, Figure 6.1300.1. The computer, FTIR spectrometer and field mirror of the White system was located inside the cabin. The reflecting mirrors of the White system were located on a tripod, 25 m away from the field mirror. The system was set to 40 passes, giving a total optical path of 1 km. The time resolution used was 5 minutes. The first year the White cell system occasionally went out of alignment, due to large diurnal temperature variations with loss of data as results. The second year the White cell was equipped with an additional alignment system to keep the optical alignment stable during the day, compensating for the diurnal temperature changes.



Figure 6.1300.1. The 1 km White system.

The spectra were evaluated applying a nonlinear retrieval, NLM, using software developed by D. Griffith at University of Wollongong, Australia. Cross sections from the HITRAN 2002 database were used in the retrieval. Figure 6.1300.2 shows the fit from the retrieval of H<sub>2</sub>CO on the 19th of September 22:08. The strong features seen correspond to absorption lines of water, and the absorption lines of formaldehyde are positioned between these. Even though the water lines are close to the formaldehyde, the retrieval is robust towards variations in the water content.

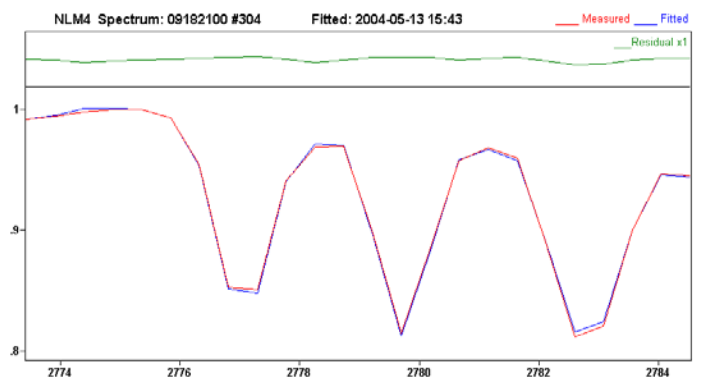


Figure 6.1300.2. Evaluation of H<sub>2</sub>CO (8 ppb). The strong absorption signatures here correspond to water and the formaldehyde absorbs between them.

Section 6: Detailed report related to overall project duration

The formaldehyde values for 2002 were compared to values obtained by other techniques with generally good agreement, considering the estimated precision of 0.3 ppb and accuracy of 0.5 ppb. In Figure 6.1300.2 a comparison between the White cell system and a Hantzsch instrument operated by IFU is shown. It can be seen that there is good agreement at higher values but an apparent offset between the techniques close to the detection limit. By utilizing simultaneous CO and CO<sub>2</sub> measurements it was possible to estimate the amount of formaldehyde typically emitted from an average vehicle in the Milano area of  $9.5 \cdot 10^{-5}$  g/g fuel and it was also possible to estimate the fraction of secondary formation of formaldehyde in the Milano plume (around 90% in the aged plume), see WP 3000.

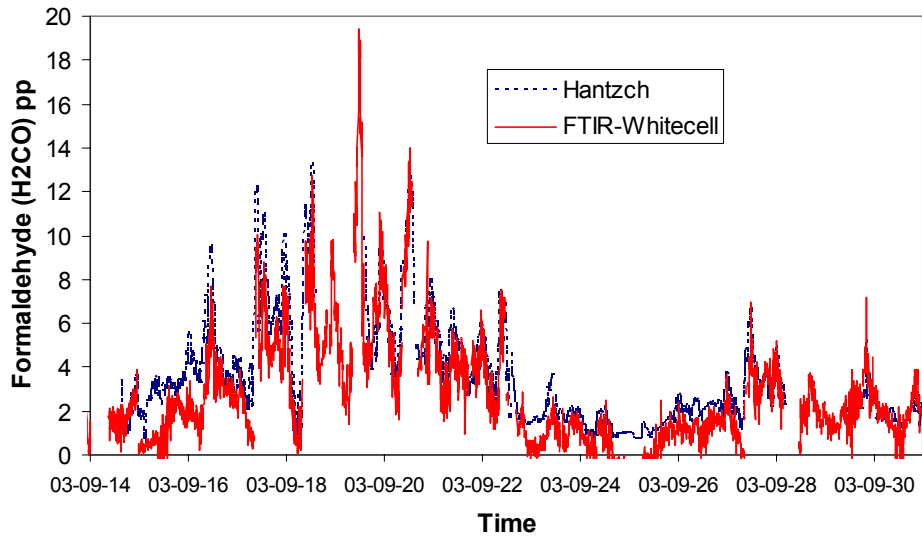


Figure 6.1300.3. Formaldehyde measured by an FTIR connected to a 1 km White cell and Hantzsch measurements by IFU.

**SOF IR and UV**

A mobile FTIR system denoted SOF (Solar Occultation Flux) was applied by Chalmers University measuring total vertical columns of  $\text{H}_2\text{CO}$  but also CO. The system consists of a commercial FTIR, (Bruker, OPAG), connected to a custom built solar tracker, see Figure 5.1300.4. The SOF system is built in to a VW-bus and measurements can be conducted both standing and while driving. In order to retrieve formaldehyde, and other species, solar measurement between  $2700$  and  $3000\text{ cm}^{-1}$  were conducted at  $0.5\text{ cm}^{-1}$  resolution, averaging for  $60\text{ s}$ . In order to improve the signal-to-noise, an interference filter was applied covering the region of interest.



Figure 6.1300.4.  $360^\circ$  rapid solar tracker connected to a  $0.5\text{ cm}^{-1}$  resolution FTIR, operating at wavelength  $2.5\text{--}14\ \mu\text{m}$  (left) and solar measurements at Bresso airport (right).

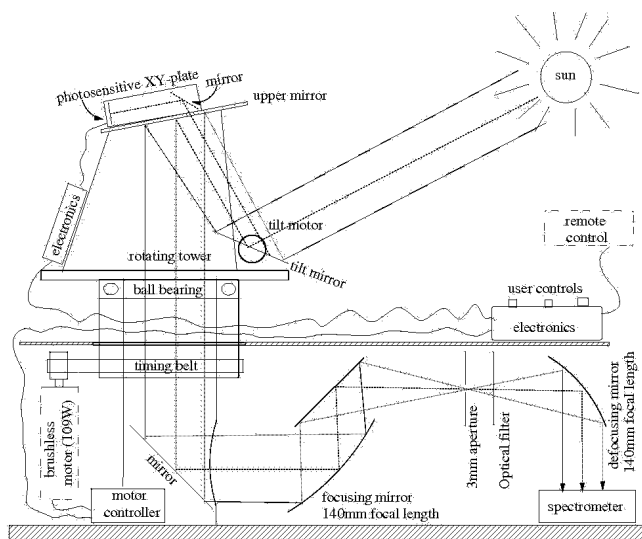


Figure 6.1300.5. Schematic of the optical setup for the SOF instrument.

Solar measurements were conducted daily both at fixed positions, Bresso, to study diurnal column variations and at different locations around the Milano area, to obtain information about spatial variations. In total there were around 10 days in 2002 (summer campaign) and 22 measurement days in 2003 (winter campaign). The measurements in 2002 were less good due to instrumental problems in the beginning of the campaign and due to the fact the concentrations of many species were lower due to the holidays. Little emphasis has therefore been put on this year in the final analysis. In 2003, 5 days were used for diurnal variation studies in Bresso and 14 for spatial column variation studies. There were also 1 refinery measurement day (Sannazzaro De Burgundi), one day at the power plant of Ostiglia and one trial measuring  $\text{H}_2\text{CO}$  at a burning field near Spessa. The

## Section 6: Detailed report related to overall project duration

solar spectra were retrieved using the Optimal estimation algorithm in a code named SFIT2 3.81, developed by NASA. In the retrieval the atmosphere was divided into 74 layers. Pressure and temperature for the layers came from NCEP, line parameter data from the HITRAN 2002 database. In the retrieval an a priori profile were used corresponding to about 2 ppb HCHO in the lowest levels and then slowly declining. This corresponds to a column of  $5.8 \cdot 10^{15}$  mol/cm<sup>2</sup>.

Figure 6.1300.6 show a spectral fit for the retrieval of HCHO, with intensity as a function of wave number and the residual of the fit on top. This region is much wider than used for the FTIR-Whitecell system since it was found to be difficult to conduct good retrievals with the narrow region. For the wide region the results seems more consistent with other techniques.

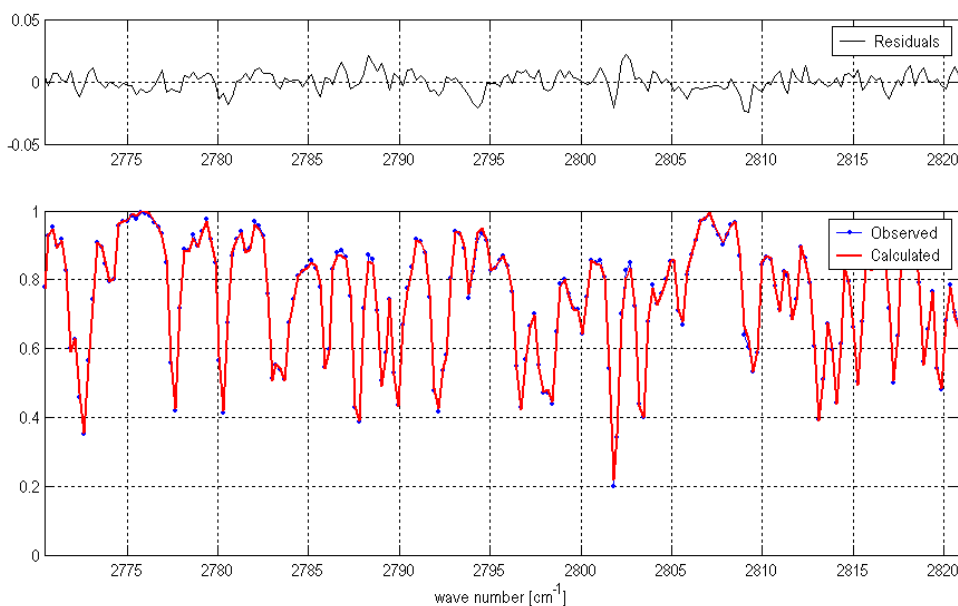


Figure 6.1300.6. Retrieval of formaldehyde using SOF, showing observed and calculated spectra and the difference between these (residual). The main features here correspond to CH<sub>4</sub> and H<sub>2</sub>O and other abundant species in the atmosphere.

In addition, to the SOF-IR system, a modified SOF system was employed extensively during both campaigns based on measuring solar spectra in the ultraviolet spectral region. Solar light from a solar tracker was here focused on the entrance hole of an integrating sphere, which was connected to a custom built UV spectrometer. The measurements, unfortunately, were too noisy for obtaining formaldehyde, since the Fraunhofer structures of the sun were not cancelled out adequately. We suspect that the problem was caused by an unstable spectrometer.

In Figure 6.1300.7 columns of formaldehyde are shown measured inside the plume of a burning grass field. Measurements conducted in the centre respectively outside of the plume are shown and clearly indicate elevated H<sub>2</sub>CO in the plume. A similar picture was obtained for CO, indicating a HCHO/CO ratio of 0.05. The plume originated from a grass field of about 100 times 100 meters, with about one fourth of the area actually burning. The wind speed at ground level was about 2-4 m/s. A rough estimate of the emissions from the burning grassland is therefore that 1 mg/m<sup>2</sup> s of HCHO is released and 20 mg/m<sup>2</sup> s of CO, respectively). Assuming that the grass burns for 5 minutes yields a total emission of 3 kg/ha HCHO.

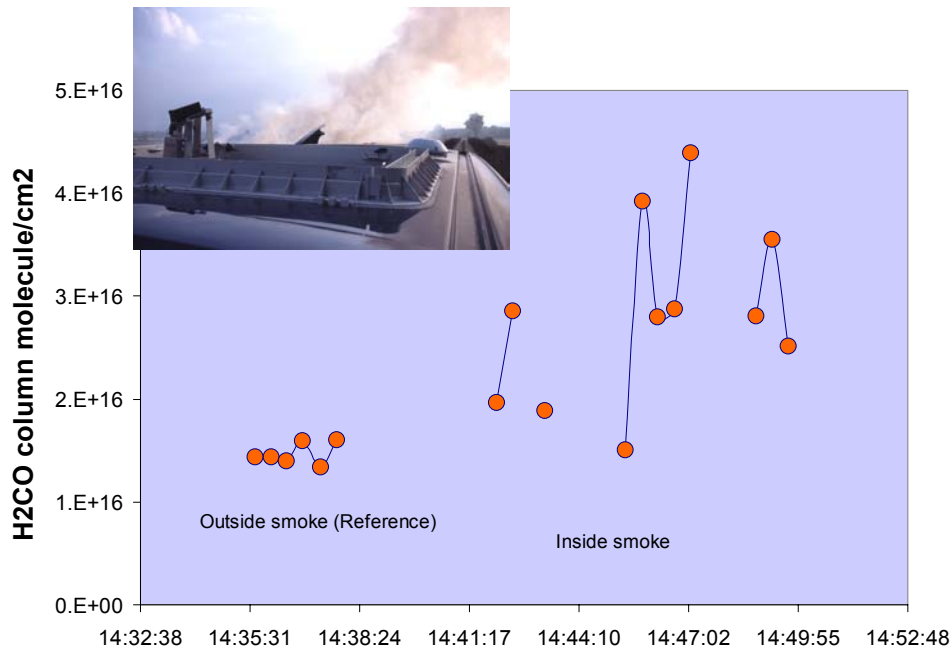


Figure 6.1300.7. Columns of formaldehyde retrieved in the plume of burning grassland using SOF.

In Figure 6.1300.8 all data taken during 2003 are shown, together with indications for the altitude and whether the data were taken standing still at Bresso airport, or moving around. It is obvious that most high altitude measurements yield low values, around  $5 \cdot 10^{15}$  molecules/cm<sup>2</sup> while most other measurements varies between  $1-2 \cdot 10^{16}$  molecules/cm<sup>2</sup>, this difference corresponds to about 4 ppb HCHO over 1 km. In Figure 6.1300.9 all measurements taken at Bresso, and their average, are shown versus hour of day. Measurements were taken both within and outside the "golden week" September 16-22, when the columns of formaldehyde were the highest. The data indicates that the values are already maximum between 9-10 in the morning and tend to decrease after 16. In Figure 6.1300.10 a latitudinal traverse is shown, starting from Bresso airfield and then moving to the mountains towards the north and then back.

Note that formaldehyde is very difficult to retrieve from solar spectra, considering the limited resolution of the instrument and that our data are the first of its kind. Further quality analysis is therefore needed to understand the uncertainty of these values.

Section 6: Detailed report related to overall project duration

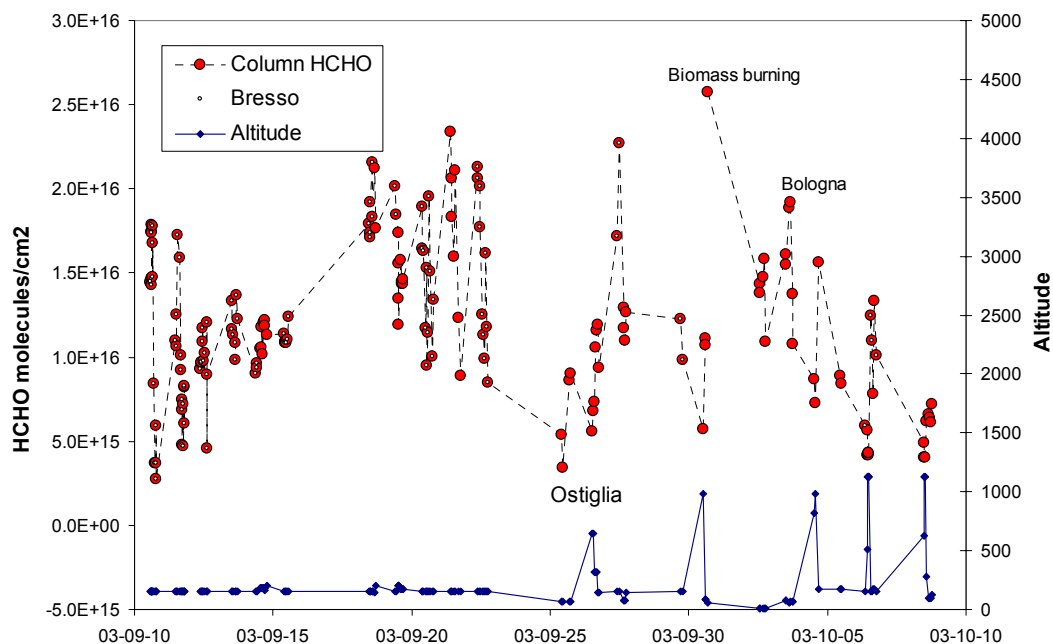


Figure 6.1300.8. The columns of HCHO for the whole measurement period taken on several locations in the Po valley. The altitude of the measurements is shown together with an indication when measurements were conducted at the Bresso airfield.

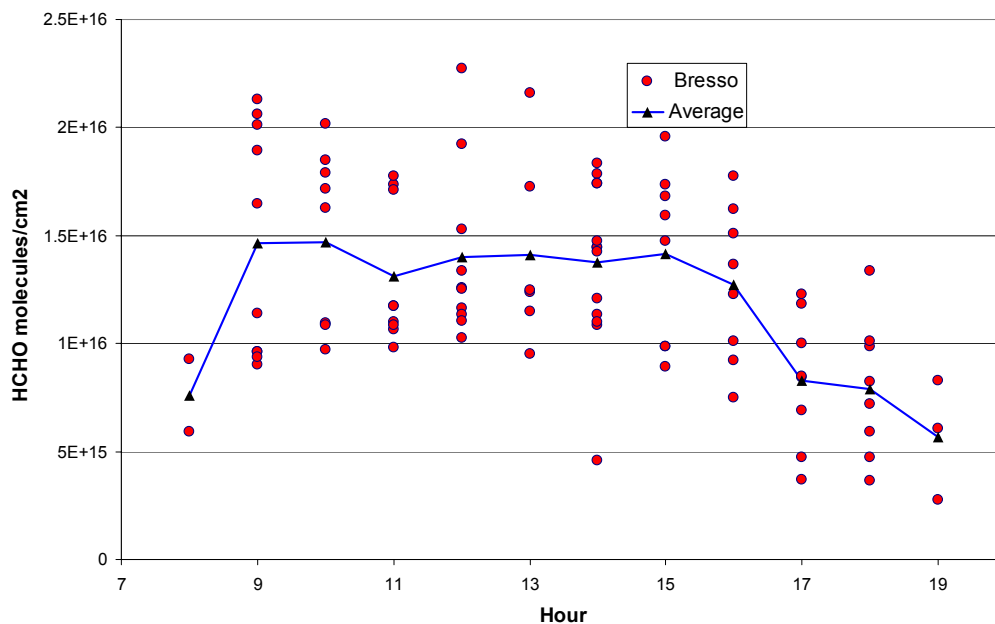


Figure 6.1300.9. Average formaldehyde evolution above Bresso on Sept 10, 11, 12, 13, 14, 15, 18, 19, 20, 22, 27, 29 and October 06. The measurements were started after the peak in the emission, occurring in the early morning and it seems as if the HCHO has already peaked at between 9 and 10 in the morning. The column at Bresso is on the average  $1.4 \cdot 10^{16}$  molecules/cm<sup>2</sup> which is around  $9 \cdot 10^{15}$  molecules/cm<sup>2</sup> above background with a 50% variation. This column corresponds to about 4 ppb HCHO over one km.

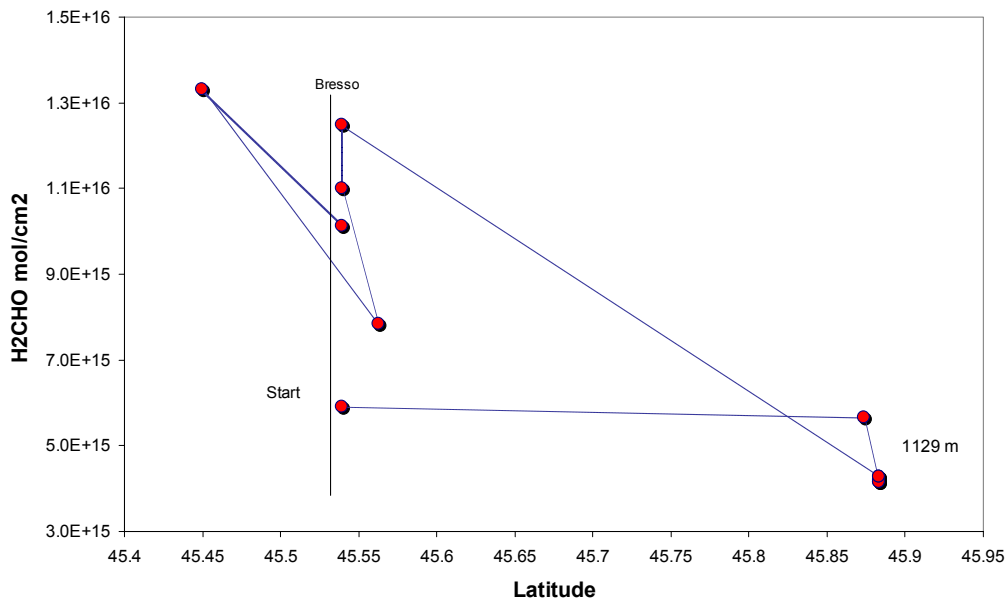


Figure 6.1300.10. Latitudinal difference in HCHO columns on October 6 measured by the SOF. The lines indicate sequential points versus time and the first measurement were conducted at Bresso airfield.

## WP 1400: Intercomparison of measurement techniques

The first FORMAT campaign in July/August 2002 was subdivided into two periods. The first addressed the comparison of measurement methods, the second phase concentrated on air chemistry measurements. The comparison of in-situ measurements was performed at Bresso, the intercomparison measurements of MAX-DOAS instruments took place at Alzate.

### 1. Intercomparison of in-situ measurements

One of the objectives of the FORMAT project was an intercomparison of the different techniques that are available for the measurement of formaldehyde. Previous intercomparisons revealed that there was still significant disagreement among the techniques used. However, there was no general pattern in the deviations that could explain the results.

Between 23 and 31 July 2002 eight instruments using four different techniques (see Table 6.1400.1) were operated at the urban site of Bresso. It was made sure that all instruments probed the same air mass by using only point measurement methods. This also applies to the White systems, used for the optical methods DOAS and FTIR. In contrast to long path integrating optical methods which average horizontally and vertically, they measure the absorption of trace gases within a very confined area of a few metres. During the intercomparison week, the CH<sub>2</sub>O mixing ratios varied between 1 and 13 ppbv.

Table 6.1400.1: Overview of the instruments used.

Instrument	Institute	Time period of operation	D.L. [ppbv]	Accuracy	Precision	Time res. [min]

## Section 6: Detailed report related to overall project duration

DOAS White system	IUP	24/07-19/08	0.9	±6%	0.45 ppbv	1-2
FTIR White system	CTH	22/07-18/08	0.4	6-27%	0.2 ppbv	5
Hantzsch AL4021	PSI	23/07-26/07	0.15	±15%	±10%	~1.5
Hantzsch AL4001	BUW	24/07-31/07	0.15	±15%	±10%	~1.5
Hantzsch AL4021	IFU	24/07-17/08	0.15	±15%	±10%	~1.5
DNPH (HPLC)	JRC	23/07-18/08	0.5	±10%	0.1 ppbv	120

Two methods were applied for the intercomparison of the measurement results. Firstly, an orthogonal regression analysis [Press et al., 1992; Riggs et al., 1978] was performed, comparing the individual results of all instrument pairs with each other. The correlation analysis showed a very good agreement among the Hantzsch results, however the slopes and intercepts from the regression analysis revealed some systematic differences. The optical techniques showed larger scattering. The second method was the analysis of fractional differences  $\delta$ , i.e. the difference between the results of each instrument and an (arbitrarily chosen) reference instrument according to  $\delta = ([\text{CH}_2\text{O}]_{\text{instr.}} - [\text{CH}_2\text{O}]_{\text{ref.}}) / [\text{CH}_2\text{O}]_{\text{ref.}}$ . Because of its long and continuous time series, the BUW Hantzsch results were chosen as the reference. Figure 6.1400.1 depicts the results of the fractional difference analysis. The nearly collocation of mode, median and average for most distribution suggests symmetry in the distributions and therefore mostly random differences. In summary, a ±11% agreement was found among the Hantzsch results. The observed discrepancies were partly attributed to different calibration standards. The agreement of the two optical methods was within 5%, which is within the uncertainties of the UV and IR absorption cross-sections (both 5%). Hantzsch and spectroscopic techniques agreed within 15%. DNPH results were generally lower than the measurements of the continuous techniques by up to 25%. A more detailed description of the methods as well as the discussion of the problems and the uncertainties of the Hantzsch and the optical methods can be found in [Hak et al., 2005].

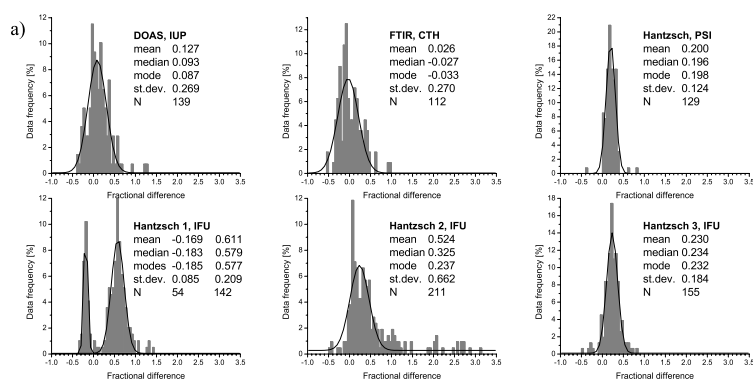


Figure 6.1400.1. Fractional difference histograms for each of the formaldehyde instruments calculated relative to the reference instrument Hantzsch BUW. Each panel shows the frequency for the data falling into 0.05 fractional difference bins.

## 2. Intercomparison with MAX-DOAS measurements

Here we show an intercomparison between IUP Bremen MAX-DOAS, IUP Heidelberg Long-Path DOAS, and IFU Hantzsch observations of Formaldehyde. The following figure gives an overview for both campaigns.

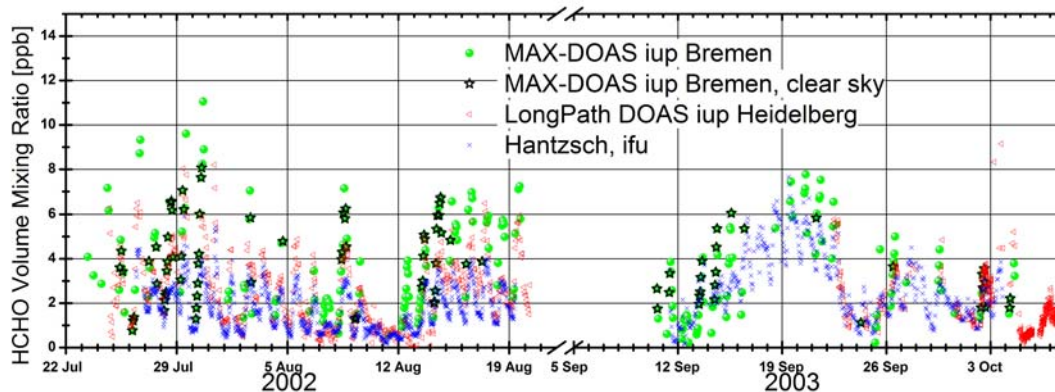


Figure 6.1400.2 Intercomparison plot showing data of a Hantzsch and a LPDOAS instrument in contrast to the HCHO mixing ratio derived using BREAM for an atmospheric bottom layer of 150 m height from the MAX-DOAS analysis. A more detailed description is available in Heckel et al., 2005 and Wittrock et al., 2005.

Most results of the intercomparison have been described in more detail in the following report, available from the lead author: Gaia Pinardi and Michel Van Roozendael: Inter-comparison of HCHO slant column measurements performed by BIRA-IASB and IUP-Bremen during the FORMAT campaign 2002 in Alzate, Belgian Institute for Space Aeronomy (BIRA-IASB) report.

### 3. Intercomparison of LP-DOAS measurements

During the autumn campaign in Alzate (13/09/2003-07/10/2003) two LP-DOAS instruments, from the University of Heidelberg and the Norwegian Institute for Air Research (NILU), have been operated in parallel. The systems have been described before. Here, we show a comparison between estimated concentrations of HCHO as well as SO<sub>2</sub>, NO<sub>2</sub> and O<sub>3</sub>. The data are from the second half of the campaign with relatively low HCHO values typical for autumn conditions with low to moderate pollution. Figure 6.1400.3 shows results retrieved from the U-Heidelberg LP-DOAS (in black) and from the NILU LP-DOAS (in red). Whereas NILU's LP-DOAS results for SO<sub>2</sub>, NO<sub>2</sub> and ozone agree well with those extracted from the U-Heidelberg LP-DOAS, it can be seen that the HCHO level are most of the time overestimated.

Section 6: Detailed report related to overall project duration

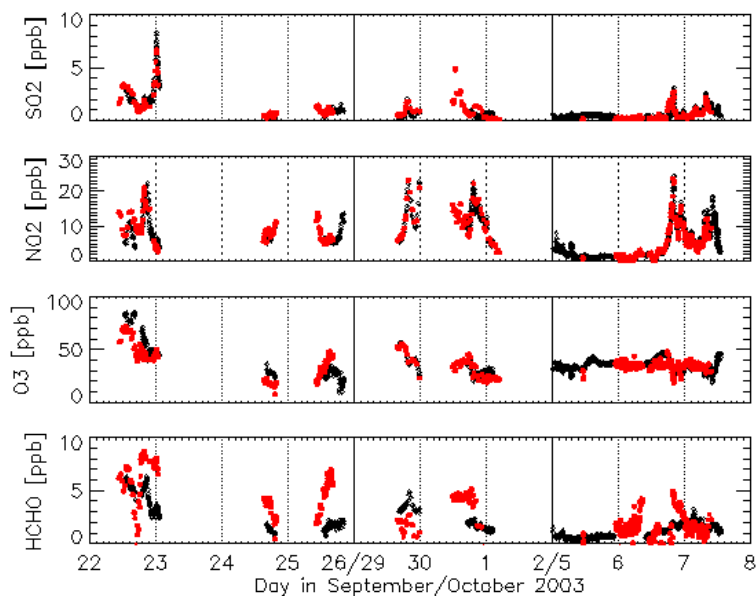


Figure 6.1400.3: Trace gas concentrations measured by LP-DOAS during the Alzate 2003 campaign. The values retrieved from the U-Heidelberg LP-DOAS are shown as black symbols, the values in red are retrieved from NILU's LP-DOAS observations.

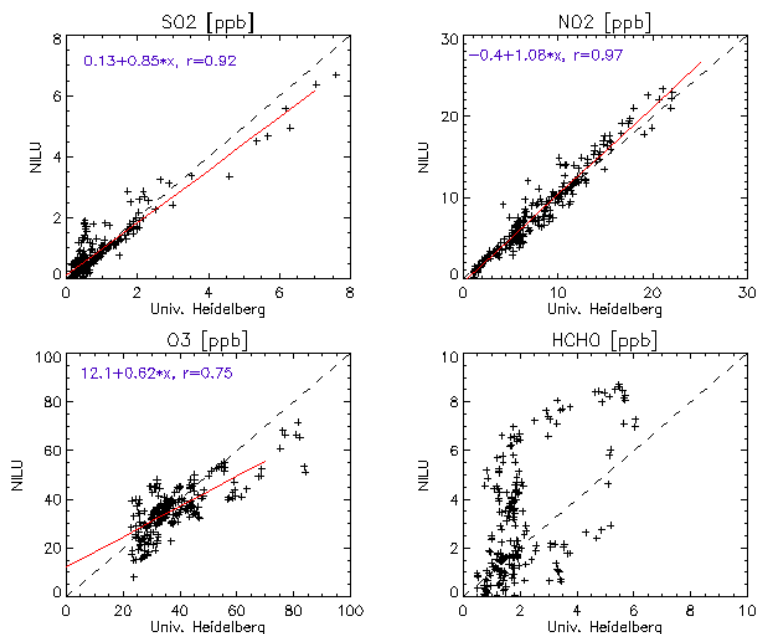


Figure 6. 1400.4: Correlation between the trace gas concentrations obtained during autumn 2003 campaign in Alzate with the LP-DOAS from University Heidelberg and NILU.

Figure 6.1400.4 shows linear correlations between the results from the LP-DOAS from University Heidelberg and LP-DOAS from NILU. Similar cross-sections have been used for the analysis.

NILU's LP-DOAS data have been averaged over three spectra (with measurement times 25 and 1000 s, depending on signal intensity) and have been compared to an average of measurements taken with the Heidelberg LP-DOAS with no more time difference than 10 minutes. Figure 6.1400.4 confirms the picture already seen in Figure 6.1400.3. The agreement is best for SO<sub>2</sub> and NO<sub>2</sub> and worst for HCHO. Unfortunately, no simultaneous data are available from the first period of the campaign, where higher HCHO concentrations occurred. For those days, we would expect a better agreement between the instruments, in particular for HCHO. The unrealistic high HCHO values derived from NILU's LP-DOAS measurements are a result of spectral fits with low quality. Instrumentally produced spikes located close to HCHO absorption bands, which not in all cases could be removed, led to an offset in the estimated trace gas concentration. An instrumental upgrade of the NILU LP-DOAS, making it more stable, mechanically as well as optically, would improve the results.

## References

Hak, C., Pundt, I., Trick, S., Kern, C., Platt, U., Dommen, J., Ordóñez, C., Prévôt, A.S.H., Junkermann, W., Astorga-Lloréns, C., Larsen, B.R., Mellqvist, J., Strandberg, A., Yu, Y., Galle, B., Kleffmann, J., Lörzer, J.C., Braathen, G.O. and Volkamer, R., Intercomparison of four different in-situ techniques for ambient formaldehyde measurements in urban air, *Atmos. Chem. Phys. Discuss.*, 5, 1-49, 2005.

Heckel, A., A. Richter, T. Tarsu, F. Wittrock, C. Hak, I. Pundt, W. Junkermann, and J. P. Burrows, MAX-DOAS measurements of formaldehyde in the Po-Valley, *Atmos. Chem. Phys.*, 5, 909–918, 2005

Press, W.H., Teukolsky, S.A., Vetterling, W.T., and Flannery, B.P.: *Straight-Line Data with Errors in Both Coordinates*. In: *Numerical Recipes in C, The Art of Scientific Computing*, Cambridge University Press, 1992.

Riggs, D.S., Guarnieri, J.A., and Addelman, S.: Fitting straight lines when both variables are subject to error, *Life Sciences*, 22, 1305-1360, 1978.

Rodgers, C. D. "Characterization and error analysis of pro\_les retrieved from remote sounding measurements", *J. Geophys. Res.*, 95, D5, 5587-5595, (1990)

Rožanov, A., Rožanov, V. V., and Burrows, J. P.: A numerical radiative transfer model for a spherical planetary atmosphere: combined differential-integral approach involving the Picard iterative approximation, *Journal of Quantitative Spectroscopy and Radiative Transfer*, 69, 491, 2001

Wagner, T., C.v.Friedeburg, M. Wenig, C.Otten and U. Platt, "UV-visible observations of atmospheric O<sub>4</sub> absorptions using direct moonlight and zenith-scattered sunlight for clear-sky and cloudy sky conditions", *Journal of Geophysical Research*, Vol. 107, No. D20, pp 4424, 2002

Wagner, T., B. Dix, C.v. Friedeburg, U. Frieß, S. Sanghavi, R. Sinreich, and U. Platt MAX-DOAS O<sub>4</sub> measurements – a new technique to derive information on atmospheric aerosols. (I) Principles and information content, *J. Geophys. Res.*, 109, D22205, doi:10.1029/2004JD004904, 2004

Wittrock, F., H. Oetjen, A. Richter, S. Fietkau, T. Medeke, A. Rožanov, and J. P. Burrows, MAX-DOAS measurements of atmospheric trace gases in Ny-Ålesund, *Atmos. Chem. Phys.*, 4, 955-966, 2004

Wittrock, F. et al., Retrieval of trace gas profiles from MAX-DOAS observations, manuscript in preparation for ACPD, 2005.

## **WP 2000 Airborne measurements and intercomparison of formaldehyde**

To obtain the desired information about the vertical and horizontal distribution airborne investigations have been carried out during both campaigns. Two different measurement techniques were used onboard three aircraft. The two measurement techniques are the Hantzsch *in-situ* technique (see also WP 1000) and the AMAX-DOAS (WP 2000). The latter technique applies a UV-VIS spectrometer, which measures the solar light coming from 8-10 different directions above and below the aircraft. This new technique is similar to commonly used DOAS techniques, e.g. from satellites (GOME, SCIAMACHY) or the ground (Zenith-sky-DOAS, MAX-DOAS, WP 1200). AMAX-DOAS is the only instrument which provides two-dimensional cross sections of HCHO below the flight altitude: tropospheric and total atmospheric columns as well as vertical profiles can be derived. It thus constitutes an excellent link between *in-situ* observations and remote sensing (in particular satellite) instruments.

On the one hand, the 3D distributions measured by the *in-situ* instruments will help to establish and improve the new AMAX-DOAS technique, on the other hand the comparison between the techniques will serve to improve both methods in the future. During comparison flights three aircraft were operated simultaneously in order to probe the same air mass, e.g. the AMAX-DOAS above the boundary layer (BL) and the *in-situ* instruments inside the BL. In this case, the *in-situ* instrumentation scanned the vertical profile while the AMAX-DOAS measures the whole column and profile from ground level up to the flight altitude simultaneously. In WP 2400, radiative transfer calculations were made to compile air mass factors for the AMAX-DOAS and also the MAX-DOAS technique.

### **WP 2100: Airborne measurements with Hantzsch**

Two different aircraft were used carrying Hantzsch monitors. The aircraft used were a DIMONA motorised glider operated by MetAir, Switzerland (in 2003 only) and a microlight operated during both campaigns by partner 3, FZK, IMK-IFU, Garmisch-Partenkirchen (Junkermann, 2001, Junkermann, 2005). Both aircraft belong to the category of 'Small Environmental Research aircraft' of the EUFAR Fleet. In ([WWW.EUFAR.NET](http://WWW.EUFAR.NET)) a detailed description of the aircraft and their capabilities can be found. The instruments on both aircraft were identical and are described in detail in Junkermann and Burger (2005). The detection limit is ~ 50 ppt with a delay time of 90 seconds. This time resolution is still sufficient to investigate vertical distributions. The horizontal resolution with a speed of 20 m/sec for the microlight and 40 m/sec for the DIMONA allows a resolution of about 2 and 4 km, respectively.



*Fig. 6.2100.1: The Hantzsch HCHO monitor in the instrument pod of the microlight aircraft D-MIFU including liquid containers for 6 hours of operation.*

The DIMONA is additionally equipped for air chemistry research while the additional microlight instrumentation is compiled for aerosol and radiation studies. The data results of the Dimona and some of the additional data from the microlight are contained in section WP 3000 and WP 3200.

#### **A) Microlight aircraft flights**

The slow microlight is especially used for vertical profiles and regional studies. The operation area in 2002 was mainly the northern part of the metropolitan area of Milano between Milano, Lecco and Como with a main focus on the vertical distribution in the area between Lecco and Como. On two days flights were extended further to the south on the eastern leg around Milano. In 2003, the operation basis was changed to Spessa and the flight tracks always included a full circle around Milano plus vertical profiles north (Lecco and Como) and south (Stradella) of Milano.

Fig. 6.2100.2 shows the aircraft map including controlled airspaces (international Airports) and airspace limitations.



Fig. 6.2100.2, Airspace of the research area, with airfields indicated. The areas marked in orange are the terminal control zones of the bigger airports of Milano Linate, Milano Malpensa, Bergamo and Piacenza. Also shown are motorways, rivers and settlements. In the area between the dotted lines north and south of Milano, the airspace allowed to operate with small aircraft under visual flight rules is restricted to 2000 ft (~ 600 m) above sea level. Vertical profiles are allowed in the north up to 9000 ft (~ 2700 m) and in the south up to 3500 ft (~ 1200 m). Above this altitude Instrumental Flying Rules, the respective equipment and detailed very stringent flight plans are mandatory. The Dimona and the microlight are not allowed within this airspace.

### WP 2110 Summer campaign

The operational basis for the microlight during the summer campaign was Lecco Monte Marenzo, a small airfield 10 km south of Lecco. Flight dates and hours with altogether about 30 flight hours are given in Table 6.2100.1.

29.07	09:12	11:31
31.07	09:13	11:25
04.08	10:16	12:04
05.08	09:16	12:18
08.08	11:28	14:51
13.08	12:48	16:32
14.08	11:57	14:31
15.08	09:41	13:40
16.08	11:55	13:32
17.08	11:24	14:07
18.08	08:39	11:02

*Table 6.2100.1 Flight dates and hours of the microlight in 2002*

Meteorological conditions during 2002 were dominated by convective processes with cumulus cloud development between about 1000 and 3000 m and a few days with foehn conditions. Foehn conditions are not suitable for the microlight aircraft and no flight was performed during these situations. During the other days, cumulus clouds grew up mainly above the first mountain ridge north of Milano, the area where vertical profiles are allowed up to 2700 m, see Fig. 6.2100.2. Cloud tops often extended above 3000 m. Only occasionally under visual flight rules the free troposphere could be reached but could not be probed more intensively as further climbing was prohibited. Data on the free troposphere mixing ratios thus could not be obtained during this campaign. The convective activity transports pollution from the planetary boundary layer into higher elevations. The typical pattern is a slight reduction of the pollution levels in a fairly well mixed boundary layer reaching up to 1000 to 1200 masl. This is also the height of the cloud base. Above this initiated by cloud venting pollution, aerosols and trace gases are transported into a second layer between cloud base and approximately 3000 m. Within this layer the pollutant concentrations steadily decrease from bottom to top as long as no cumulonimbus cloud develops. A detailed description of the processes of cloud venting and redistribution of pollutants can for example be found in Cotton et al, (1995). In the vicinity of Milano most probably two effects are superimposed, the local small scale transport phenomena associated with thermal convection and the effects of an urban heat island (<http://www.actionbioscience.org/environment/voogt.html>) Crutzen, (2004). That can lead to a horizontal redistribution or advection of pollution in higher elevations.

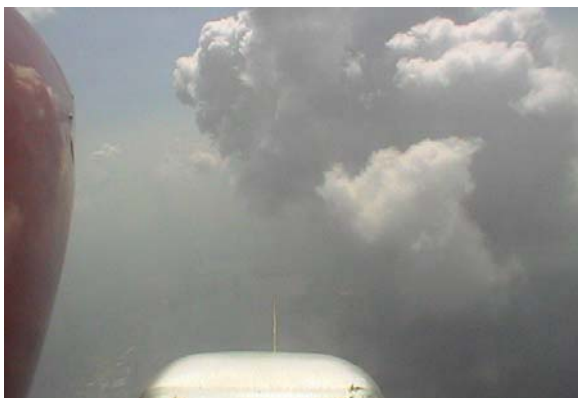


Fig. 6.2100.3, Convective clouds above the north of the research area in 2002.

Fig. 6.2100.4 shows the vertical distribution of small and large aerosols, the potential temperature and the HCHO vertical distribution on August 17 between Lecco and Como. The brown colour in the formaldehyde graphic indicates the horizontal variability in low level below 600 m in the area north of Milano. The HCHO in the profile above Lecco is higher than above Como, although in the flat area close to the main motorway between Milano and the Swiss border at Como/Chiasso on the average 20% more HCHO is measured than above the eastern part of the area. In the graph for the large particles also the potential temperature (outside the clouds) is indicated. The slope of this curve indicates that there is no vertical mixing likely above 600 m and no mixing possible above 1200 m. Nevertheless some HCHO is found up to 2700 m. The particle concentration of the small particles supports that there was no mixing between 600 m and 1200 m and the big increase in mid elevations is most probably the result of horizontal advection processes.

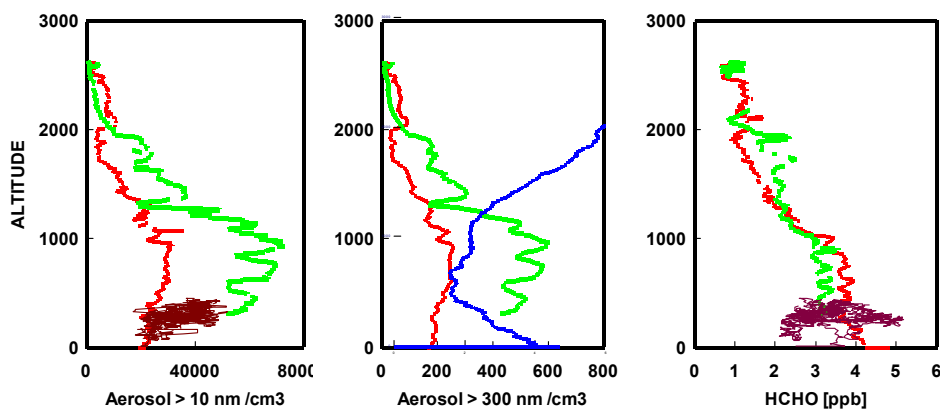


Fig. 6.2100.4, Concentrations of small and large particles and formaldehyde north of Milano on August 17, 2002. The colours indicate the ascent at Lecco (red), the descent above Como (green) and the data during the horizontal flight pattern between Como, Milano and Lecco (brown). The blue line in the middle graph is the potential temperature.

## WP 2120 Winter campaign

The operational basis for the microlight was changed to Spessa for the winter campaign. The advantages of Spessa were the collocation with a ground site, and the more stable weather conditions in the southern part of the Po Valley. With convective conditions in the mountain areas

Section 6: Detailed report related to overall project duration

of Lecco Monte Marenzo the danger of thunderstorms or severe showers increases within the afternoon making flight planning especially in the afternoon more difficult. A picture of the site in Spessa is given in section WP 1000 (ground measurements). The flight dates and hours for the 2003 campaign, altogether 34 hours, are given in Table 6.2100.2.

16.09	10:56	12:48
18.09	10:28	13:48
19.09	11:00	14:28
20.09	09:00	09:58
20.09	10:45	13:10
21.09	10:25	13:33
22.09	10:20	13:32
25.09	12:00	15:05
26.09	09:11	11:28
26.09	13:15	16:36
27.09	10:12	13:47
30.09	11:20	13:54
04.10	12:08	12:56

Table 6.2100.2 Flight dates and hours of the microlight D-MIFU in 2003.

Meteorological conditions in the 2003 campaign were simpler than in 2002. In most cases, especially in the second and third week of the campaign no severe convection cloud production was observed. The lower atmosphere was in a stable stratified condition with a heavily polluted but not always well-mixed layer up to 1200 to 1500 m (see also WP 3200). Accordingly most of the particles and most of the formaldehyde were found in the lowest 1200 m. Fig. 6.2100.5 shows an example for a flight track in 2003 with a complete circle around Milano avoiding the control zone of Linate and with profile measurements north and south of Milano. During the return track a biomass burning plume was passed for about 12 seconds.

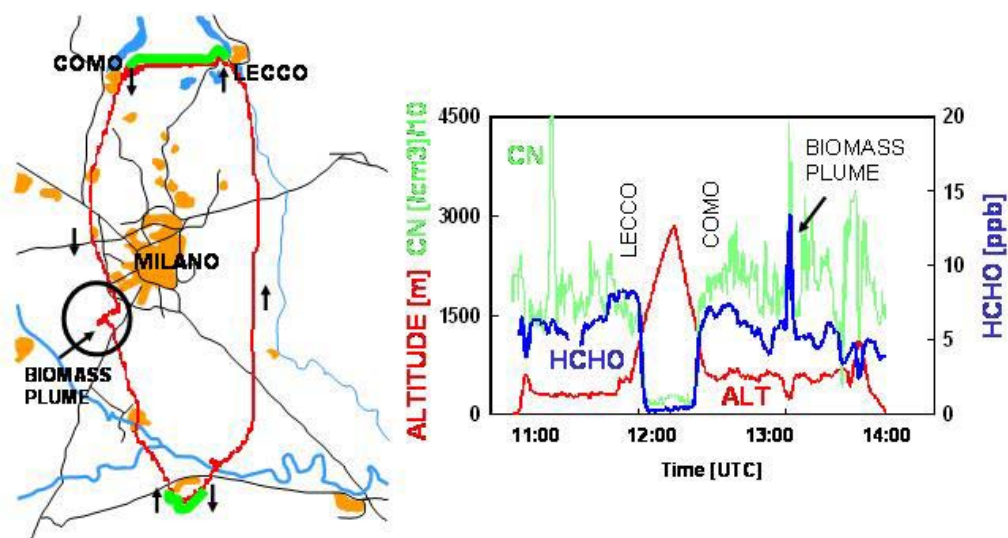
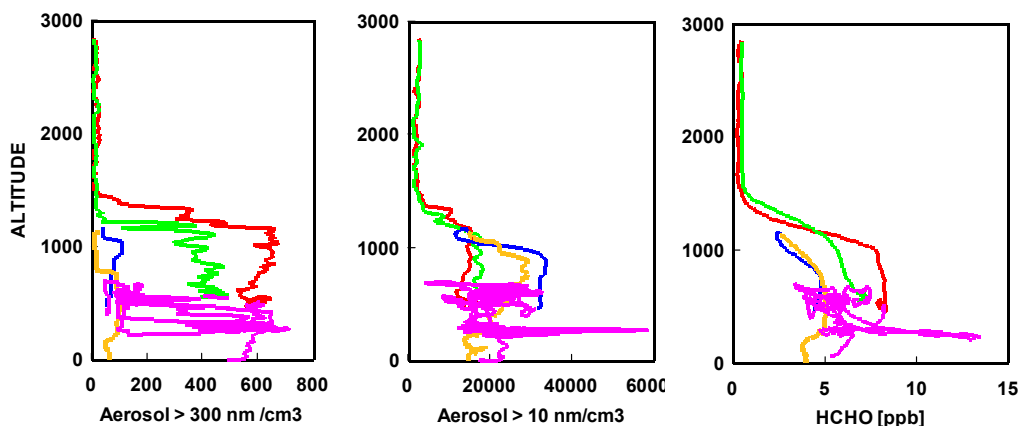


Fig. 6.2100.5: Flight track from Spessa via Lecco, Como and back to Spessa with ascent and descent at Lecco and Como (marked by arrows). The green line marks flight levels above 600 m.

*The right side of the graphic shows the corresponding HCHO and particle mixing ratios. A biomass plume was passed on the return from Como to Spessa.*

The corresponding vertical distributions of small and large particles and of HCHO are given in Fig. 6.2100.6. Red and green are the profiles in the north, yellow and blue in the south. An interesting feature during this flight is that mainly large particles (> 300 nm) were found in the north, whereas in the south there were mainly small particles. These particles often correlate to the biomass burning plumes that were also identified as a source of HCHO. In this case, HCHO levels are higher in the north despite the high fire frequency in the south at that particular day.



*Fig. 6.2100.6. Vertical distributions of large particles (> 300 nm), small particles (sum of all particles > 10 nm) and HCHO in ppb. red (Lecco), green (Como), yellow and blue (Stradella), pink variability during the horizontal fraction of the flight. The absolute maxima are correlated with a biomass burning plume passage.*

The two HCHO profiles in the north differ in the planetary boundary layer by about 25% with higher mixing ratios in the Lecco area.

### **B) Dimona aircraft flights:**

The Dimona aircraft performed 13 flights during the 2003 FORMAT campaign. Figure 6.2100.7 shows the vertical distribution of HCHO over the Po Basin measured during 9 afternoon flights, including flights around the agglomeration of Milano as well as flights to the east of the Po Basin. Most of the HCHO amounts are accumulated within the lowest 1800 m for most of the flights.

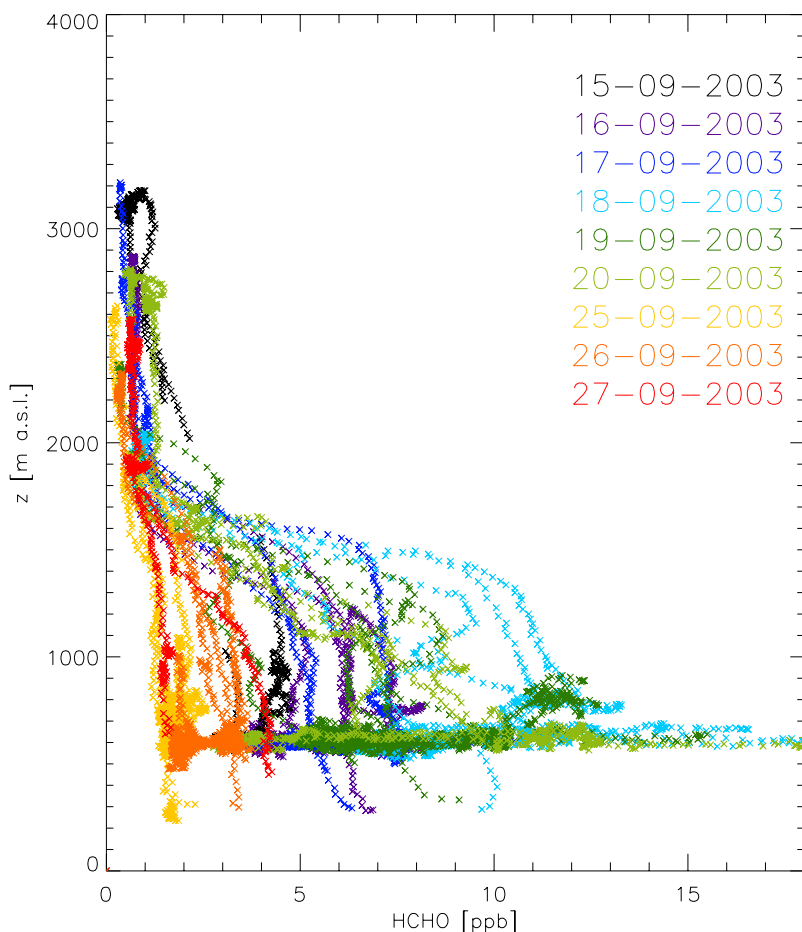


Figure 6.2100.7: Vertical profiles of HCHO (10-second average concentrations) around Milano on 9 afternoon flights in September 2003.

During box flights, the Dimona flew around the agglomeration of Milano to assess the ambient concentrations (at around 500-800 m altitude a.s.l.) of HCHO and other species upwind and downwind of Milano. Due to the prevailing southerly wind direction during the day, higher HCHO concentrations were generally measured downwind (North,  $\sim 45.7^\circ\text{N}$ ) than upwind (South,  $45.2^\circ\text{N}$ ) of the Milano metropolitan area during the afternoons, as seen in Table 6.2100.3 and Figure 6.2100.8. Low HCHO concentrations are observed north of  $45.8^\circ\text{N}$  (see figure) as the aircraft had to fly at an altitude higher than 1000 m over that area due to the presence of the Alpine Crest.

Table 6.2100.3: Average measured concentrations of HCHO (in ppb) north and south of Milano on afternoon flights in September 2003.

	15-Sep	16-Sep	17-Sep	18-Sep	19-Sep
South	3	4	4.8	8	6.7

North	4.35	7.2	7.5	12.8	11.4
-------	------	-----	-----	------	------

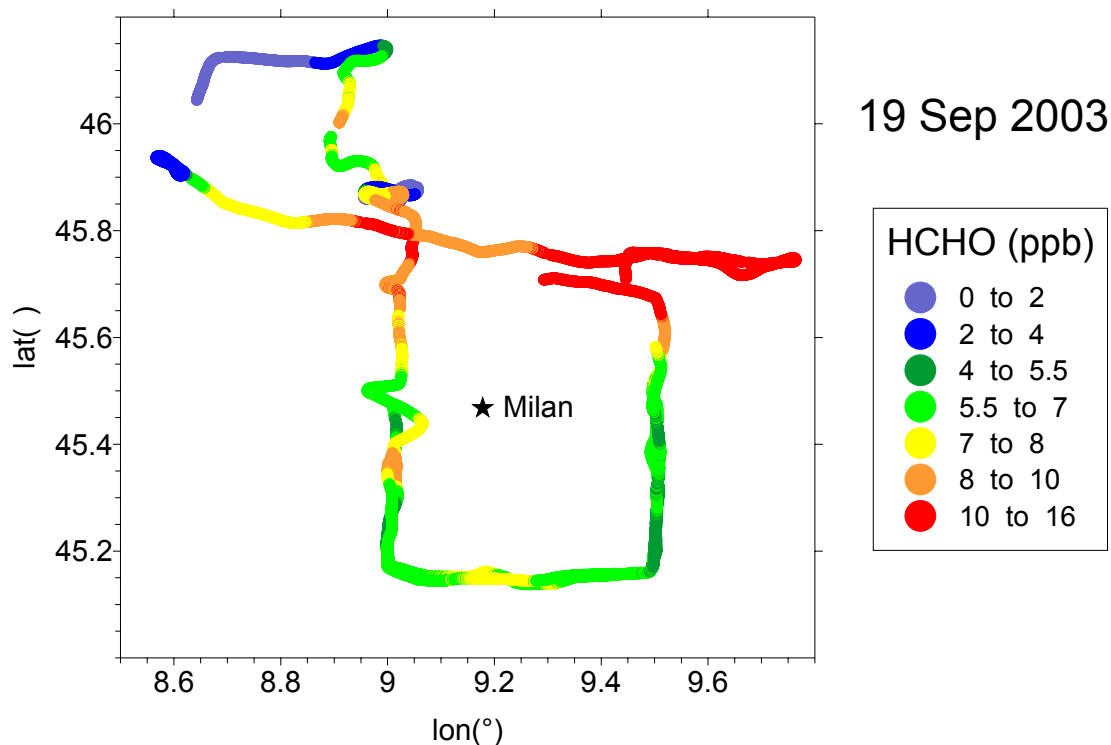


Figure 6.2100.8: HCHO concentrations measured during an afternoon flight on 19 Sep 2003.

## References

- Crutzen, P. J. New Directions: The growing urban heat and pollution island effect-impact on chemistry and climate, *Atmospheric Environment* 38: 3539–3540, 2004.
- Cotton, W.R., Alexander, G.D., Hertenstein, R., Walko, R.L., McAnelly, R.L., and Nicolls, M., Cloud venting – A review and some new global annual estimates, *Earth Science Reviews*, 39, 169-206, 1995.

## WP 2200: Airborne measurements with AMAX-DOAS

The aircraft measurements were conducted by partner 2 in co-operation with partner 4. In contrast to the two other aircraft, the AMAX DOAS (Air-borne Multi AXis Differential Optical Absorption Spectroscopy) was operated for the first time inside the planetary boundary layer. Therefore, we briefly explain its measurement principle/strategy during the two campaigns.

### The AMAX DOAS Instrument

Section 6: Detailed report related to overall project duration

The instrument comprises two separate grating spectrometers, one for the UV (300 to 440 nm) and one for the visible (400 to 570 nm). These are connected to 10 telescopes. Two fibre bundles transmit the light from the upper and lower window where the telescopes are mounted to the spectrographs. The fibre bundles are split to enable both spectrometers to be supplied with light. The detectors contain two-dimensional CCD arrays, which allow the simultaneous measurement of up to ten distinct spectra of different viewing angles. On the CCD, the light is dispersed in x-direction and the different spectra for the light from different fibres are separated in y-direction (with each spectrum covering about 20 lines of the CCD array). Thus, it is possible to measure the different spectra simultaneously using a similar instrumental transmission function. The measurements are automatically controlled by a PC, which also stores the data.

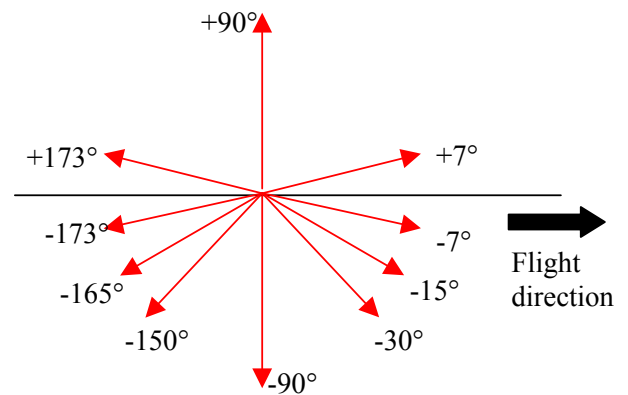
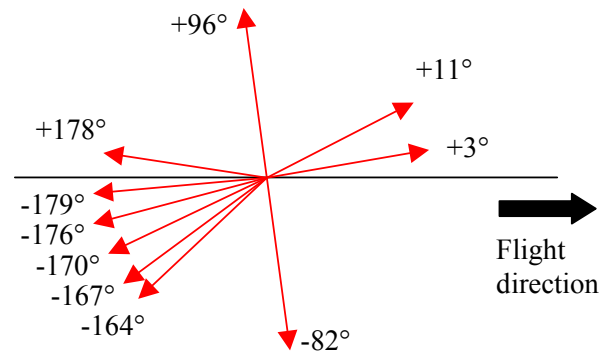


Figure 6.2200.1: Upper photo: The Partenavia aircraft and the two telescope boxes fixed above and below the aircraft, respectively, as used during the first campaign. Lower photo. Improved telescope box as used during the second campaign

Figure 6.2200.2: Telescope viewing directions. Upper panel: first campaign, Lower panel: second campaign (note that the angles are vertically stretched). Angles are relative to the flight direction.

During the first campaign, the configuration was as follows: a) four of the telescopes were pointed upwards at the angles,  $+2^\circ$ ,  $+84^\circ$  backward,  $+3^\circ$ ,  $+11^\circ$  forward relative to the horizontal and, b) six of the telescopes were pointed downwards ( $-1^\circ$ ,  $-4^\circ$ ,  $-10^\circ$ ,  $-13^\circ$ ,  $-16^\circ$  backward,  $-82^\circ$  forward). For the second campaign, the entrance optics of the instrument was slightly improved in order to adapt for boundary layer measurements (Figures 6.2200.1 and 6.2200.2).

**A) Flights**

Section 6: Detailed report related to overall project duration

During the first campaign, the aircraft was based at Lugano airport (Switzerland). From there, ten flights (of about two hours each) on nine days were performed in the Milano area. The table 6.2200.1 gives an overview on the flight times, tracks, types, working spectrometer, weather conditions, and the quality of the spectra.

No.	Date Time	Flighttrack	Type	Spectro -meter	Weather	Results
5	29 July 8:45-10:20	Alzate	Inter comp.	UV/Visible	very few clouds	Very Good
6	31 July 9:30-12:00	Pavia - Alzate	Inter comp.	UV/Visible	Some clouds at the beginning, rain during landing	Very Good
7	05 Aug. 9:12-10:48	Pavia - Alzate	Measur.	Visible (bad resolution)	Clear sky, clouds in the south Bad viewing conditions	Qualitatively good
8	12 Aug. 12:34-15:07	Pavia – Alzate	Measur.	Visible	Very few clouds, turbulences, Very clear viewing conditions	Good
9	13 Aug. 12:48-15:22	Pavia- Alzate	Measur.	Visible	No clouds, very clear viewing conditions – worse than the day before	Good
10	14 Aug. 10:05-11:37	U-round Milan	Measur.	Visible	Very few clouds, clear viewing conditions – worse than the day before	Good
11	14 Aug. 13:00-15:24	3 x Box around Milan	Measur.	Visible	Very few clouds, clear viewing conditions – as the flight before	Good
12	15 Aug. 10:54-13:26	Voghera-cross Milan	Measur.	Visible	Good viewing conditions, first large clouds develop, Large fire south east of Milano city	Good
13	16 Aug. 12:56-15:37	Box around + 1 cross over Milan	Measur.	Visible	Smog over Milano – some small clouds, larger ones in the south, many cirrus clouds above flight-level, not constant in time	Good
14	18 Aug. 10:13-11:55	Box around + 1 other cross-over Milano	Measur.	Visible	Smog over Milano – some small clouds in the south, more clouds in the north	Good

Table 6.2200.1: Flight times, -tracks, -types, working spectrometer, weather conditions, and quality of the spectra of the AMAXDOAS aircraft measurements. The first two flights were dedicated to the intercomparison with other instruments operating on ground or aircraft.

During the second campaign, the aircraft was based at Bresso airport in the northern part of Milano. From there, nine flights (of about two hours each) were performed in the Milano area and in the Po Basin. Table 6.2200.2 gives an overview on the flight times and tracks as well as on the weather conditions.

No	Date Time	Flight track	Type	Spectro meter	Weather conditions
----	-----------	--------------	------	---------------	--------------------

## Section 6: Detailed report related to overall project duration

1	14.09.03 11:10 -13:00	Bresso – Pavia – Cremona box (two times) – Power plant in Cremona box (two times) with a trajectory like a fish – Pavia – Bresso	Meas.	UV /Visible	No clouds / sunny
2	16.09.03 10:15 –12:15	Bresso – one box around Milano - three boxes around refinery in Sannazzaro(two times near refinery)	Meas.	UV /Visible	No clouds / sunny
3	17.09.03 10:30 –12:30	Bresso – one box around Milano – three boxes around refinery in Sannazzaro (two times near refinery)	Meas.	UV /Visible	No clouds / sunny
4	18.09.03 11:50 –13:50	Bresso – Pavia – Tavazzano – Cassano – Calusco – Como – Saronno – Rho – Alzate( two times box around Milan)	Meas.	UV /Visible	No clouds / sunny
5	19.09.03 12: 20 -14:30	Bresso – one small box around Rho – Saronno – Como – Calusco – Alzate (just flight in northern region)	Meas.	UV /Visible	No clouds / sunny
6	20.09.03 12:48 –15:22	Bresso– Voghera–Codogno – Calusco – Linate–Voghera – Saronno – Linate – Calusco – Saronno – Rho – Bresso (complicated trajectory of one box around Milano and crossing Milano Linate )	Meas.	UV /Visible	No clouds / sunny
7	25.09.03 13:00 –15:24	Bresso – Cremona – Mantova – Sermide – Intercomparison with Dimona	Meas.	UV /Visible	No clouds / sunny, strong NE wind in the afternoon
8	26.09.03 10:54 -13:26	Bresso – Cremona – box in Sermide – Porto Tolle. Profile intercomparison with Microlight.	Meas.	UV /Visible	No clouds / sunny
9	27.09.03 12:56 –15:37	Bresso – Cremona – Sermide – Porto Tolle. Intercomparison with SCIAMACHY	Meas.	UV /Visible	A little cloudy / sunny

Table 6.2200.2 Flight times and tracks as well as weather conditions of the AMAXDOAS aircraft measurements.

Flights were conducted only for almost cloud free conditions. During both campaigns, the speed of the aircraft was about 70 m/s, and one solar spectrum was taken every second kilometre. After each flight, tungsten lamp and HgCd lamp reference spectra were taken with each telescope.

### B) Spectral analysis algorithms

The retrieval of the atmospheric spectra was carried out using the WINDOAS software of IASB (Fayt and van Roozendaal, 2001) and the DOAS analysis technique. Several reference spectra of the trace gases which show structured absorptions in the respective wavelength regions were fitted to the logarithm of the measured spectrum using a non linear least squares algorithm. Absorption cross sections were taken from the literature and convoluted with the instrument's slit function, which varied only slightly from one flight to the next. The used literature cross sections are listed in Table 6.2200.3.

<u>Absorption cross section</u>	<u>Reference</u>
NO <sub>2</sub> (293K)	Voigt et al., 2002
HCHO	Meller and Moortgat, 2000
O <sub>3</sub> (293K) & O <sub>3</sub> (223K)	Voigt et al., 2001
O <sub>4</sub>	Greenblatt et al., 1990.
BrO (298K)	Wilmouth et al., 1999.

Table 6.2200.3 Cross sections used for the spectral analysis of HCHO.

The analysis procedure is as follows: Initially, the strong Fraunhofer structures of the measured spectra are removed using a solar reference spectrum taken at the standard flight altitude in a remote area. In contrast to satellite observations where the solar reference spectrum (direct sun light) contains no atmospheric absorption structures, the spectral analysis yields no absolute atmospheric slant column densities (SCD) but the difference in the column densities between the measurement and the solar reference spectrum, i.e. a differential SCD (DSCD). The fitting range is 323 - 368 nm. Apart from the absorption cross sections, a polynomial of third degree and a Ring correction spectrum are fitted. An intensity offset is allowed to be added in the fitting procedure. The Ring spectrum is calculated with the WINDOAS software and a highly resolved Fraunhofer spectrum.

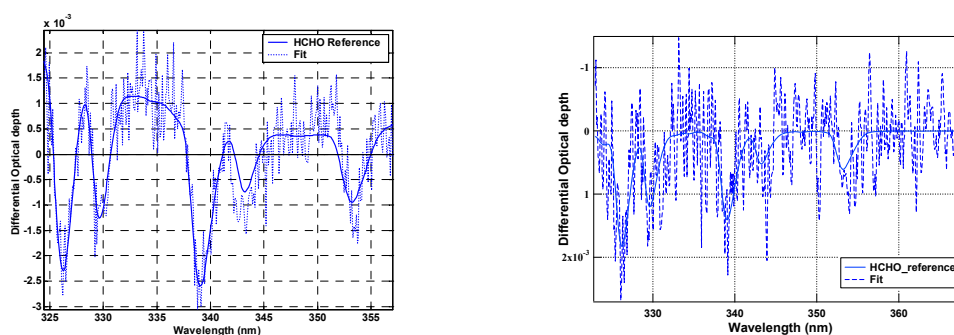


**Fig. 6.2200.3:** Left panel: HCHO DOAS fitting result for a spectrum taken with the UV spectrometer on 29 July 2002 Right panel: DOAS fitting result for a spectrum taken with the visible spectrometer on 16 August 2002. The laboratory spectra of HCHO (thick line) is fitted to the absorptions found in the solar spectrum (dashed line)

## References:

Greenblatt G. D., Orlando, J.J., Burkholder, J.B., and Ravishankara, A.R.: Absorption measurements of oxygen between 330 and 1140 nm, *J. Geophys. Res.*, 95, 18577-18582, 1990.

Meller, R. and G. K. Moortgat: Temperature dependence of the absorption cross sections of formaldehyde between 223 and 323 K in the wavelength range 225 - 375 nm, *J. Geophys. Res.*, 201 (D6), 7089 - 7101, 2000.

Fayt, C and van Roozendaal, M., WinDOAS 2.1., Software User Manual, 2001.

Voigt, S., J. Orphal, and J. P. Burrows, J.P.: The temperature- and pressure-dependence of the absorption cross-sections of NO<sub>2</sub> in the 250-800 nm region measured by Fourier-transform spectroscopy, *J. Photochem. and Photobiol.*, A, 149, 1-7, 2002.

Voigt, S., J. Orphal, K. Bogumil, and J.P. Burrows, J.P.: The temperature dependence (203-293 K) of the absorption cross sections of O<sub>3</sub> in the 230-850 nm region measured by Fourier-transform spectroscopy, *J. Photochem and Photobiol.*, A, 143, 1-9, 2001.

### C) Differential Slant Column results

**Figure 6.2200.4** shows HCHO and O<sub>4</sub> differential slant column densities from one flight performed on the 16 August 2002, as function of the geographic position for one downward looking telescope

(-4°). One square- and one triangle-formed flight track were flown in sequence, followed by a repetition of both tracks. The length of the square is approx. 40 km, and the centre of Milano is located inside the square. The wind direction was 135° (obtained by balloon soundings at Linate (45.43°N, 9.28°E, 103 masl), which was typical for the afternoon during the campaign. The high HCHO values measured at the North West side of the flight track and the city of Milano correspond well with what is expected from the wind direction. A few clouds were encountered only during the west-east transverse at the southern side of the flight track. The flight altitude was 1100 m above ground level during the entire flight. O<sub>4</sub> seems to be anticorrelated to HCHO. As can be seen also in Figure 6.2200.4, the lowest values are encountered in the northwest corner of the flight track. This can be explained by the very steep vertical profile of O<sub>4</sub> and the aerosol loads in the atmosphere: Most of O<sub>4</sub> is located very close to the surface and the vertical profile decreases exponentially with a scale height of approximately 4 km. With increasing aerosol load the sunlight is scattered in the upper layers of the plume, where the O<sub>4</sub> mixing ratio is low. Only in areas with low aerosol loads more light measured by the telescope, comes from the lower layers of the atmosphere. Low O<sub>4</sub> values therefore indicate high aerosol loads, in consistency with high aerosol loads which are expected in the Milano plume. The differences between high and low O<sub>4</sub> values decrease with increasing (downward) viewing angles (Figure 6.2200.5). At -82° viewing angle, the light comes from lower layers independent of the aerosol load in the atmosphere. For small viewing angles, O<sub>4</sub> depends strongly on the viewing angle. This yields to artefacts around the corners of the flight track, when the pitch and roll of the aircraft change tremendously.

Section 6: Detailed report related to overall project duration

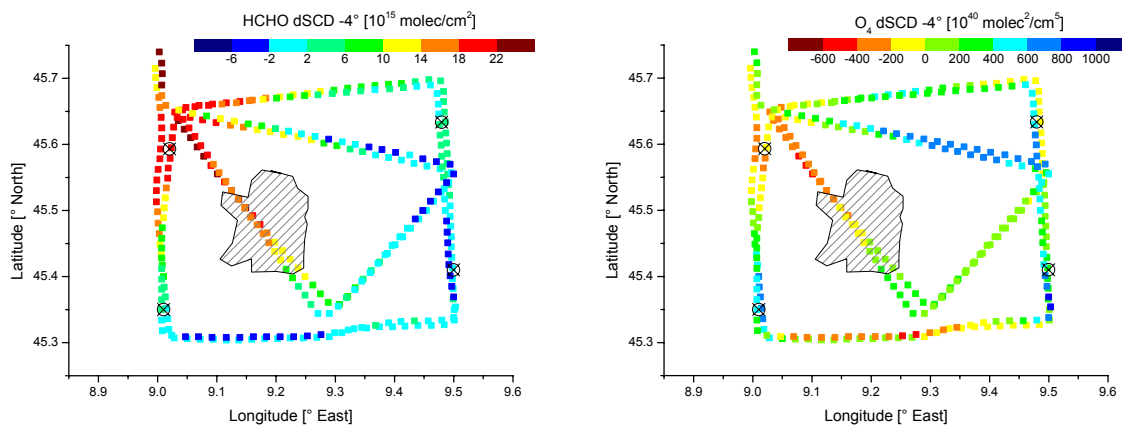


**Figure 6.2200.4** (left panel): HCHO differential slant column density as function of the flight track (geographic) position on 16 August 2002, measured with the telescope  $-4^\circ$ . (right panel): the same for  $O_4$ . The four studied locations Pavia (SW), Saronno (NW), Calusco (NE) and Codogno (SE) are marked by circles.

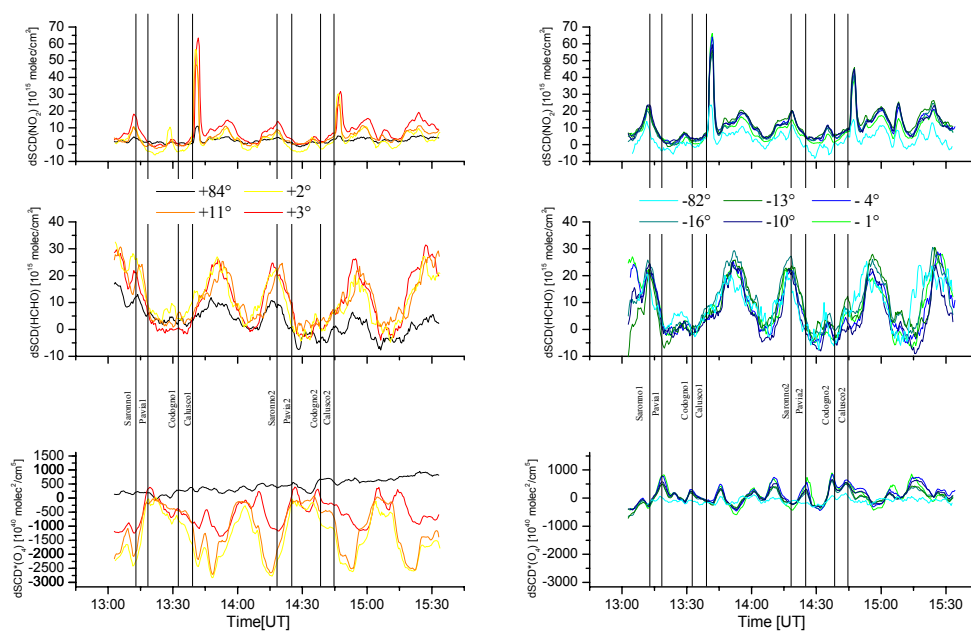


**Figure 6.2200.5:** DSCDs for  $NO_2$ ,  $HCHO$ , and  $O_4$  as a function of time for the measurements made by the ten telescopes on the 16 August 2002. Results of the four upward looking telescopes are shown in the left hand figures; results of the six downward looking telescopes are shown in the right hand figures. Four positions have been studied more in detail (they are marked by the vertical lines), each of them has been over flown twice. In the  $NO_2$ -series, two strong peaks at 1341 UT and 1447 UT are observed, which can be attributed to the cement works in Calusco. As expected, no  $HCHO$  peaks are observed here.

## Section 6: Detailed report related to overall project duration

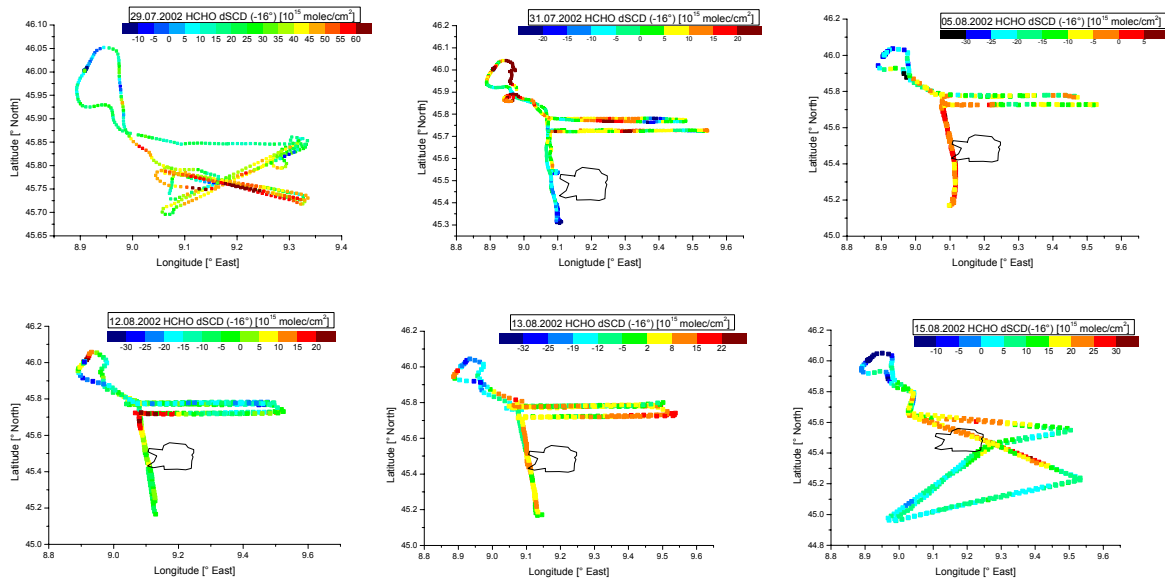


Figure 6.2200.6: Differential slant columns of HCHO measured with the telescope viewing direction  $-16^\circ$  during six flights of the first campaign as function of geographic position. The city area of Milano is marked. Note that the axis and the colour scales are different for each flight.

Section 6: Detailed report related to overall project duration

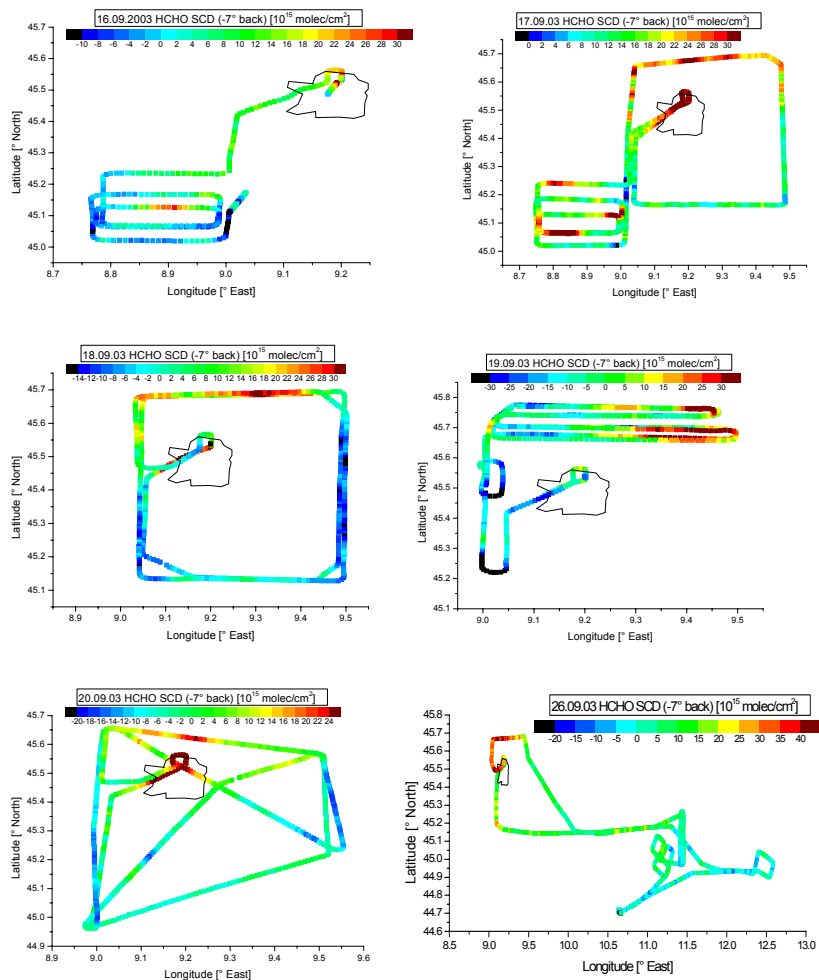


Figure 6.2200.7: Differential slant columns of HCHO measured with the telescope viewing direction  $-7^\circ$  during six flights of the second campaign as function of geographic position. The city area of Milano is marked. Note that the axis and the colour scales are different for each plot.

## D) HCHO vertical column distribution in the measurement area

Vertical column distributions have been derived by means of the procedure explained in WP 2400. The data of three telescope directions have been averaged. A horizontal map of the average HCHO vertical columns of the flight of 16 August 2002 is shown in Figure 6.2200.8a. The HCHO mixing ratio derived at ground is displayed in Figure 6.2200.8b. The Milan plume is located north west of Milan according to the wind direction of  $135^\circ$ . The mixing ratios inside the Milano plume vary between 6 and 8 ppbv whereas the background values are only 2-5 ppbv.

There are two major error sources, that of the DOAS analysis and that of the radiative transfer AMF calculations. The DOAS error consists of a systematic and a random error. The systematic error is mainly given by the uncertainty of the absorption cross-section of HCHO, which is quoted to be 5% (Meller and Moortgat, 2000). The random error results from the limited numbers of photons and the detector characteristics for each spectrum. The error is about  $3.5 \times 10^{15}$  molec/cm<sup>2</sup> for one spectrum. When averaging the 60 measurements (20 positions multiplied with 3, number of telescopes) along one straight line of the flight track (e.g., the side length of the square), this contribution diminishes to  $4.5 \times 10^{14}$  molec/cm<sup>2</sup>. The total uncertainty of the VCDs due to errors in the radiative transfer calculations is estimated to be within 15%.

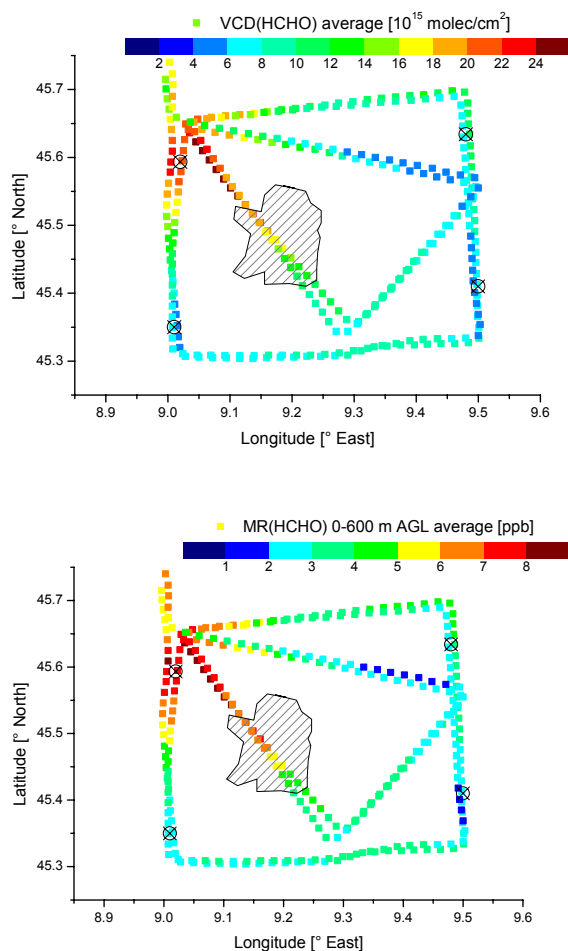


Figure 6.2200.8 a,b: Left (a): HCHO Vertical columns measured on 16 August 2002 as function of the geographic position: (data average of the three elevation angles  $-4^\circ$ ,  $-10^\circ$ , and  $-16^\circ$ ). Right (b): Horizontal distribution of the HCHO mixing ratio at ground (0-600m AGL). The shaded area presents the city of Milano.

With the vertical column densities it is possible to calculate the total HCHO flux (molec/s) from the city. The flux is calculated as follows:

$$Flux = v_{aircraft} \int_{t_1}^{t_2} v_{wind}(t) VCD(t) dt \quad (7)$$

Here,  $v_{wind}$  is the wind speed perpendicular to the flight direction, (it changes with time due to the changing flight direction);  $v_{aircraft}$  is the speed of the aircraft, VCD the vertical column density and  $t$  the time period needed for the measurement of the cross section. On 16 August, the wind speed was  $1.5 \pm 0.5$  m/s, the speed of the aircraft was  $270 \pm 10$  km/h and the entire time span across the photochemical plume lasted about 300 seconds. Using the above formula we derive a total net flux of  $4.4 \times 10^{24}$  molec/s originating from the town (Pundt et al., paper in preparation).

## WP 2300: Intercomparison of measurement techniques

### A) Measurement overview on Aircraft and SOF operations

There are a large number of time intervals, which can be used for intercomparison. Table 6.2300.1 summarises the flight times of the two aircraft, which were used during the first campaign. The locations of the aircraft are mostly different due to different airspace limitations for the different aircraft. The two first flights of the first campaign (2002), performed during the intercomparison week, were dedicated to the intercomparison between the two aircraft and the groundbased MAX-DOAS instruments. The location of the groundbased instruments (Alzate) was overflown at least ten times. Also both aircraft met at this location in order to exclude temporal variations when comparing the results. Also during the other flights, the ground locations were overflown (Pavia, Bresso and Alzate), so comparisons will be possible here for the entire campaign.

Date	PARTENAVIA	MICROLIGHT
	Time	Time
29. July	8:45-10:20	9:12 -11:31
31. July	9:30-12:00	9:13 -11:25
04. Aug.	-	10:16 -12:04
05. Aug.	9:12-10:48	9:16 -12:18
08. Aug.		11:28 -14:51
12. Aug.	12:34-15:07	-
13. Aug.	12:48-15:22	12:48 -16:32
14. Aug.	10:05-11:37	-
14. Aug.	13:00-15:24	11:57 -14:31
15. Aug.	10:54-13:26	9:41 -13:40
16. Aug.	12:56-15:37	11:55 -13:32
17. Aug.	-	11:24 -14:07
18. Aug.	10:13-11:55	8:39 -11:02

Table 6.2300.1: Overview on the Partenavia (AMAXDOAS) and Microlight (Hantzsch) flights of the first campaign.

Table 6.2300.2 summarises the times of measurements of the three aircraft and the SOF mobile instrument for the second campaign. During most of the measurements the instruments were operated at different locations. However, the ground locations were overflown frequently (Spessa, Bresso, and Alzate), therefore, comparisons were possible here during the entire campaign. The

## Section 6: Detailed report related to overall project duration

data intercomparison from the AMAXDOAS, MAX-DOAS, airborne Hantzsch, and SOF measurements could be done for several flights and is still ongoing.

Date		PARTENAVIA	DIMONA	MICROLIGHT	SOF
14.09.03	Sunday	11:10 -13:00 4x Cremona box		-	X
16.09.03	Tuesday	10:15 -12:15 2x to Sannazzaro	12:15-16:05 Boxes around Milan	10:56 – 12:48 Box southeast of Milan	
17.09.03	Wednesday	10:30 -12:30 2x to Sannazzaro	10:25-12:41 Boxes	-	
18.09.03	Thursday	11:50 -13:50 Two boxes around Milan	13:20-17:04 Boxes around Milan	10:28 – 13.48 Box around Milan	X
19.09.03	Friday	12: 20 -14:30 To the north	9:11-10:21 12:23-16:29	11:00 – 14:28 Box around Milan	X
20.09.03	Saturday	12:48 -15:22 Box+cross (Milan)	9:42-12:54 Boxes around Milan	09:01 – 13:10 Box around Milan	X
25.09.03	Thursday	13:00 -15:24 -> Sermide (Int. Dimona)	12:40-16:34 Eastward (Intercomp.)	12:00 – 15:05 Box around Milan	X
26.09.03	Friday	10:54 -13:26 -> Eastward Porto Tolle (Intercomp.)	9:02-10:08 13:15-16:34 Eastward	9:11 –11:28 13:15 – 16:36 Eastward, Montagnana	X
27.09.03	Saturday (SCIA)	12:56 -15:37 -> Porto Tolle (SCIA)	9:15-13:34 Eastward (Intercomp.)	10:12 – 13:47 Box around Milan	X

Table 6.2300.2: Overview of the Partenavia (AMAXDOAS), Dimona (Hantzsch), Microlight (Hantzsch), and the SOF operations of the second campaign.

## B) Results

### Horizontal distribution: AMAXDOAS /Hantzsch

The horizontal distribution of the AMAXDOAS ground level mixing ratio data is compared to that of the Microlight (Figure 6.2300.1). Note that for the Microlight only the flight track south of 45.75°N can be used. North of the area Lecco – Alzate – Como its flight altitude was above the mixing layer, ~2900 m above sea level. East of 9.1 °E, there is a very good agreement between the measurements of the two aircraft taking into account the wind direction of 135° N which leads to a shift of the data towards the west for the microlight data which are located more in the north. The mixing ratio is about 3-4 ppbv almost everywhere except the sharp increase in the west of 9.2 °E due to the Milano emission and photochemical plume. Comparisons can be done for the data inside the parallelogram. In this region, the agreement between the HCHO measurements of the two aircraft is excellent.

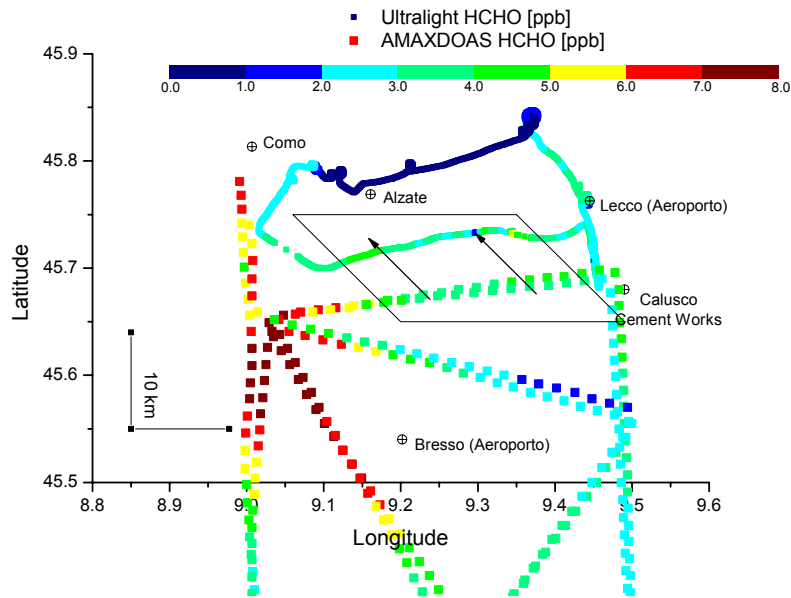


Figure 6.2300.1: Horizontal distribution of HCHO mixing ratios derived by the Microlight Hantzsch (thin line) and the AMAXDOAS instrument (squares). The time difference between the measurements of the two aircraft is only 30 minutes. North of Lecco – Alzate – Como the flight altitude of the Microlight was above the mixing layer, 1900 m – 2200 m above sea level. The wind direction was 135°N (see arrow).

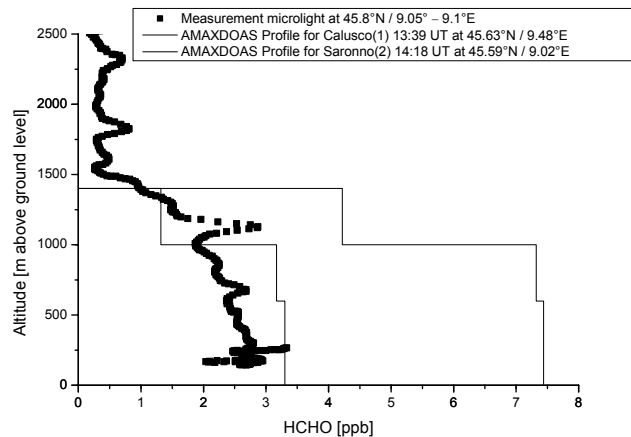


Figure 6.2300.2: Vertical distribution of HCHO mixing ratios derived by the Microlight Hantzsch (squares) and that of the AMAXDOAS instrument (thin lines) on 16 August 2002.

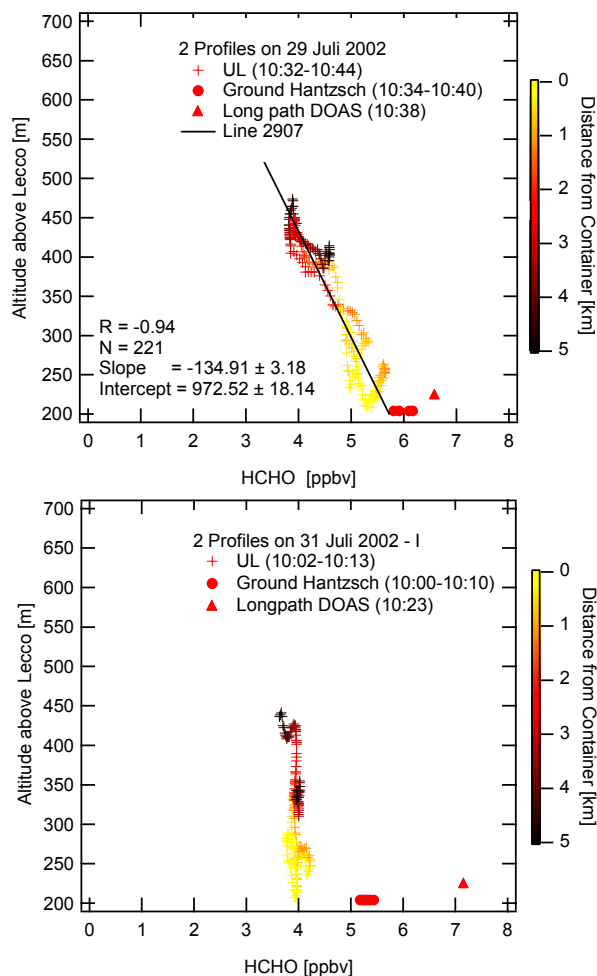


Figure 6.2300.3: HCHO mixing ratio vertical distributions derived by the Microlight (crosses) and that of the ground instruments Hantzsch and long path DOAS (circles and triangles) on 29 and 31 July 2002 at Alzate. The colour of the Microlight data points corresponds to the distance between the aircraft and the groundbased instruments.

#### Vertical distribution: Hantzsch/AMAXDOAS

The vertical distribution of the AMAXDOAS data as derived for the two locations Saronno and Calusco are compared to the vertical distribution of the Microlight data (Figure 6.2300.2). The Microlight HCHO profile was taken in the background air and compares very well with the AMAXDOAS profile of Calusco, which is located in the background air as well. Note that the Microlight is sensitive to small horizontal or vertical fluctuations whereas the AMAXDOAS measures average concentrations of larger areas.

#### Vertical distribution: Hantzsch/Ground instruments

Figure 6.2300.3 shows an intercomparison between HCHO vertical profiles measured with the Microlight Hantzsch and ground measurements (Hantzsch and long path DOAS) at Alzate. The agreement of the data of the three instruments is very good on 29 July 2002, but it is poorer on 31 July 2002. The difference of 2 ppbv between the groundbased Hantzsch data and the long path DOAS data on this day suggests that there is a small scale spatial variation (over some tens to hundreds of metres). This variation can be the reason for the discrepancy between the three instruments.

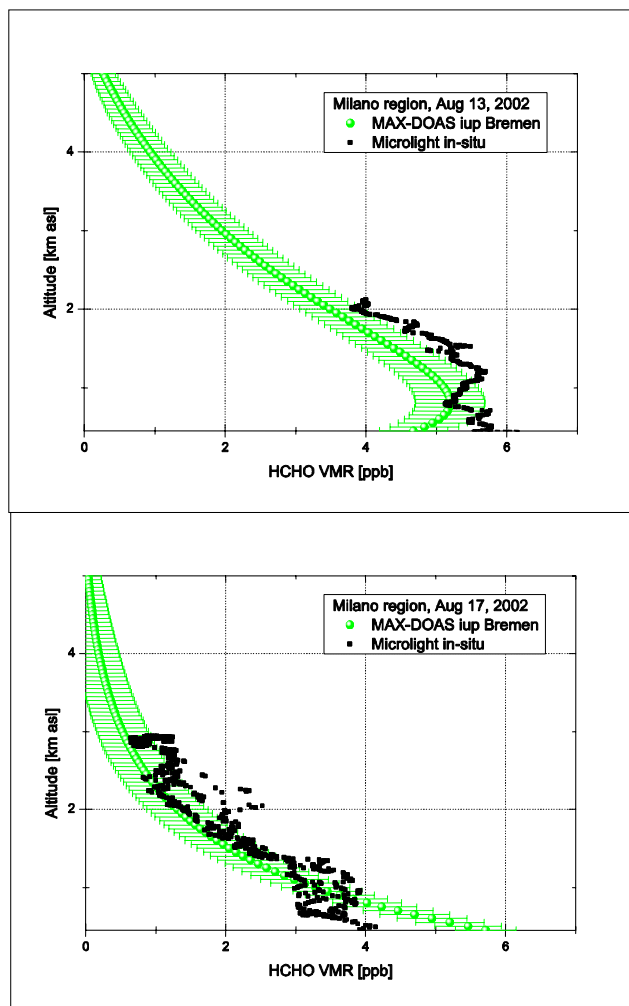


Figure 6.2300.4: HCHO vertical column derived from the Microlight and the groundbased MAX-DOAS measurements. Top figure: 13 August 2002, Bottom figure: 17 August 2002.

Vertical distribution: Hantzsch/MAX-DOAS

The agreement between the vertical profiles derived from the ground based MAX-DOAS data and the Microlight data is excellent (Figure 6.2300.4), despite the fact that the MAX-DOAS profile approximation may lead to higher discrepancies of up to 2 ppbv in the first 300 m above ground.

Vertical column time series: MAX-DOAS / SOF

The Alzate MAX-DOAS is compared to the SOF instrument for the days when the SOF instrument was installed at Alzate (Figure 6.2300.5). The data agreement is good to excellent, however, the SOF was not installed at the location during the entire day. Some data have been measured at different locations with a distance of up to 40 km from Alzate.

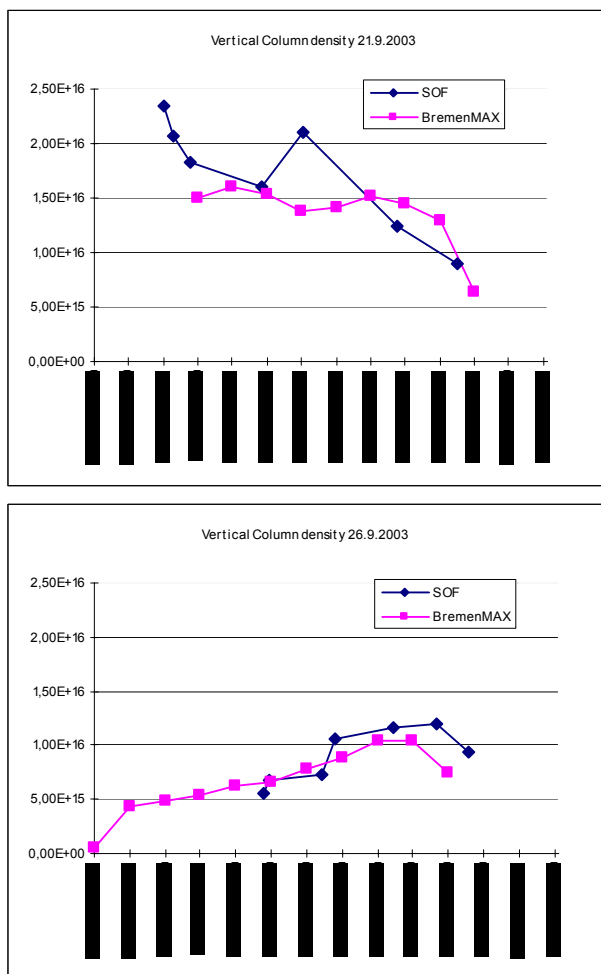


Figure 6.2300.5: HCHO vertical column measured with the SOF and the MAX-DOAS instruments over Alzate on 21 and 26 September 2003.

## WP 2400: AMF modelling for MAX- and AMAXDOAS

### A) MAX-DOAS:

#### Air mass factors for MAX-DOAS for selected conditions including uncertainties (D2400.1)

#### HCHO vertical profiles with error bars from MAX-DOAS measurements (D2400.3)

During the first part of the project, most effort was spent on the investigation of the radiative transport through the atmosphere for the MAX-DOAS geometry. For this purpose, three radiative transport models were applied:

- SCIATRAN (the CDIPI-version: is a combined differential-integral approach involving the Picard iterative approximation). In this model, the full spherical radiative transfer equation is converted into an integral form by using the characteristic method. This integral form depicts an iteration scheme for the intensity. As initial estimation for the radiation field the output of a pseudo-spherical approach to the radiative transfer equation is used. The interested reader can find a detailed description of the model SCIATRAN together with all relevant equation elsewhere (Rozanov et al., 2001).
- AMFTRAC. In this model, the Monte-Carlo method is applied. Thus, it is in particular possible to include full spherical geometry and multiple scattering (Von Friedeburg et al., 2003; see also the

workshop contribution): Weighting functions and Air Mass Factors for balloon-borne nadir and limb measurements of stratospheric trace species using a 3D Monte Carlo RT model

(<http://www.iup.physik.uni-bremen.de/sciamachy/services/meetings/limbWS2003/limbProgram.html>).

- 1D pseudo-spherical discrete-ordinates model libRadtran ([www.libradtran.org](http://www.libradtran.org))

All radiative transport models were shown to produce good results in the model intercomparison described below.

Different sensitivity studies have been performed to investigate the possible information content on the vertical resolution which can be derived from MAX-DOAS measurements of HCHO. One example (using SCIATRAN) of the different studies is described in the following. In situ measurements have shown that the boundary layer near to Milano is often split into two sublayers. To answer the question, whether a stratification like this could be detected by the MAX-DOAS instrument, air mass factors (AMF) have been calculated for three different profiles shown in Fig 6.2400.1a. The absolute vertical column for each profile was kept constant to guarantee the comparability. The relative differences for the AMF compared to AMF for one homogenous layer (profile 1) are shown in Fig 6.2400.1b. Deviations in the range of 10 to 20% should be visible also from experimental data. This conclusion is also supported by the excellent agreement between MAX-DOAS, Hantzsch and LP-DOAS observations shown in WP 1400.

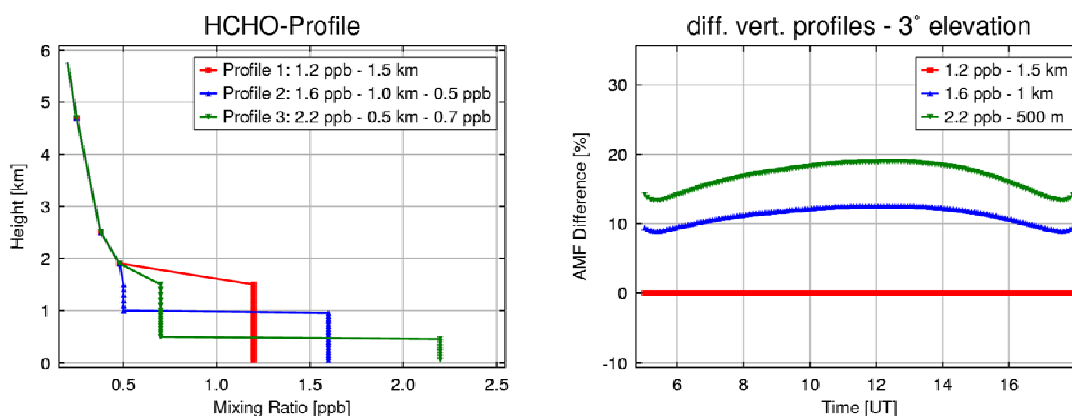


Fig. 6.2400.1: Left: different assumed vertical HCHO concentration profiles used for the AMF calculation. Right: Differences between the AMFs (for 3° elevation) calculated for the selected profiles (left). The differences between the sensitivities for the different profiles clearly indicate the potential of the MAX-DOAS measurement for profile retrieval.

Similar sensitivity studies were also performed with the AMFTRAC model. This study contains several assumed HCHO profiles elevation angles and ground albedos (see Fig. 6.2400.2 and 6.2400.3).

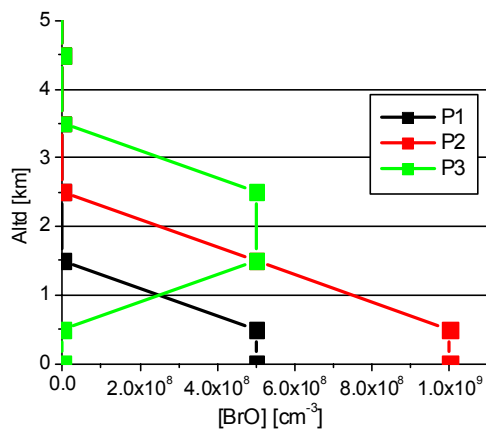


Fig. 6.2400.2 Assumed profiles for the MAX-DOAS sensitivity study.

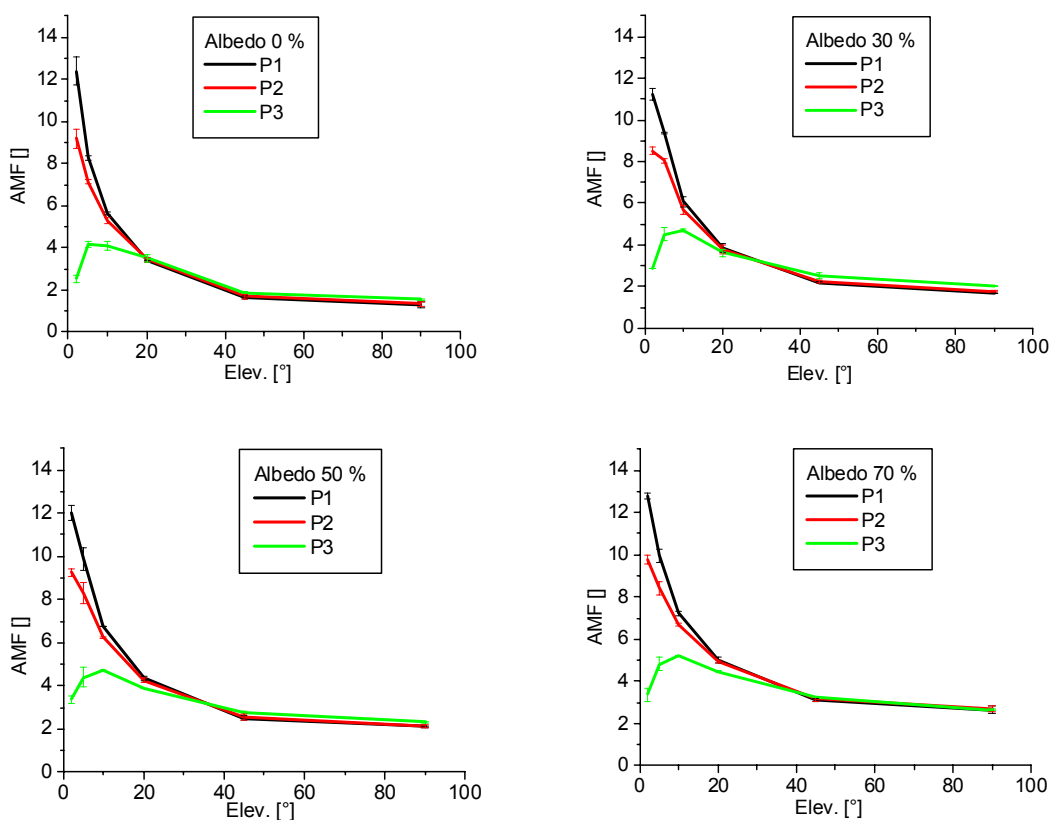


Fig. 6.2400.3 Dependence of the MAX-DOAS HCHO AMFs depending on ground albedo and elevation angle. While the absolute values of the AMF significantly depend on the ground albedo, the overall behaviour is very similar for the different scenarios. In particular it becomes evident that profile information can be retrieved for measurements at low elevation angles (Von Friedeburg et al., 2003).

UHei

During the second part of the project UHei concentrated on radiative transfer modelling of MAX-DOAS O<sub>4</sub> observations at different atmospheric aerosol conditions, which are important to derive atmospheric vertical extinction profiles, which are needed as input for the HCHO analysis. The simulations are carried out with the Monte Carlo model ‘TRACY’, which takes into account multiple scattering and full sphericity [von Friedeburg, 2003; Hönninger et al., 2004].

### Reduction of the direct light path along the line of sight

In Fig. 6.2400.4 the modelled O<sub>4</sub> AMFs for different elevation angles and different aerosol profiles are shown as a function of SZA. The azimuth angle was set to zero. While additional aerosol scattering has only a small influence on the AMFs for zenith direction, the AMFs for the low elevation angles are strongly affected by the different aerosol loads. In general the finding that the AMFs become smaller for increasing aerosol extinction is clearly confirmed. In particular, it is shown that especially the telescopes at small elevations are very sensitive to aerosol scattering near the surface. One additional interesting finding is that especially the telescopes at low elevation angles are very sensitive to the aerosol height profile. In particular for the two aerosol profiles with the same total optical depth (0.05) from either 0 to 2 km or 0 to 1km the respective O<sub>4</sub> AMFs are significantly different.

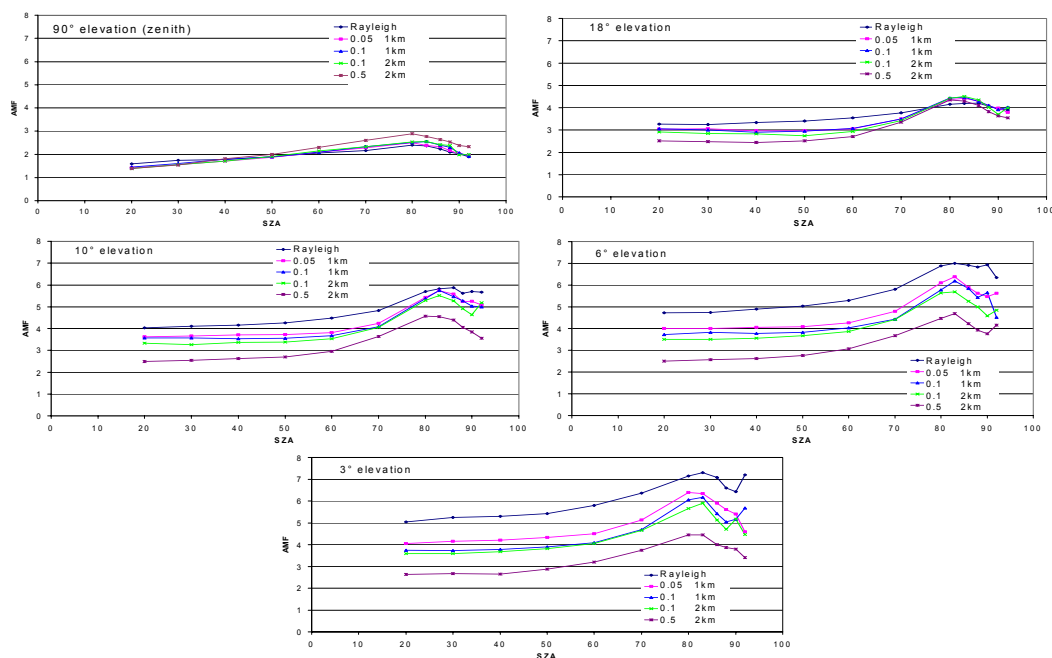


Fig. 6.2400.4 O<sub>4</sub> AMF calculated with the Monte Carlo model ‘TRACY’ [Von Friedeburg, 2003] for different MAX-DOAS elevation angles and aerosol scenarios. The first number in the legend indicates the aerosol extinction per km, the second number the upper boundary of the aerosol layer (see Table 6.2400.1).

Table 6.2400.1 Properties of the aerosol profiles used for the radiative transfer simulations

Profile name	Aerosol extinction	Altitude range	Total extinction aerosol	Visibility [km] (Mie only)
0.05_2	0.05/km	0 – 2km	0.1	78
0.1_1	0.1/km	0 – 1km	0.1	39
0.1_2	0.1/km	0 – 2km	0.2	39

0.5	1	0.5/km	0 – 1km	0.5	8
-----	---	--------	---------	-----	---

### Influence on the penetration depth of the incident sun light

In Fig. 6.2400.4 it can also be seen that the amplitude of the AMF variation during the day is influenced by the aerosol profile. For the zenith viewing telescopes it is slightly increased if the aerosol scattering is enhanced: from about 0.8 for a pure Rayleigh atmosphere to about 1.1 for the aerosol layer with an optical depth of 0.5 (see table 6.2400.1).

### The effects of multiple scattering

We investigated the effects of multiple scattering inside vertically extended clouds.  $O_4$  AMFs for MAX-DOAS observations were calculated for three different cases: a) a cloud with a total optical depth of 5 and a vertical extension from 0.1 to 5 km, b) a cloud with a total optical depth of 20 and a vertical extension from 0.1 to 2 km, and c) a cloud with a total optical depth of 50 and a vertical extension from 0.1 to 5 km. The results are summarised in Fig. 6.2400.5. We find that the  $O_4$  AMF is strongly enhanced for optically thick clouds and depends only slightly on elevation angle. The number of scattering events can become very large: for the cloud with an optical depth of 50 it is almost 1000.

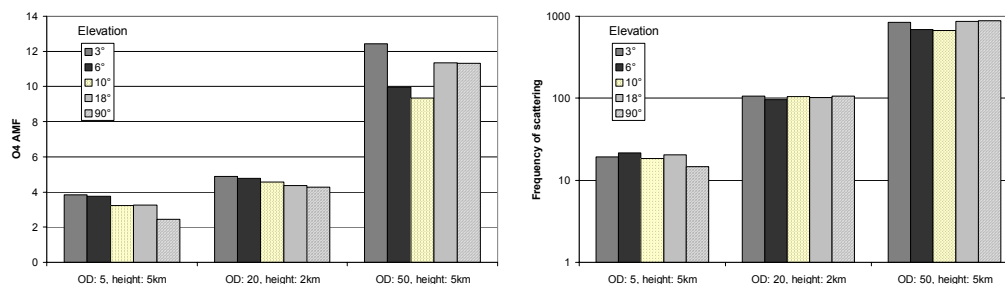


Fig. 6.2400.5 top:  $O_4$  AMFs for clouds with different optical depths and different vertical extensions. The assumed clouds are located close to the ground (cloud base height 100m) and the  $O_4$  AMF only slightly depends on the elevation angle. Bottom: Number of scattering events for clouds with different optical depths and different vertical extensions. The assumed clouds are located close to the ground (cloud base height 100m).

### Influence of aerosol absorption

We investigated how strongly the absorbing properties of aerosols affect the MAX-DOAS  $O_4$  observations. It turned out that in contrast to the total intensity of the observed light the  $O_4$  absorption is only weakly affected (Fig. 6.2400.6). This finding can be explained by the fact that even for strongly absorbing aerosols the average photon path lengths are still high; it indicates one specific advantage of  $O_4$  MAX-DOAS observations for the determination of aerosol properties.

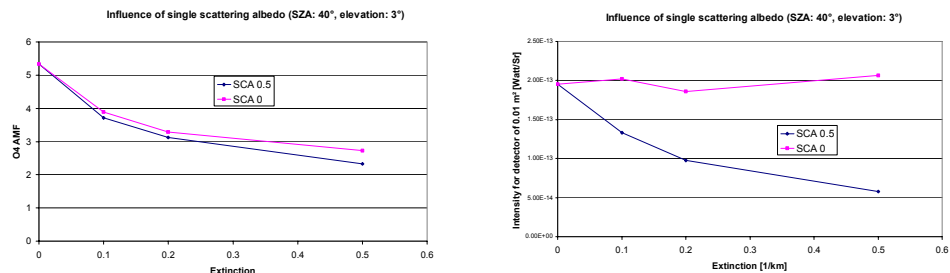


Fig. 6.2400.6: top: dependence of the MAX-DOAS O<sub>4</sub> AMF (for 3° elevation) for different aerosol optical depths and different values of the single scattering albedo. The MAX-DOAS O<sub>4</sub> depends only weakly on the absorbing properties of aerosols. Bottom: dependence of the observed intensity (for 3° elevation) for different aerosol optical depths and different values of the single scattering albedo. It strongly depends on the absorbing properties of aerosols.

### Influence of the scattering phase function

We modelled MAX-DOAS O<sub>4</sub> AMFs, the intensity and the Ring effect (Fig. 6.2400.7) as a function of the azimuth angle (between the telescopes and the sun). As expected, the O<sub>4</sub> AMFs are smallest for an azimuth angle of zero. For this angle, single scattering on aerosols has a larger relative contribution to the total intensity compared to other azimuth angles. Accordingly, for an azimuth angle of 0° the intensity is highest and the Ring effect is smallest because of the preferred forward scattering of aerosols. These findings are in excellent agreement with our observations.

It should be noted here that our radiative transfer model so far does not include a realistic module for the detailed simulation of the Ring effect. Within this study, we approximated the relative strength of the Ring effect from the relative contribution of photons having undergone molecular scattering to the total number of scattering events.

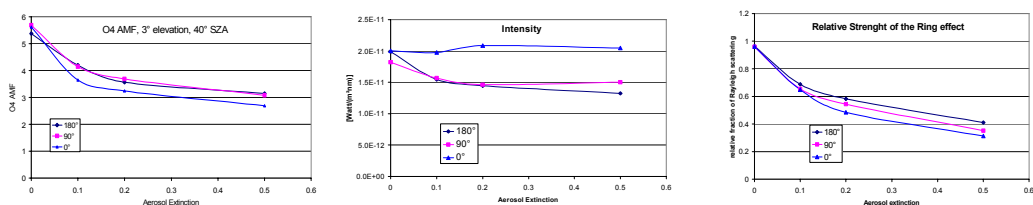


Fig. 6.2400-7 O<sub>4</sub> AMF, intensity, and Ring effect calculated for different MAX-DOAS elevations and azimuth angles. In agreement with MAX-DOAS observations the smallest O<sub>4</sub> absorptions (as well as the highest intensity and the smallest Ring effect) are found for an azimuth angle of zero. This indicates the strong forward preference of aerosol scattering.

### IUP Bremen

During the second part of the project IUP Bremen has continued the work on sensitivity studies for AMF calculations. One paper has been published, which applies the outcome of AMF modelling to MAX-DOAS measurements from IUP Bremen during the first field campaign (Heckel et al., 2005). This paper illustrates the possibilities of the MAX-DOAS method to get profile information for HCHO using realistic input parameters for radiation transport calculations.

The following figure shows a comparison between MAX-DOAS and other instruments published in this paper.

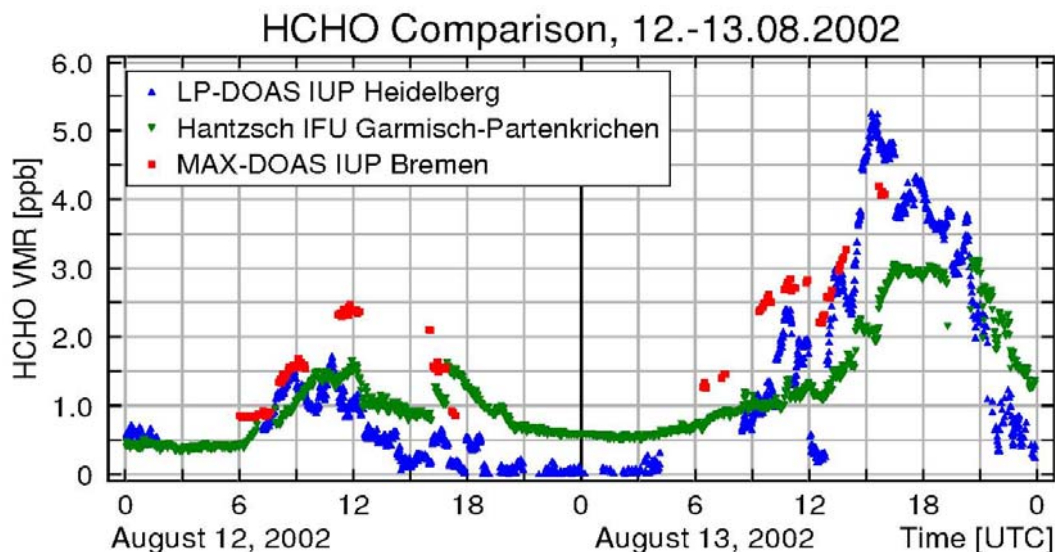


Fig 6.2400.8: Intercomparison plot showing data of a Hantzsch and a LP-DOAS instrument in contrast to the HCHO mixing ratio derived for a atmospheric bottom layer of 500m height from the MAX-DOAS analysis. The agreement is excellent and well within the error bars for both in the absolute values and the diurnal variation. This comparison provides a first validation for the retrieval method, although clearly the air sampled by the three instruments was not identical (Heckel et al., 2005).

### Norwegian Institute for Air Research (NILU)

NILU has performed sensitivity studies of air mass factors in order to improve the retrieval of formaldehyde columns and profiles from AMAX and MAX-DOAS measurements.

Various radiative transfer models have been intercompared in terms of air mass factors computed for selected scenarios. All models, including those applied within the FORMAT project, produced agreeable results. This task was completed jointly with the QUILT project. A full report is available at [http://nadir.nilu.no/quilt/rtm\\_validation\\_package\\_wp2500.zip](http://nadir.nilu.no/quilt/rtm_validation_package_wp2500.zip). A manuscript has been submitted to a scientific journal with peer-review (Hendrick et al., ACPD).

For air mass factor sensitivity studies we used the 1D pseudo-spherical discrete-ordinates model libRadtran ([www.libradtran.org](http://www.libradtran.org)), which was shown to produce good results in the above model intercomparison. Air mass factors are sensitive to atmospheric composition and surface reflection, as well as observation and sun geometry. We used formaldehyde profiles simulated by both regional and global CTMs (Chemistry Transport Models). For example, the regional 3D NILU-CTM produced 6-hourly profiles over Milano throughout the FORMAT 2 campaign (7 Sept. – 14. Oct. 2003). Simulations based on all these profiles for a zenith looking surface instrument at solar zenith angles of  $87^\circ$  for a 336 nm wavelength resulted in air mass factors of  $1.95 \pm 0.64$  ( $2\sigma = 33\%$ ). We found that air mass factors can vary between 1.05 and 9.17. The mean constitutes the recommended air mass factor when no a priori knowledge on formaldehyde profiles is available.

Air mass factors are highly sensitive to surface albedo. For a zenith looking surface instrument, the air mass factor can vary between 1.6 for no surface reflection to 4.5 for a fully reflecting surface

## Section 6: Detailed report related to overall project duration

(albedo of unity). There is a slight solar zenith angle dependency with a maximum at around 65 degrees.

Air mass factors seem much less sensitive to aerosol profiles. For a zenith looking instrument, assuming a typical surface visibility of 25 km, the airmass factor for a typical autumn profile deviates less than 2% from a spring profile with a maximum deviation for a solar zenith angle at about 75 degrees. The aerosol loading, on the other hand has a stronger effect on the air mass factor, increasing it by 13% when transforming a clear atmosphere to a turbid one (5 km visibility).

**B) AMAXDOAS**

For the interpretation of the AMAXDOAS slant column data, and the inversion into vertical concentration distributions, the radiative transfer Monte Carlo Model TRACY was used (Von Friedeburg, 2003). One issue for the interpretation of scattered light measurements such as those from the AMAXDOAS is the scattering of light by the aerosol loading, which has a significant influence on the light path. Knowledge of the aerosol load is hence a necessary prerequisite to interpret the scattered light measurements. For example, for the flight presented before, the variation of the O<sub>4</sub> data (fig. 6.2400.9), during the flight indicates that the aerosol loading is much higher inside the Milano plume (e.g., Saronno, 45.61°N 9.02°E) than outside the plume (e.g., Pavia, 45.36°N 9.0°E). This implies that AMFs have to be calculated for different locations and aerosol conditions.

As described above the solar reference spectrum was taken from the same flight and the same viewing direction to remove Fraunhofer structures and to reduce any instrumental structures. This procedure leads to slant column differences (the differential slant column densities, dSCD) between the specific location along the flight and the reference location. Thus, retrievals for aerosols, HCHO and NO<sub>2</sub> have to be performed also for the reference locations. Four locations were chosen for a detailed investigation: Saronno (45.61°N 9.02°E), Pavia (45.36°N 9.0°E), Codogno (45.4°N 9.5°E), and Calusco (45.6°N 9.0°E). Pavia, which is situated south west of Milano, was taken as reference location.

To reproduce expected high gradients of aerosol and HCHO near the ground, five boxes reaching from 0-600 m, 600-1000 m, 1000-1400 m, 1400-2000 m and above 2000 m, respectively, were used in the analysis. For the chosen wavelength range, the albedo of the landscape below the aircraft was 2% (Feister and Grewe, 1995). A single scattering albedo of 90% was assumed using AERONET data (Dubovik, 2001). A standard phase function representing an asymmetry coefficient of 0.65 was chosen for the aerosol. The complete analysis of the HCHO profiles was done in four steps. In the first step some preparation for an easier handling were made. In the second step the aerosol profiles were modelled and the corresponding Box-AMFs were calculated and in the third step a forward modelling of HCHO was done. Finally, the AMF data were interpolated in order to derive AMFs for the entire flight (fourth step).

- 1) The O<sub>4</sub> dSCD\* as result of the DOAS analysis are in the order of 10<sup>43</sup> molecules<sup>2</sup>/cm<sup>5</sup>. For mathematical and numerical convenience, a “differential AMF”, dAMF, is introduced. It is defined as:

$$\begin{aligned} dAMF_{Loc\_Ref,i} &= AMF_{Location,i} - AMF_{Reference,i} = \frac{SCD_{Location,i} - SCD_{Reference,i}}{VCD} \\ &= \frac{dSCD_{Location,i} - dSCD_{Reference,i}}{VCD} \end{aligned} \quad (5)$$

The dAMF is the difference between the AMF at the measurement location and that of the reference point; “i” refers to the respective telescope angle. Here, the VCD of O<sub>4</sub> is 1.22 × 10<sup>43</sup> molecules<sup>2</sup>/cm<sup>5</sup> for all locations. Note that this relation is not valid for trace gases with changing vertical concentration profiles because of the varying VCD. It is obvious that dAMF<sub>Pavia</sub> = 0. The dAMF were calculated using the measurement data for the telescope elevations (+2°, -1°, -4°, -10°, -16°) and all seven locations.

- 2) After that the aerosol profiles of the two locations were varied in the model until the following function is minimised:

$$F = dAMF_{Loc\_Ref}(measurement) - dAMF_{Loc\_Ref}(model) \quad (6)$$

Here, two AMF(*model*) were calculated with the radiative transfer model at the two locations, whereas dAMF (*measurement*) was calculated from the measurements as described above. A maximum error in both modelled and measured AMF data of 0.1 was allowed. The aerosol loads were changed iteratively. Some general sensitivity aspects were used for the simulation. It was found that the slant elevations (+2°, -1° and -4°) are sensitive to changes in the aerosol loading close to the flight altitude, whereas the higher (steeper) elevations are more sensitive than the lower elevations to aerosol loading near the ground. All O<sub>4</sub>-AMFs decrease when aerosols are added above the flight altitude. The O<sub>4</sub> measured and simulated AMF is displayed in Figure 6.2400.9a for the ten different telescope angles for two locations: Calusco (first overflight) and Saronno (second overflight).

For all locations a linear decay of the aerosol extinction coefficient turned out to yield the best fits (Figure 6.2400.9b). The maximum extinction coefficient was observed in the plume of Milano (Saronno) reaching 1.5 km<sup>-1</sup>. This corresponds to a visibility of 5 km in the visible wavelength.

Then the Box-AMFs were calculated with the modelled aerosol profiles as shown in Figure 6.2400.10. As predicted by earlier simulations (Bruns et al. 2004), the highest sensitivity is achieved close to the flight altitude, and it decreases with increasing aerosol extinction. The sensibility close to the ground is poor at this flight altitude.

- 3) In principal if the Box AMFs are known, it should be possible to retrieve the vertical profile based on the data of 10 viewing directions for the 8 locations. Here, the following functions are minimised for all elevations (i) simultaneously:

$$F_i = \left| dSCD(measurement) - dSCD(model) \right|_i = \left| dSCD_{loc,i}^{meas}(HCHO) - \left( \sum_j BAMF_{loc,j,i} * c_{loc,j} * V_j - \sum_j BAMF_{ref,j,i} * c_{ref,j} * V_j \right) \right| \quad (6)$$

Here, c<sub>j</sub> stands for the concentration in the box (j) and V<sub>j</sub> is the vertical extension of the box, (see also equation (3)). Unfortunately, the matrix equation was found to be insufficient to calculate HCHO vertical profiles for any position without assuming a priori information. Therefore, some a priori information was included in the optimisation procedure: we assumed the HCHO to be well mixed in the boundary layer (0 to 1000 m), and a 30-50% lower mixing ratio in the layer between 1000 and 1400 m. For the concentration in the box 1400-2000 m no a priori information was assumed. The maximum mixing ratio was fixed to be less than 9 ppbv and for the background an average mixing ratio of 2 ppbv was taken as a priori information. The information is based on independent in situ measurements performed by the Microlight aircraft on the same day in the same area (W. Junkermann, pers. comm.), and ground based measurement being part of the FORMAT project (C. Hak, pers. comm.). The optimisation procedure was performed in two steps: First the HCHO profiles for the seven locations and the reference points were changed manually to minimise the difference between model and measurement. Then, a least square procedure was used to optimise this minimisation. The result of three locations is shown in Figure 6.2400.11. As expected, the HCHO mixing ratios are high (6-8 ppbv) inside the photochemical plume of Milano (Saronno) and low (0-5 ppbv) outside the plume (Pavia and Calusco).

- 4) A high correlation between the O<sub>4</sub> and HCHO AMFs for the eight measurement points for several telescope directions was found. This is probably due to a specific relationship between the HCHO and the aerosol vertical concentration distribution inside the plume; both are emitted continuously over the area of Milano. This does not imply that the concentrations are proportional to one another. However, we found that results of the telescope direction -13° are too noisy probably due to the location of the spectra on the edge

of the CCD chip. They are therefore excluded in the following. The linear relationship between the two AMFs was used to calculate the vertical HCHO vertical column for each position.

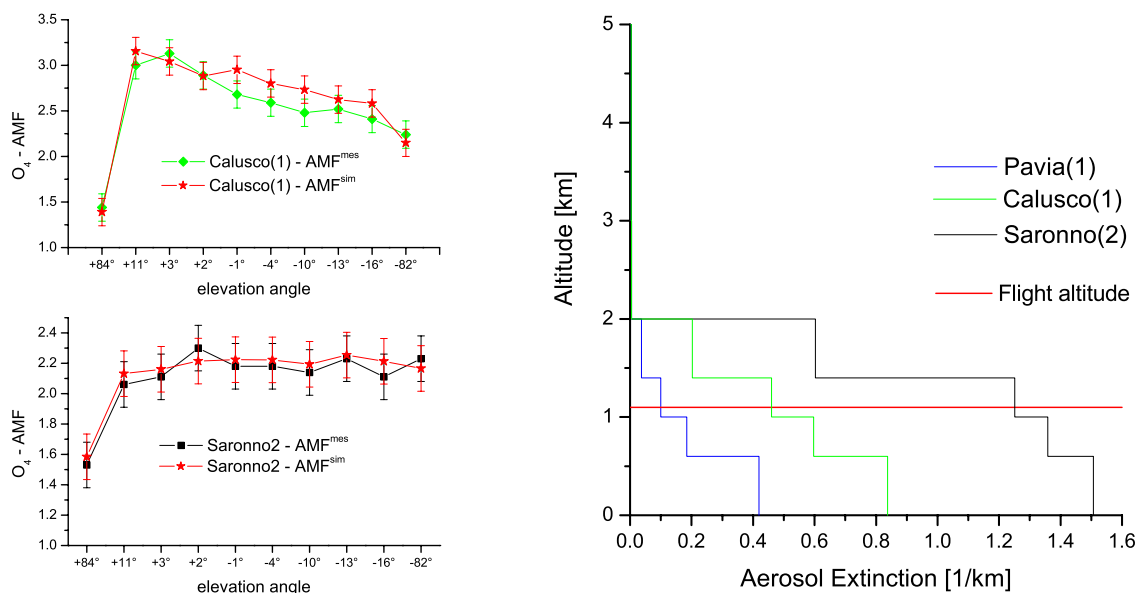


Figure 6.2400.9a: Simulated and measured  $O_4$  air mass factors (AMF) for the different telescope elevation angles at the locations Calusco and Saronno after optimisation of the vertical extinction profile. Due to the high aerosol load, the AMF in the Milano plume over Saronno does not depend on the elevation angle (except from the upward looking telescopes)

Figure 6.2400.9b: Vertical extinction coefficients for Saronno (45.61°N 9.02°E), Pavia (45.36°N 9.0°E) and Calusco (45.6°N 9.0°E) derived from the  $O_4$  measurements used for the calculation of Box-AMF. The number inside parentheses corresponds to the number of the overflight. The flight altitude of 1.1 km was constant during the entire flight.

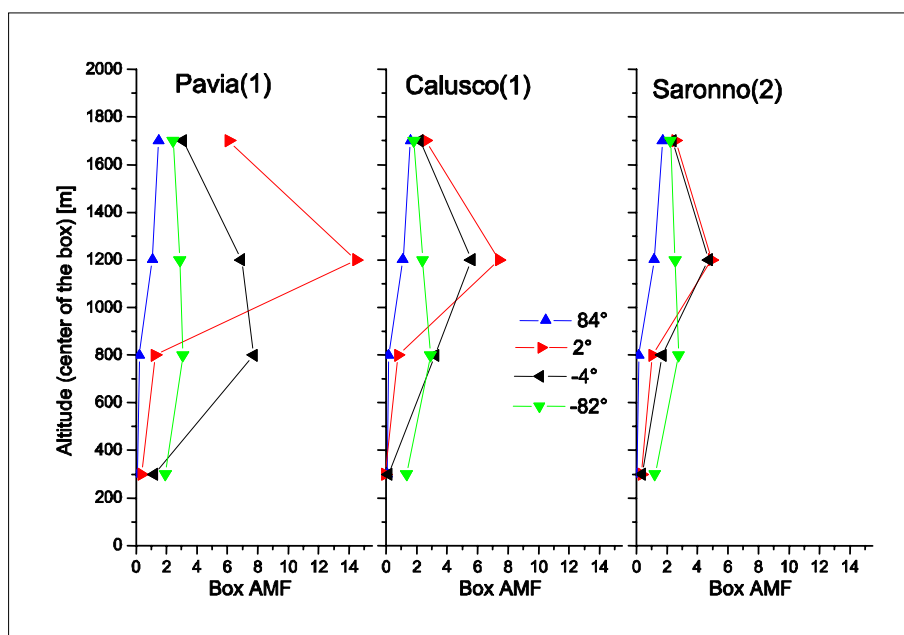


Figure 5.2400.10: Box-AMF on 16 August 2002 for the three locations Pavia, Calusco, and Saronno calculated with the radiative transfer model using  $O_4$  measurements. Four boxes were used in the model. The concentrations above 2 km were set to zero.

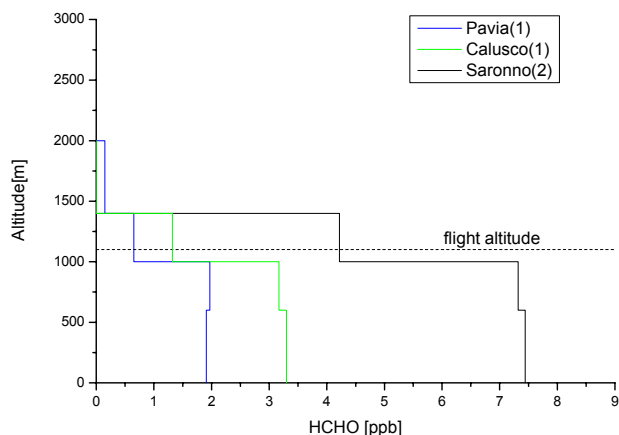


Figure 6.2400.11: HCHO concentration profiles on 16 August 2002 derived for three locations Pavia, Saronno and Calusco. All profiles are well mixed inside the boundary layer, which is located below the flight altitude. Saronno, which is located inside the photochemical plume of Milano, contains about 5 ppbv more HCHO than the two background locations Pavia and Calusco.

## References

- Dubovik, O., Holben, B., Eck, T., Smirnov, A., Kaufman, Y., King, M., Tanré, D., and Slutsker, I.: Variability of Absorption and Optical Properties of Key Aerosol Types Observed in Worldwide Locations, *J. Atmos. Sciences*, 59, 590-608, 2001.
- Feister, U. and Grewe, R.: Spectral Albedo measurements in the UV/visible region over different types of surfaces, *J. Photochem. Photobiol.*, 62(4), 736-744, 1995.

- Rozanov, V. Rozanov, and J.P. Burrows, A numerical radiative transfer model for a spherical planetary atmosphere: combined differential-integral approach involving the Picard iterative approximation, *Journal of Quantitative Spectroscopy & Radiative Transfer*, 69, 491, 2001.
- Von Friedeburg, C., A. Butz, F. Weidner, S. Sanghavi, K. Pfeilsticker, U. Platt and T. Wagner, Weighting functions and air mass factors for balloon-borne nadir and limb measurements of stratospheric trace species using a 3D Monte Carlo RT model, *Geophysical Research Abstracts*, European Geophysical Society 2003, 5, 11311, 2003.
- Von Friedeburg, C.: Derivation of Trace Gas Information combining Differential Optical Absorption Spectroscopy with Radiative Transfer Modeling, PhD thesis, Heidelberg, 2003.

## WP 3000: Measurements of additional compounds

### WP 3100: Measurement of additional species

Additional compounds as well as diverse meteorological parameters were measured from ground stations and mobile / airborne platforms during the 2002 and 2003 field campaigns.

#### 1. Ground-based measurements

The Tables 6.3100.1-6.3100.5 summarise the ground-based measurements performed at the different sites during the two FORMAT campaigns. Most of the processed data have been averaged in 30 minute intervals and submitted to the NADIR data centre at NILU:

<ftp://zardoz.nilu.no/nadir/projects/other/format/>

*Table 6.3100.1: Measurements at Alzate during FORMAT 2002. The field no. in the tables refers to the contractor number of the institution that performed each measurement.*

No.	Instrument	Parameters
1, 2	Longpath-DOAS	O <sub>3</sub> , NO <sub>2</sub> , SO <sub>2</sub> , HONO
2	Radon Monitor	Rn activity
2, 4	Max-DOAS	NO <sub>2</sub> , O <sub>4</sub> , AOD
5	O <sub>3</sub> instrument (UV absorption)	O <sub>3</sub>
5	CO analyser AL5002	CO
5	Thermoenvironment 42c trace level	NO
5	NOxTOy instrument (chemiluminescence + NOy converter)	NO <sub>2</sub> , NO <sub>x</sub> , total nitrate, PANs
5	PTR-MS	VOCs
5	GC	VOCs
5	Canisters	VOCs
5	Meteo station	T, p, r.h., wind dir and speed, global radiation

Section 6: Detailed report related to overall project duration

8	DNPH cartridges	CH <sub>3</sub> CHO, CH <sub>3</sub> (CO)CH <sub>3</sub>
---	-----------------	--

Table 6.3100.2: Measurements at Bresso during FORMAT 2002.

No.	Instrument	Parameters
2	White system, DOAS	O <sub>3</sub> , NO <sub>2</sub> , SO <sub>2</sub> , HONO
2	Max-DOAS	NO <sub>2</sub> , O <sub>4</sub>
2	Ozone monitor	O <sub>3</sub>
2	NO monitor	NO
2	Spectroradiometer	J of NO <sub>2</sub> , HONO, O( <sup>1</sup> D), HCHO
2	J(NO <sub>2</sub> ) sensor	J (NO <sub>2</sub> )
2	Weather station	T, p, r.h., wind dir and speed, global radiation
2	Sonic anemometer	3D-wind field measurements
2	Aerosol monitor	Particle size distribution, surface, volume, weighted sum of particles
7	FTIR White system	CO
8	DNPH cartridges	CH <sub>3</sub> CHO, CH <sub>3</sub> (CO)CH <sub>3</sub>
8	PTR-MS	benzene, toluene

Section 6: Detailed report related to overall project duration

Table 6.3100.3: Measurements at Alzate during FORMAT 2003.

No.	Instrument	Parameters
1, 2	Longpath-DOAS	O <sub>3</sub> , NO <sub>2</sub> , SO <sub>2</sub> , HONO
2	Radon Monitor	Rn activity
4	Max-DOAS	NO <sub>2</sub> , O <sub>4</sub> , AOD
5	O <sub>3</sub> instrument (UV absorption)	O <sub>3</sub>
5	CO analyser AL5002	CO
5	CRANOX Ecophysics	NO <sub>2</sub> , NO
5	GC Varian	VOCs
5	J(NO <sub>2</sub> ) sensor	J(NO <sub>2</sub> )
5	Meteo station	T, p, r.h., wind dir and speed, global radiation
8	DNPH cartridges	CH <sub>3</sub> CHO, CH <sub>3</sub> (CO)CH <sub>3</sub>

Table 6.3100.4: Measurements at Bresso during FORMAT 2003.

No.	Instrument	Parameters
2	Multibeam Longpath DOAS	O <sub>3</sub> , NO <sub>2</sub> , SO <sub>2</sub> , HONO
2	MAX-DOAS	NO <sub>2</sub> , O <sub>4</sub>
2	Spectral radiometer	J of NO <sub>2</sub> , HONO, O( <sup>1</sup> D)
2	Weather station	T, p, r.h., wind dir and speed, global radiation
2	Aerosol monitor	Particle size distribution, surface, volume, weighted sum of particles
7	FTIR White system	CO, CO <sub>2</sub> , H <sub>2</sub> CO, CH <sub>4</sub> , NO, C <sub>4</sub> H <sub>10</sub> , N <sub>2</sub> O
8	DNPH cartridges	CH <sub>3</sub> CHO, CH <sub>3</sub> (CO)CH <sub>3</sub>
8	GC-MS	VOCs

Table 6.3100.5: Measurements at Spessa during FORMAT 2003.

No.	Instrument	Parameters
2	Multibeam Longpath DOAS	O <sub>3</sub> , NO <sub>2</sub> , SO <sub>2</sub> , HONO
1	Weather station	T, p, r.h., wind dir and speed, global radiation
8	DNPH cartridges	CH <sub>3</sub> CHO, CH <sub>3</sub> (CO)CH <sub>3</sub>

Figures 6.3100.1 and 6.3100.2 depict the time series of the daily average global radiation (average only during daylight hours) as well as the half-hourly average temperature and ozone concentrations measured at Alzate during FORMAT 2002 and FORMAT 2003, respectively. Data in red correspond to fair weather days: days with averaged global radiation exceeding  $350 \text{ W/m}^2$  (for FORMAT 2002) or  $300 \text{ W/m}^2$  (for FORMAT 2003). A lower radiation threshold was chosen for the second campaign as it took place in September, with lower solar declination than during the first campaign, which was conducted mainly in August.

During the 2002 campaign, ozone and temperature usually reached their highest values on the selected fair weather days (see Figure 6.3100.1), with some exceptions like some North Foehn days as it will be explained later. The ozone levels hardly exceeded 80 ppb, concentration considerably lower than expected for this region in summer. These low values are probably due to both the low emissions during the August vacation in Northern Italy and the absence of stable multi-day episodes of fair weather during that campaign.

Much higher ozone concentrations were registered during the 2003 campaign, especially during the period 17-21 September (see Figure 6.3100.2), as a consequence of the stable and warm weather conditions. The ozone concentrations reached 130 ppb on the 19<sup>th</sup>, 20<sup>th</sup> and 21<sup>st</sup> of September 2003. On the 22<sup>nd</sup> September (green colour in the figure), ozone decreased due to a drop in the atmospheric pressure (not shown), followed by less stable weather with lower radiation and temperature than on the previous days. From the 23<sup>rd</sup> September on, the temperatures and the ozone concentrations represented conditions typical for autumn.

The presence of the alpine foothills north of the Alzate measurement site favoured southerly winds during the day and northerly winds at night and in the early morning during both field campaigns. This might lead to the advection of polluted air masses from Milano during the afternoon hours.

North Foehn cases were observed on 7, 12 and 13 Aug 2002, and on 12 Sep 2003. Clean and very dry air masses were advected from North of the Alps to the Po Basin during those events, leading to anomaly low ozone levels considering the temperatures registered on those days.

Section 6: Detailed report related to overall project duration

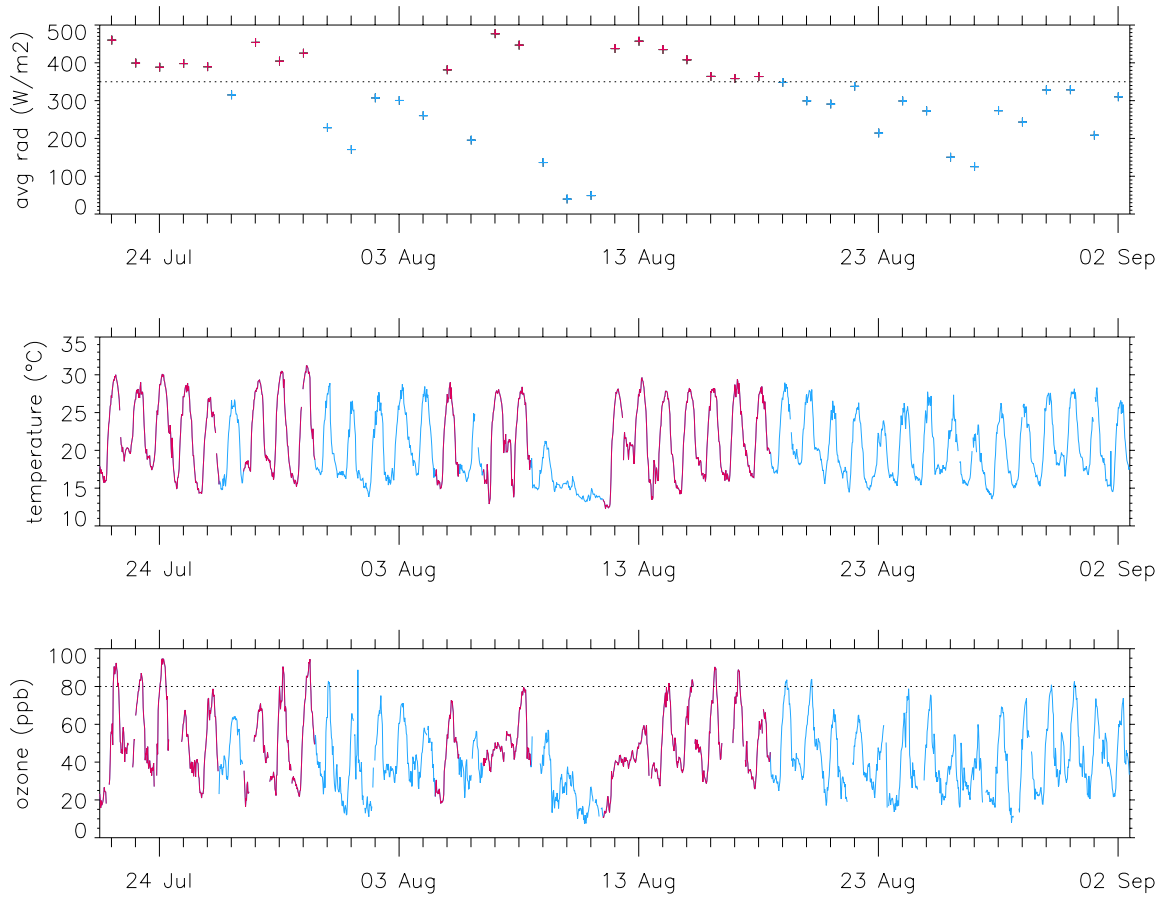


*Figure 6.3100.1. Time series of the daily averaged global radiation (average only during daylight hours) as well as half-hourly temperature and ozone concentrations measured at Alzate during the 2002 campaign. The ticks on the x axes correspond to 12:00 CEST (i.e. UTC+2).*

Section 6: Detailed report related to overall project duration

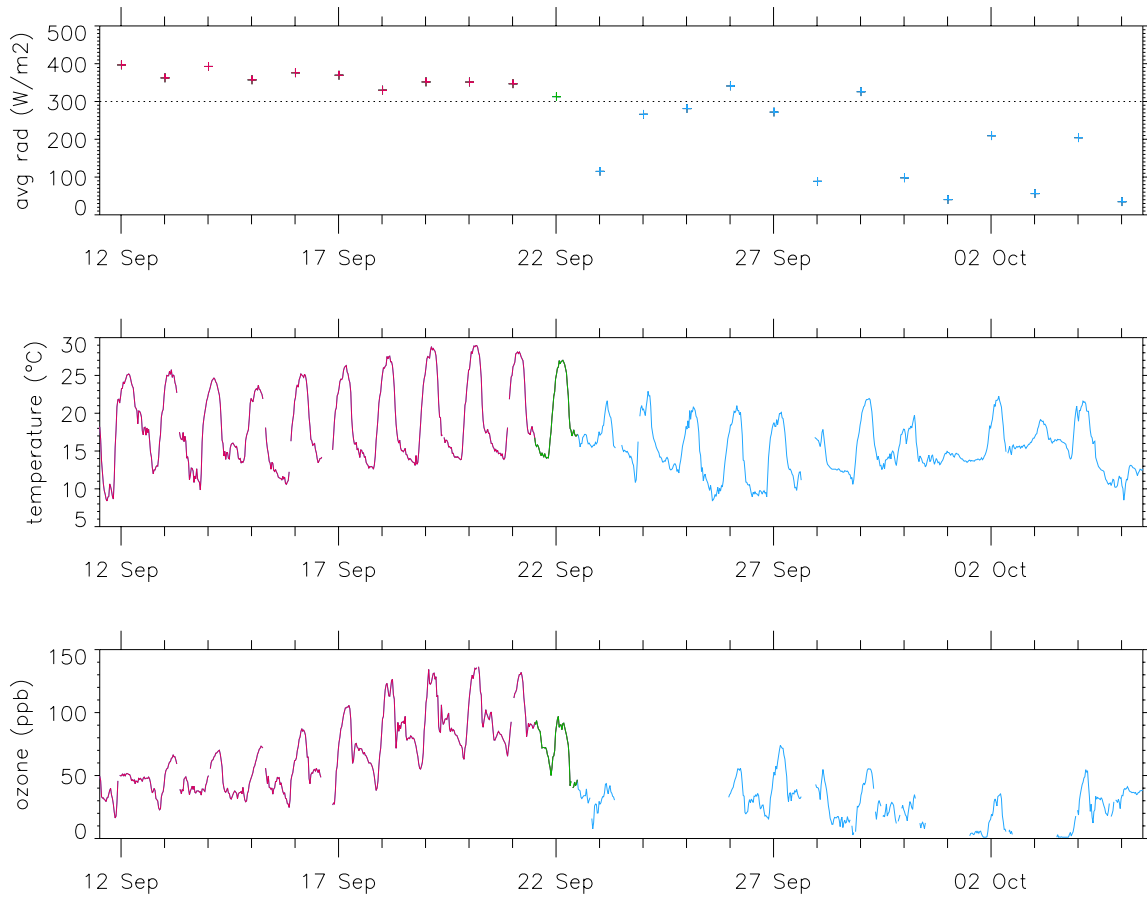


Figure 6.3100.2. Same as Figure 6.3100.1 but for the 2003 campaign.

## 2. Measurements from aircraft and mobile platforms

### Measurements from the Dimona aircraft

After a crash in 2002, the Dimona aircraft could be fixed and operated successfully during the 2003 campaign (see Figure 6.3100.3). The main species measured are included in Table 6.3100.6. Measurements were performed during 13 flights in September. Table 6.3100.7 provides a short overview. During box flights, the aircraft flew around the agglomeration of Milano in order to assess the ambient concentrations of various parameters up-wind and down-wind of Milano. The ferry flights include measurements over the Alps from the home base north of the Alps to the Po basin or the other way around. During the eastward flights, the air quality of the eastern part of the Po basin was probed. During two of these flights, the different aircrafts performed vertical profiles in order to compare the performance of the various instruments on board.

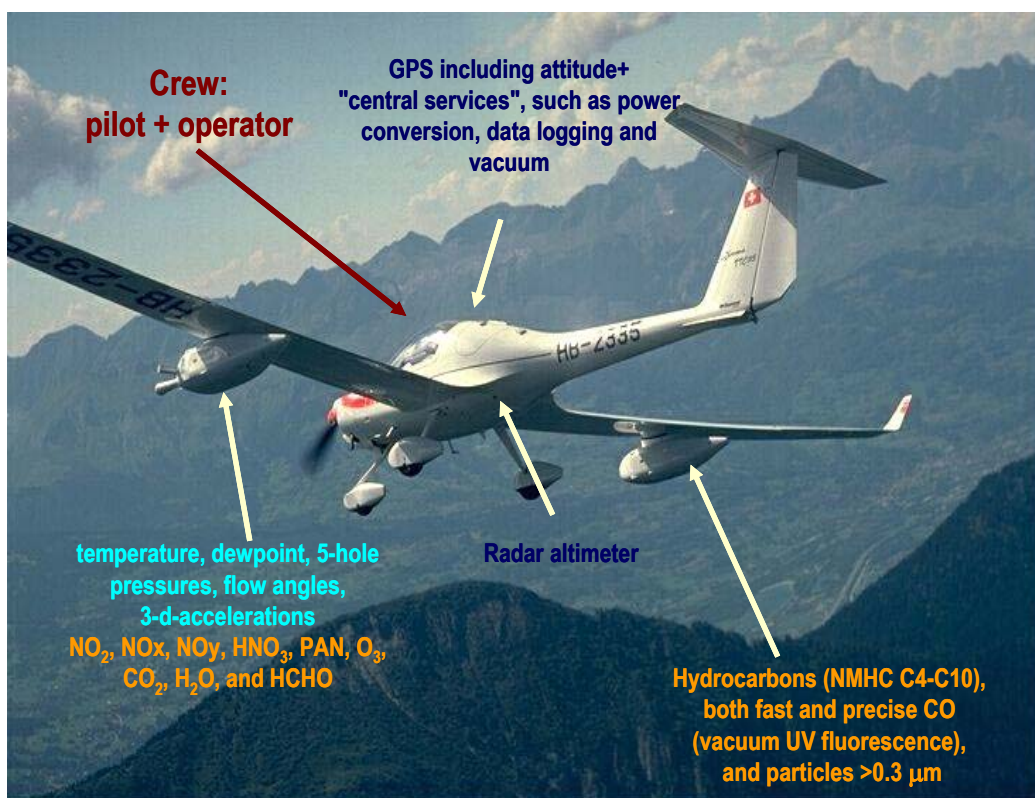


Figure 6.3100.3: Dimona aircraft with the setup of the instruments (with the courtesy of MetAir, subcontractor of PSI, partner 5).

*Table 6.3100.6: Airborne measurements performed by the Dimona during FORMAT 2003.*

No.	Instrument	Parameters
5	Hantzsch monitor	HCHO
5	O <sub>3</sub> instrument (UV absorption)	O <sub>3</sub>
5	NOxTOy instrument (chemiluminescence + NO <sub>y</sub> converter)	NO, NO <sub>2</sub> , NO <sub>x</sub> , PAN, HNO <sub>3</sub>
5	CO analyser AL5002	CO
5	LICOR CO <sub>2</sub> /H <sub>2</sub> O gas analyser (IR absorption)	CO <sub>2</sub> , water vapour
5	Gas Chromatography	VOCs
5	Canisters	VOCs

*Table 6.3100.7: Overview of the Dimona aircraft flights during the second FORMAT campaign, including the different flight patterns.*

Date	Morning	Afternoon
15 Sep. 2003		ferry
16 Sep. 2003		boxes
17 Sep. 2003		boxes
18 Sep. 2003		boxes
19 Sep. 2003	sounding	boxes
20 Sep. 2003	box, ferry back	
25 Sep. 2003	Ferry	eastwards, intercomparison
26 Sep. 2003	Sounding	eastwards
27 Sep. 2003	eastwards, intercomparison	ferry

### Measurements from the microlight aircraft operated by IMK-IFU

Partner 3 (IMK-IFU) operated a microlight aircraft in both campaigns carrying instrumentation listed in [Table 6.3100.8](#) (see also [Figure 6.3100.4](#)). The aircraft operated out of Lecco Monte Marenzo (a small airfield 10 km south of Lecco) in 2002 and out of Spessa (30 km south of Milan) in 2003. Flight patterns for 2002 covered mainly the area north and east of Milano while in 2003 complete circles around Milano were flown. Additional to the horizontal flight legs, the aircraft was used during each flight to perform at least one vertical profile up to ~ 2700 m (the limit of the airspace allowed for visual flying rules) north of Milano between Lecco and Como to probe the vertical structure of the planetary boundary layer. In 2003, vertical profiles up to ~ 1200 m were also investigated south of the Po river to check the homogeneity of the planetary boundary layer thickness in the observation area. Between Lecco / Como and Spessa the airspace restrictions above 2000 ft (~ 600 m) prevent further vertical flight profiles.

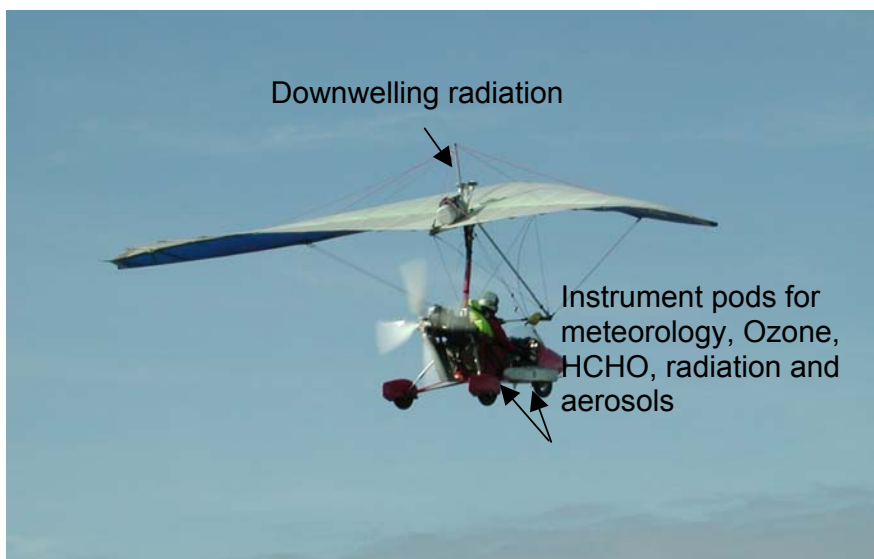


*Fig 6.3100.4: The microlight aircraft with instrument pods and radiation sensors.*

*Table 6.3100.8: Airborne measurements performed by the microlight during FORMAT 2003.*

No.	Instrument	Parameters
3	Hantzsch monitor	HCHO
3	O <sub>3</sub> instrument (UV absorption)	O <sub>3</sub>
3	TSI 3010 counter	Particles (number) > 10 nm < 1 um
3	Grimm 1.108 Spectrometer	Particle size distribution > 300 nm – <15 um 15 size bins
3	Actinic Filtradiometers	Actinic UV-radiation at 300 nm and 380 nm, up and downwelling hemispheres, JO1D and JNO2
3	LICOR Pyranometers	Global radiation balance
3	Chilled Mirror	Temperature, dewpoint

The vertical structure of the lower troposphere was rather different during the two campaigns. In 2002 the vertical structure of the troposphere north of Milano was characterized by humid convective conditions with a lower surface layer up to about 1200 m, topped by cumulus clouds extending up to 3000 m, with strong production of haze and aerosols between the clouds. Often it was not possible to reach the free troposphere with the 9000 ft (~ 2800m) limit of the open airspace. In 2003, with more stable conditions, a cleaner layer without direct exchange with surface air was typically reached in about 1500 m often with additional residual aerosol layers. Typical situations are shown in [Figure 6.3100.5](#).



*Figure 6.3100.5: Typical meteorological conditions for 2002 (left) and 2003 (right) above the flat terrain and the first mountain range north of Milano.*

An overview about the microlight flights of both campaigns is given in WP 1400, airborne measurements using the Hantzsch Technique. Besides the additional instrumentation on the aircraft, IMK-IFU supplied a spectrophotometer (MICROTOPS III) for measurements of the ozone column density and the aerosol optical depth. This instrument was operated in 2002 at Alzate by partner 4 (Univ. of Bremen) for quasi-continuous diurnal measurements, and in 2003 by partner 3 for three soundings per day at the locations of the three ground stations during the daily maintenance of the HCHO monitors.

### **SOF mobile measurements by CTH**

A mobile FTIR system denoted SOF (Solar Occultation Flux) was applied for the first time by Chalmers University for vertical column measurements of CO, in addition to measurements of H<sub>2</sub>CO, as described in WP 1000. By alternating between fixed positions around the Milano area, information was gained about both diurnal and spatial variations. In total there were around 10 days with measurements in 2002 (summer campaign) and 22 days in 2003 (winter campaign). The measurements in 2002 were less good due to instrumental problems and little emphasis has therefore been put on this year in the final analysis. In 2003, 5 days were used for diurnal variation studies in Bresso and 14 for spatial column variation studies. The available CO data corresponds to the same as for HCHO, as shown in WP 1000.

The conditions in the Milano area during the campaign were such that the height of the meteorological mixing layer was a few hundred meters above the ground in the morning hours, raising to 1.2-1.5 km during the day. The ground concentration of CO and HCHO, primarily originating from traffic emissions, was increasing in the morning hours but then rapidly decreased due to the dilution effect caused by the increase of the mixing layer height, as can be seen in Figure 6.3100.6. This was not the case for the SOF column measurements since these are insensitive to the dilution in the vertical plane. In theory, the columns of CO should actually increase over the day, as long as there is no inflow of clean air, i.e. horizontal advection. As long as the boundary layer is not significantly diluted, the ratio between the mixing ratio and column should correspond to the mixing height. In this case the mixing height can be estimated to about 2 km at 11:00, when the columns were at their maximum.

Figure 6.3100.7 depicts measurements of CO and HCHO conducted around Milano and in the mountains towards Como on October 6, 2004. The measurements at 1150 m altitude show that the background of CO and HCHO corresponds to  $1.8 \cdot 10^{18}$  molec/cm<sup>2</sup> and  $4 \cdot 10^{15}$  molec/cm<sup>2</sup>,

respectively. In the upper layer over 500 m the CO column drops  $2.7 \cdot 10^{17}$  molec/cm<sup>2</sup>, and this corresponds to approx 200 ppb of CO. Around the Milano area the CO column is much more variable. For HCHO the drop in the upper layer between 500 m and 1000 m corresponds to an average mixing ratio of about 1.5 ppb.

SOF measurements of CO and HCHO both north and south of Milano at varying altitudes are shown in Figure 6.3100.8. Linear regression fits to the data are included in the figure, indicating that the average CO concentration in the Po valley is  $3 \cdot 10^{12}$  molec/cm<sup>3</sup>, or 120 ppb.

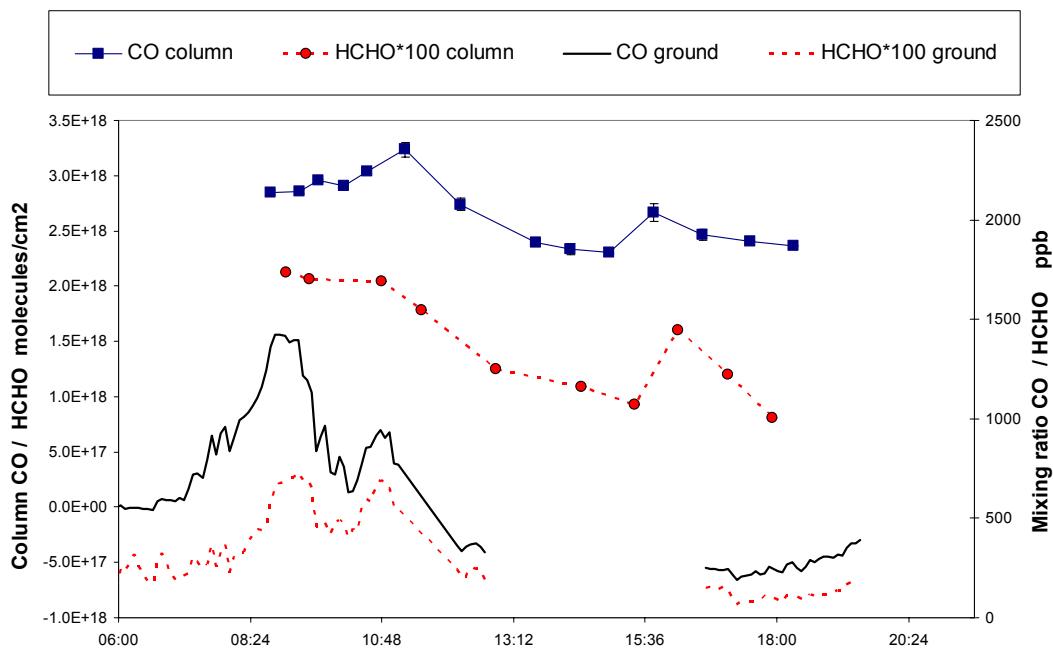


Figure 6.3100.6. Columns and ground mixing ratios of CO and HCHO from the SOF and the Whitecell instrument. The measurements were conducted at Bresso airfield on Sep 22, 2004. The drop in columns is probably caused by advection, since there was a change in the weather conditions (drop in the atmospheric pressure followed by a frontal passage) in the afternoon of this day.

Section 6: Detailed report related to overall project duration

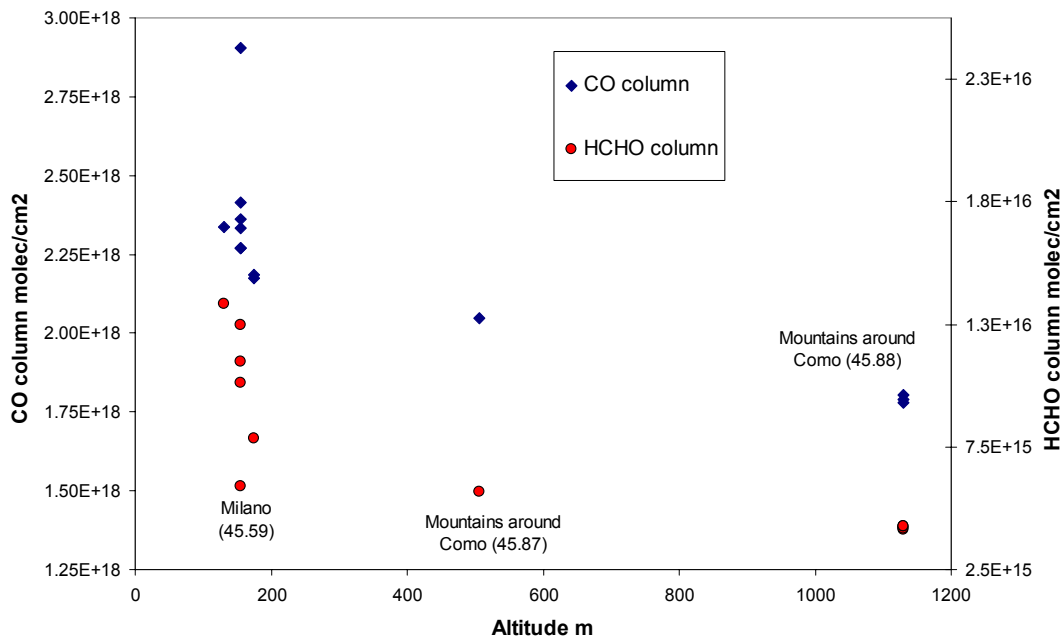


Figure 6.3100.7. Columns of CO and HCHO measured by SOF around Milano and in the mountains towards Como, on October 6, 2004.

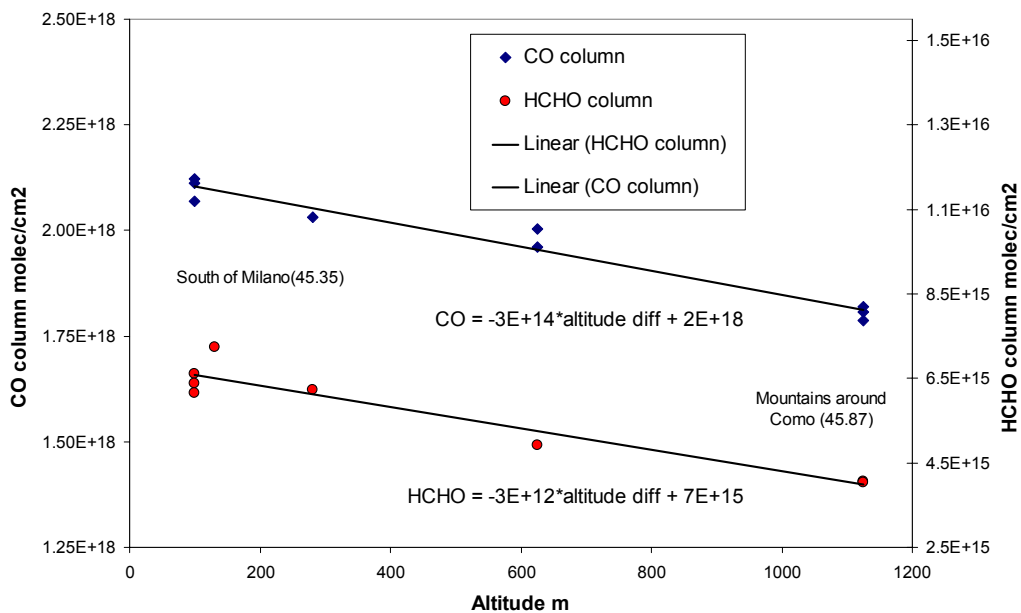


Figure 6.3100.8. Columns of CO and HCHO on October 8, 2004, obtained by SOF. The measurements were conducted both south and north of the Milano area at different altitudes.

In addition to measurements of the CO columns on many places along the Po valley emission measurements were also conducted. On one occasion the SOF system was used to measure columns of formaldehyde and CO in the centre of the plume from a burning grass field, and as explained in WP 1000 a crude estimate of the CO emissions were  $20\text{ mg s}^{-1}\text{ m}^{-2}$ . Emission measurements using the SOF technique were also tried at a refinery, Sannazzaro De' Burgondi. Due to unfavorable

## Section 6: Detailed report related to overall project duration

weather conditions total emission estimates could not be made. Significant VOC columns of up to 160 mg/m<sup>2</sup> were observed however.

The ongoing results of this analysis will be included in the manuscript [Mellqvist et. al., in prep., planned for submission to *Atm. Chem. Phys.*].

### References

Mellqvist, J., Samuelsson, J., Strandberg, A., Galle, B., Ordóñez, C, Prevot, A.S.H., Junkerman W., Wagner, T., Neiniger, B. Temporal and spatial distribution of CO and HCHO columns using mobile solar FTIR, on-road and flight measurements, and model calculations 2002-2003, in prep., for ACP.

### Measurements from the PSI mobile van

In addition to what was planned in the work plan, HCHO and CO simultaneous measurements (see [Table 6.3100.9](#)) were performed with the Paul Scherrer Institute (PSI) mobile pollutant measurement laboratory during the 2003 FORMAT field campaign. These measurements allowed for the estimation of HCHO/CO emission ratios.

*Table 6.3100.9: On-road measurements performed by the PSI mobile lab on 4 days during the second FORMAT campaign: 19, 20, 25 and 26 September 2003.*

No.	Instrument	Parameters
5	Hantzsch monitor	HCHO
5	CO analyser AL5002	CO

## WP 3200: Analysis of the measurements

This workpackage includes analyses of the measurements from WP 3100. Data from the field campaigns of August 2002 and September 2003 were used. In order to put the data into perspective of existing data, measurements of 1998 were also taken into account for some of the analyses.

### 1. Ozone and HCHO levels in 1998, 2002, and 2003

During the FORMAT campaign 2002, considerably lower ozone and HCHO concentrations than in PIPAPO 1998 were found. In addition, the slopes of the linear regressions of the afternoon ozone and HCHO concentrations against temperature were rather small in FORMAT 2002 (see [Figure 6.3200.1](#)). Theoretically, this could have been interpreted as a downward trend in the pollutant concentrations. However, the ozone and HCHO data in September 2003, measured with much more stable meteorological conditions than in August 2002, show similar values to those ones of 1998. This leads to the conclusion that the low ozone and HCHO levels of August 2002 were most probably due to both the low emissions during the August vacation in Italy and the absence of multi-day episodes of fair weather during that campaign.

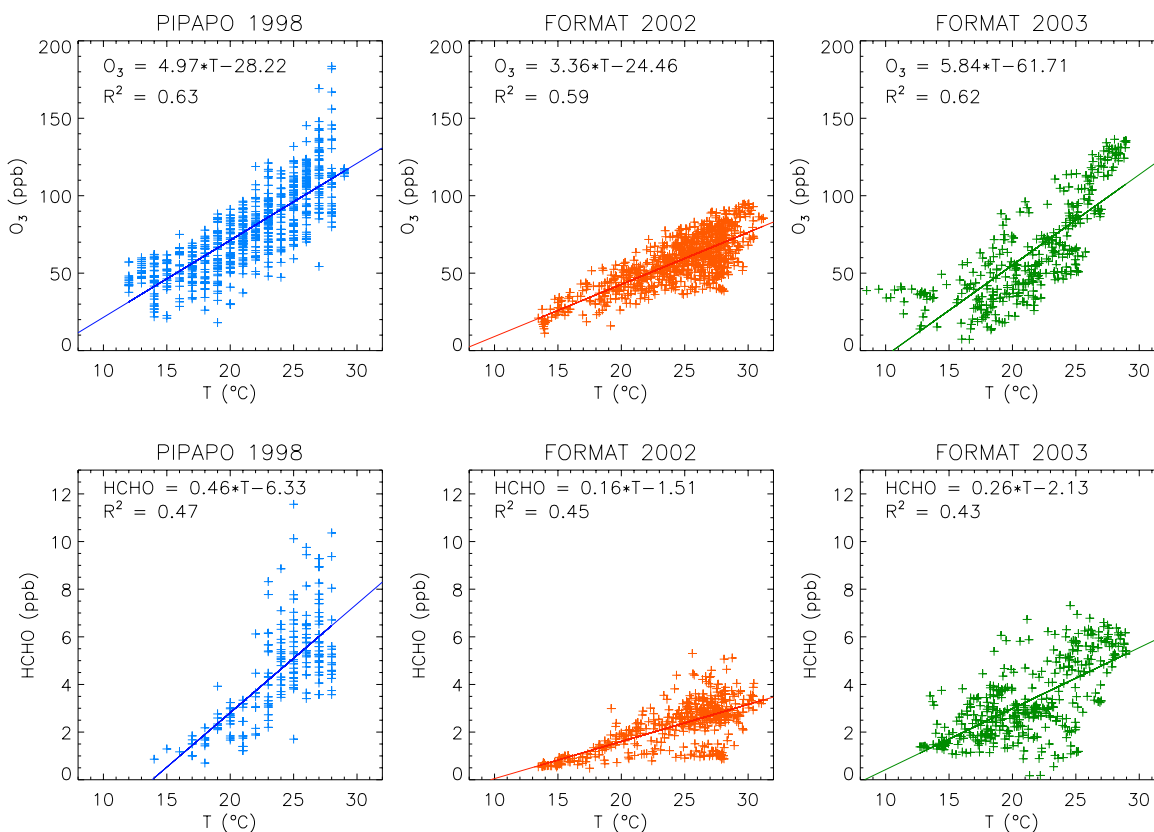


*Figure 6.3200.1: Regression of the afternoon ozone and HCHO concentrations against temperature for three field campaigns: PIPAPO 1998 (May-Jun), FORMAT 2002 (Jul-Aug), and FORMAT 2003 (Sep-Oct).*

## 2. Analysis of VOC data in Alzate

### Anthropogenic VOCs

Measurements at Alzate during the field campaigns PIPAPO 1998, FORMAT 2002, and FORMAT 2003, as well as measurements from some fixed stations (Direzione Generale Qualità dell'Ambiente, Regione Lombardia) close to roads, showed the significant impact of the weekend and the vacation time on the concentrations of anthropogenic VOCs. Low toluene concentrations as well as low toluene to benzene ratios were found at weekends compared to weekdays (see [table 6.3200.1](#)) and during August compared to July and September (see [table 6.3200.2](#)), as a consequence of the low anthropogenic emissions due to less traffic and reduced industrial activities in those periods. In addition, no cyclohexane peaks were found at weekends.

*Table 6.3200.1: Mean ( $\pm$  standard error of the mean) toluene to benzene ratios at Alzate on weekdays, Saturdays, and Sundays, for three different campaigns.*

Campaign	toluene/benzene ratio		
	Weekday	Saturday	Sunday
PIPAPO 1998	3.77 $\pm$ 0.04	2.84 $\pm$ 0.07	2.30 $\pm$ 0.03
FORMAT 2002	3.26 $\pm$ 0.11	2.89 $\pm$ 0.08	2.57 $\pm$ 0.07
FORMAT 2003	3.35 $\pm$ 0.11	3.21 $\pm$ 0.11	2.13 $\pm$ 0.08

*Table 6.3200.2: Mean afternoon (10 AM to 6 PM) toluene and benzene mixing ratios (in ppb), and toluene to benzene ratios for July and August. %: obtained from the Direzione Generale Qualità dell'Ambiente, Regione Lombardia, \*: 22 July to 04 August 2002,  $\nabla$ : 05 August to 25 August 2002. Como, Monza, and Milano data were available from 1996 - 2003, 2000 - 2003, and 2001 - 2002, respectively.*

Station	July			August		
	tol	benz	tol/benz	tol	benz	tol/benz
Como <sup>%</sup>	8.5	1.9	4.8	6.6	1.5	4.4
Monza <sup>%</sup>	7.5	1.5	7.1	4.7	1.1	5.3
Milan <sup>%</sup>	3.9	1.1	3.5	2.4	0.9	2.7
Verzago	0.8*	0.3*	3.9*	0.6 $\nabla$	0.3 $\nabla$	2.3 $\nabla$

### Biogenic VOCs

Isoprene is emitted by plants and is often a very important precursor of formaldehyde. The isoprene measurements at Alzate exhibited a bimodal diurnal cycle with high concentrations in the morning and evening. This diurnal cycle might seem inconsistent with the isoprene emissions (see [Figure 6.3200.2](#)), which were estimated with the Guenther algorithm [Guenther et al., 1993]. This algorithm considers the isoprene emissions only as a function of light and temperature, due to the light- and temperature-dependent activity of the isoprene producing enzyme. Time series of the main products of the isoprene degradation – methyl vinyl ketone (MVK) and methacrolein (MACR) – showed rising concentrations shortly after the isoprene morning peak (see [Figure 6.3200.2](#)). This

supports that the photochemical influence was at least partly responsible for the isoprene decay at noontime. The second isoprene peak in the late afternoon was not followed by an increase of MVK + MACR as it would be expected if the isoprene + OH reaction was the dominant process of the nighttime isoprene decay. A box model was used to analyse around 40 days from the campaigns PIPAPO 1998, FORMAT 2002 and FORMAT 2003. This analysis showed that the reaction of isoprene with the NO<sub>3</sub> radical is the most important factor for the isoprene degradation in the evening. The main features of the diurnal cycles of isoprene have been reproduced with a 3-dimensional model calculation (Figure 6.3200.3).

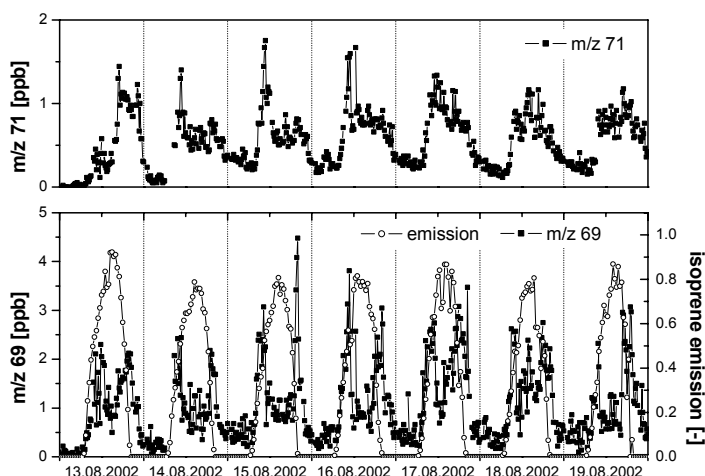


Figure 6.3200.2. Isoprene mixing ratios (*m/z* 69), estimated isoprene emissions according to the Guenther algorithm [Guenther et al., 1993], and methyl vinyl ketone + methacrolein mixing ratios (*m/z* 71) for a 7-day period in 2002.

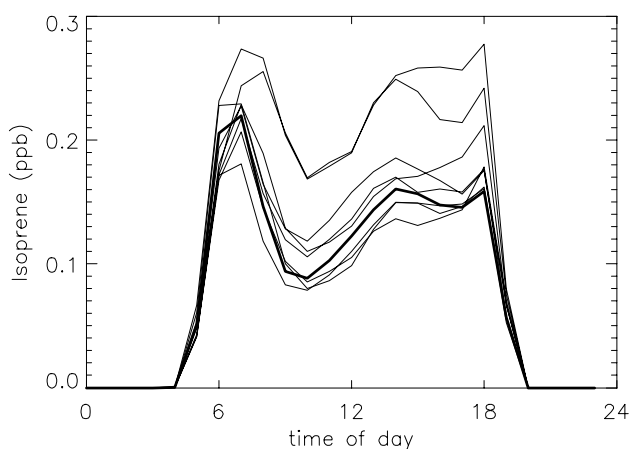


Figure 6.3200.3. Diurnal cycle of isoprene for Alzate (bold line) and 8 adjacent grid cells modelled with a 3-D Eulerian model for a clear day.

Another important biogenically emitted molecule at this site is methanol. In contrast to most of the previous publications that reported methanol emissions driven by temperature and stomatal conductance [MacDonald and Fall, 1993], solar radiation [Das et al., 2003], or due to cutting [Das

## Section 6: Detailed report related to overall project duration

*et al.*, 2003, *Warneke et al.*, 2002], considerable methanol peaks were observed at Alzate during several nights at the end of August 2002. The very high methanol concentrations, with very high variations (probably due to emission bursts), were most probably of local origin as they were found during the night with low wind speed and high relative humidity.

More details on the analysis of anthropogenic and biogenic VOCs at Alzate can be found in [*Steinbacher et al.*, 2005a] and [*Steinbacher et al.*, 2005b], respectively. The interpretation of these VOC patterns forms an important basis to investigate the production of formaldehyde from different VOCs and the role of formaldehyde as an intermediate of the VOC oxidation in the boundary layer.

### References

Das M., Kang D., Aneja V. P., Lonneman W., Cook D. R., Wesely M. L.: Measurements of hydrocarbon air-surface exchange rates over maize, *Atmospheric Environment* 37, 2269-2277, 2003.

Guenther, A. B., Zimmerman, P. R., Harley, P. C., Monson, R. K., Fall, R.: Isoprene and Monoterpene Emission Rate Variability: Model Evaluation and Sensitivity Analyses, *Journal of Geophysical Research*, 98 (D7), 12609-12617, 1993.

MacDonald R. C., Fall R.: Detection of Substantial Emissions of Methanol from Plants to the Atmosphere, *Atmospheric Environment* 27A (11), 1709-1713, 1993.

Steinbacher, M., Dommen, J., Ordóñez, C., Reimann, S., Grüebler, F. C., Staehelin, J., Prévôt, A. S. H.: Volatile organic compounds in the Po Basin. Part A: anthropogenic VOCs, *Journal of Atmospheric Chemistry*, 2005a, in press.

Steinbacher, M., Dommen, J., Ordóñez, C., Reimann, S., Grüebler, F. C., Staehelin, J., Andreani-Aksoyoglu, S., Prévôt, A. S. H.: Volatile organic compounds in the Po Basin. Part B: biogenic VOCs, *Journal of Atmospheric Chemistry*, 2005b, in press.

Warneke C., Luxembourg S., de Gouw J. A., Rinne H. J. I., Guenther A. B., Fall R.: Disjunct eddy covariance measurements of oxygenated volatile organic compounds fluxes from an alfalfa field before and after cutting, *Journal of Geophysical Research* 107 (D8), art.-no.: 4067, 10.1029/2001JD000594, 2002.

### 3. Receptor modelling for source apportionment of ozone precursor hydrocarbons in Bresso

The results on VOC measurements during the September 2003 campaign demonstrate how combined ambient air monitoring of an urban air mass and vehicle emission measurements (obtained from the JRC laboratories) of individual C<sub>2</sub>-C<sub>9</sub> hydrocarbons specified in the Ozone Directive 2002/3/EC can be used as the basis for source apportionment with multivariate receptor modelling.

The results of semicontinuous analysis of ozone precursor hydrocarbons in air and vehicle exhaust with cryogen-free, on-line sampling and dual column Deans' switch chromatography point to the fact that the C<sub>2</sub> and C<sub>3</sub> hydrocarbons together with aromatic compounds are the main ozone precursors. The used method proved to be a robust and practical (cryogen-free) technology for on-line monitoring of ozone precursors in field and laboratory applications at the levels required for both ambient air and vehicle emission testing.

The use of two multivariate receptor models – chemical mass balance (CMB) and positive matrix factorization (PMF) – which are fundamentally different and complementary, is essential for the source apportionment of ozone precursor hydrocarbons. One (CMB) initiates its calculations from the assumed knowledge of the main source profiles for the Bresso air mass and calculates their contribution to the air pollution. The other (PMF) takes its starting point in the statistical analysis of the variability in the ambient air concentration data and identifies latent variables (factors) consisting of co-varying hydrocarbons, which in this study could be attributed to the major emission sources, namely gasoline exhaust (30-38%), gasoline evaporation (17-26%), diesel exhaust (13-16%) and natural gas leakage (around 8%) (see Figure 6.3200.4). Both CMB and PMF rely on an estimated uncertainty for each input data. The successful source apportionment calculations were attained through the use of a new approach, by which the uncertainty is allowed to float as function of the photochemical reactivity of the atmosphere and the stability of each individual compound.

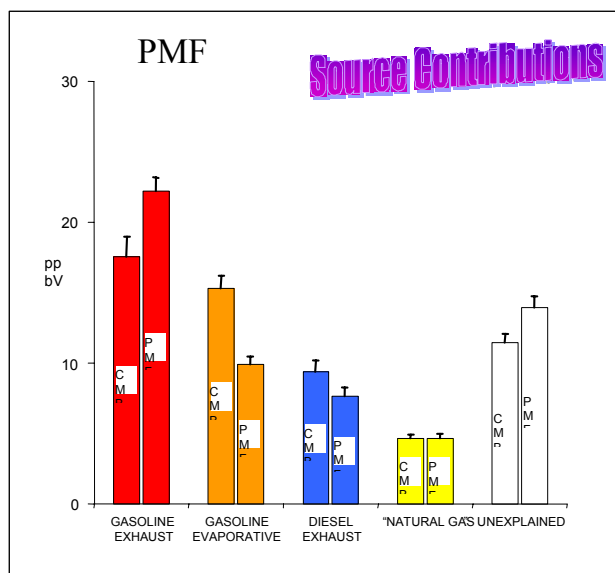


Figure 6.3200.4. Source contribution estimates (mean  $\pm$  95% confidence interval) from chemical mass balance (CMB) and positive matrix factorization (PMF) modelling of 163 VOC measurements in Milano (Bresso), September 2003.

Section 6: Detailed report related to overall project duration

The maximum incremental reactivity calculation of the potential ozone formation of the emitted ozone precursor hydrocarbons points to a 50% contribution to the ozone in the Bresso air mass by gasoline vehicles and 25% by diesel vehicles (Figure 6.3200.5).

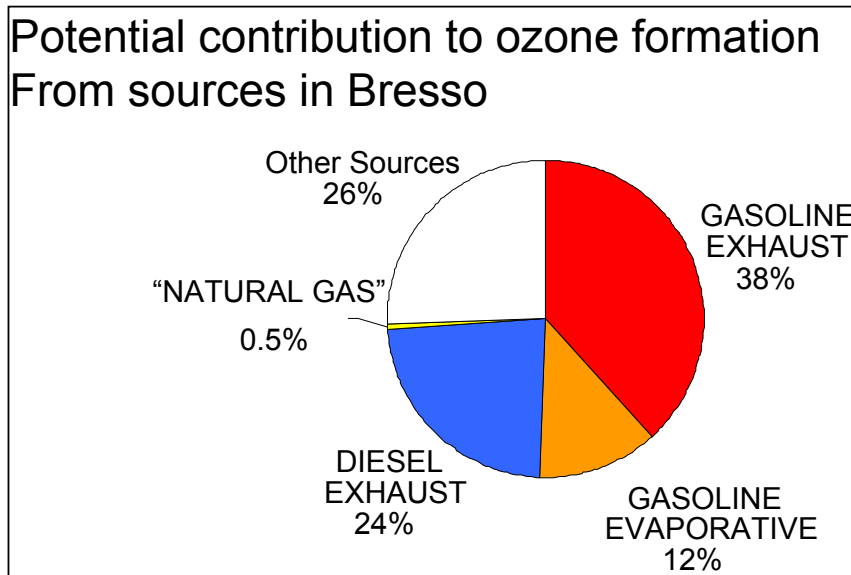


Figure 6.3200.5. Potential contribution to ozone formation calculated from the maximum incremental reactivity approach.

#### 4. Vertical structure of the boundary layer as derived from the microlight flights

The vertical structure of the planetary boundary layer can be derived from different parameters available from the microlight aircraft. Basic meteorological information like temperature and dewpoint allows calculating the potential temperature within the profile and thus gives numbers about a possibility to mix air masses in a certain altitude region. That does not guarantee that this mixing is actually happening or tells us anything about the time constants for mixing. It can be used to define the absolute height of the polluted boundary layer. Additionally the distribution of water vapour and small and large particles can be used. Very small particles in the accumulation mode (~ 50 to 200 nm) are typically related to ground based sources like car exhaust or biomass burning. Biomass burning injects particles into an otherwise stable atmosphere in elevations of a few hundred meters where they can produce distinct aerosol layers unless thermal convection destroys these layers again. Thus the vertical distribution of ultrafine particles provides information about the intensity of the vertical exchange processes within the planetary boundary layer (PBL). This is especially important within FORMAT as sources of HCHO are often identical to sources of small particles. It is relevant for budget considerations as well as for air mass factor calculations.

As an example the vertical profiles of dewpoint, potential temperature and small particles are given in Figure 6.3200.6. All vertical profiles were flown in the central Po Valley, in an area ~ 30 km east of Milano, close to Cremona and Mantova. While all the dewpoint profiles – with the exemption of the first profile from 10:00 in the morning – show no restriction up to 1500 m, the potential temperature profiles allow mixing up to this altitude only for the last profile in the late afternoon (pink colour in the figure). This is reflected in the aerosol profiles of small particles that show a pronounced stratification with several different layers until the early afternoon and homogeneity only in the late afternoon. On September 27 (Figure 6.3200.7.), with further stabilization of the high pressure conditions, the aerosol extends up to 1500 m in the north and 1200 m in the south of the Po Valley. However, according to the potential temperature profile, thermodynamically no mixing is possible above 500 m. The aerosol layers observed above 500 m are residuals from the previous day with no exchange with the surface layer.

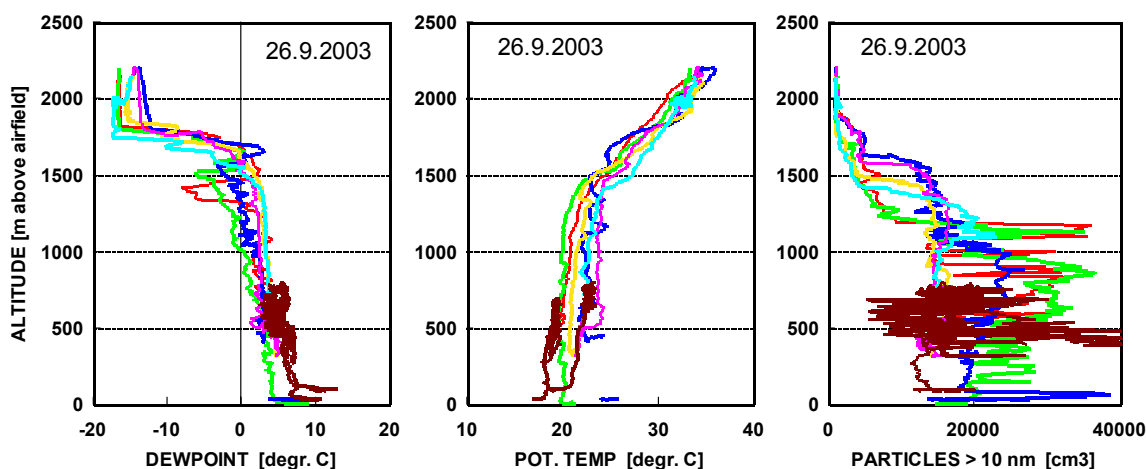
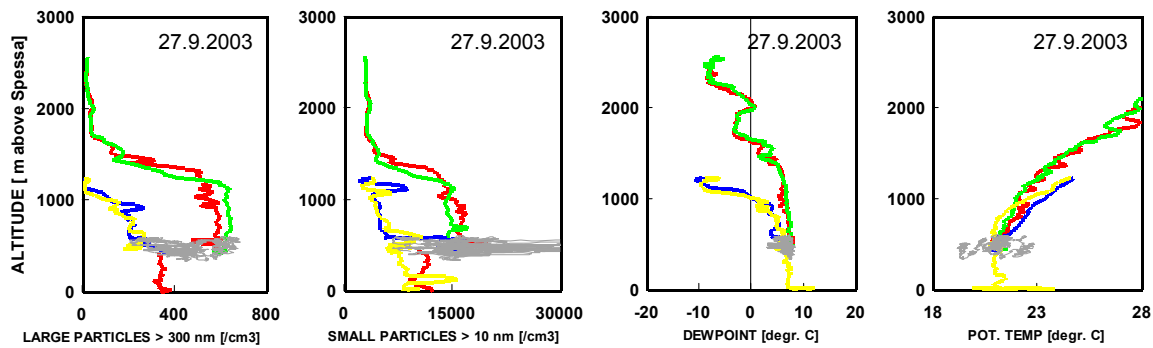


Figure 6.3200.6. Vertical profiles of dewpoint, potential temperature and small particles during a flight from Spessa to Montagnana in the morning (from 9:00 to 11:00 UTC) and back in the afternoon (13: 00 - 17:00 UTC). The brown lines indicate the data during horizontal flight legs between Spessa and Montagnana. The only profile that allows vertical mixing up to 1500 m during that day is the last one (descent close to Cremona, pink).

The apparent difference between the vertical distributions north and south of Milano may have several reasons. In the north, flying higher than 2000 ft (~ 600 m) is allowed only close to the mountains that reach about 2000 m. Although upslope effects are unlikely due to the potential temperature profile they cannot be excluded. More probably the profiles are generated by regional diurnal flow and horizontal advection patterns between the flat terrain and the mountains. A tilted upper rim of the planetary boundary layer with higher altitudes towards the mountain is a general pattern that is observed during alpine pumping events. However, that would require higher wind speeds close to the ground than observed in both campaigns in the valleys south of Lecco and Como. A heat island (<http://eetd.lbl.gov/HeatIsland/>) above Milano could also break the boundary layer topping inversion and inject particles into higher elevations where they would be horizontally transported.



*Figure 6.3200.7. Vertical profiles of large and small particles, dewpoint, and potential temperature during a flight from Spessa around Milano on September 27, 2003. Grey colour indicates data during horizontal flight legs between Spessa and Lecco and between Como and Spessa. No vertical mixing possible above 500 m. Red and green are profiles over Lecco and Como (north), blue and yellow are profiles south of Spessa (south). The high numbers of small particles during the horizontal legs were recorded during passage of biomass fires.*

#### *Horizontal distribution of particles*

Occasionally, higher numbers of small particles are observed in the north than in the south of the observing area but this distribution was not a general feature. The frequent fires all over the agricultural areas were a large contribution to the particle budget in the south. These local emissions can compensate fully for the lower population density and traffic density of the north.

## 5. North–south gradients in the distribution of pollution from airborne measurements.

During box flights performed in the second FORMAT campaign, the Dimona aircraft flew around the agglomeration of Milano in order to assess the ambient concentrations (at around 500-800 m altitude a.s.l.) of various species up-wind and down-wind of Milano. Due to the prevailing southerly wind direction during the day, higher concentrations were generally measured North ( $\sim 45.7^\circ\text{N}$ ) than South ( $\sim 45.2^\circ\text{N}$ ) of the Milano metropolitan area during the afternoons, as seen in [Table 6.3200.3](#) and [Figure 6.3200.8](#). Low pollutant concentrations are observed north of  $45.8^\circ\text{N}$  in the figure as the aircraft had to fly at an altitude higher than 1000 m over that area due to the presence of the Alpine Crest.

Aircraft measurements carried out in the summers of 1992 and 1993 already showed very high ozone concentrations with high spatial variability south of the Alps in the afternoon. Those ozone levels were extraordinarily high in comparison with the typical levels measured North of the Alps, and they were found 3-5 hours downwind of Milano during summer smog situations [Prévôt et al., 1997].

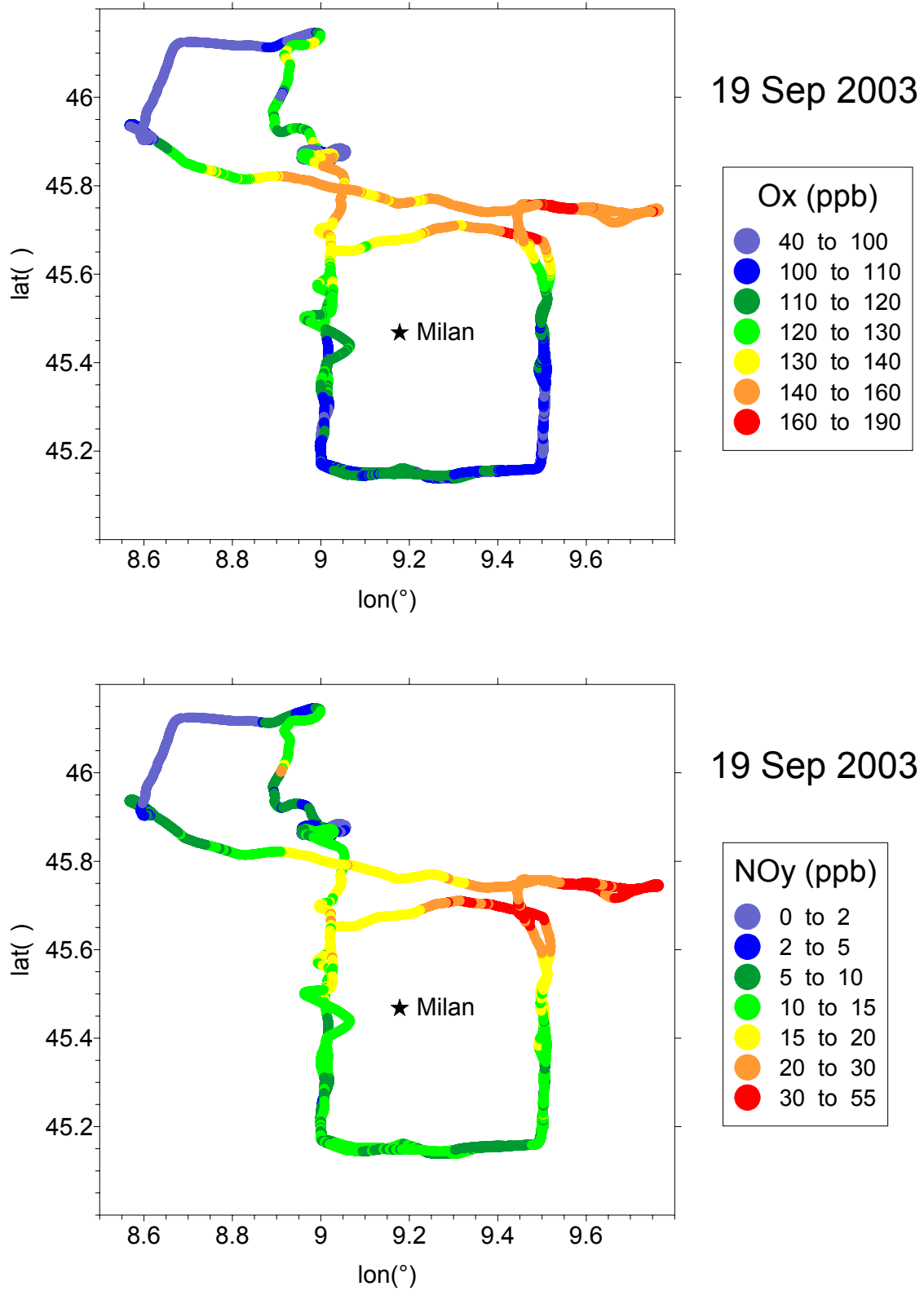
**Table 6.3200.3:** Average measured concentrations of  $\text{O}_x$ ,  $\text{NO}_y$ , and CO around Milano on afternoon flights in September 2003.

day	$\text{O}_x$ (ppb)		$\text{NO}_y$ (ppb)		CO (ppb)	
	South	North	South	North	South	North
15 Sep	62 <sup>(*)</sup>	63.2 <sup>(*)</sup>	--	--	168	202
16 Sep	84	105	6	25	182	341
17 Sep	88	113	8	15	216	331
18 Sep	113	134	9.7	24.6	227	419
19 Sep	110	153	10	28.6	239	473

<sup>(\*)</sup>  $\text{O}_3$  instead of  $\text{O}_x$  on 15 Sep.

### References

Prévôt, A. S. H., J. Staehelin, G. L. Kok, R. D. Schillawski, B. Neiningner, T. Staffelbach, A. Neftel, H. Wernli, J. Dommen: The Milano photooxidant plume, *J. Geophys. Res.*, 102(D19), 23375-23388, 10.1029/97JD01562, 1997.



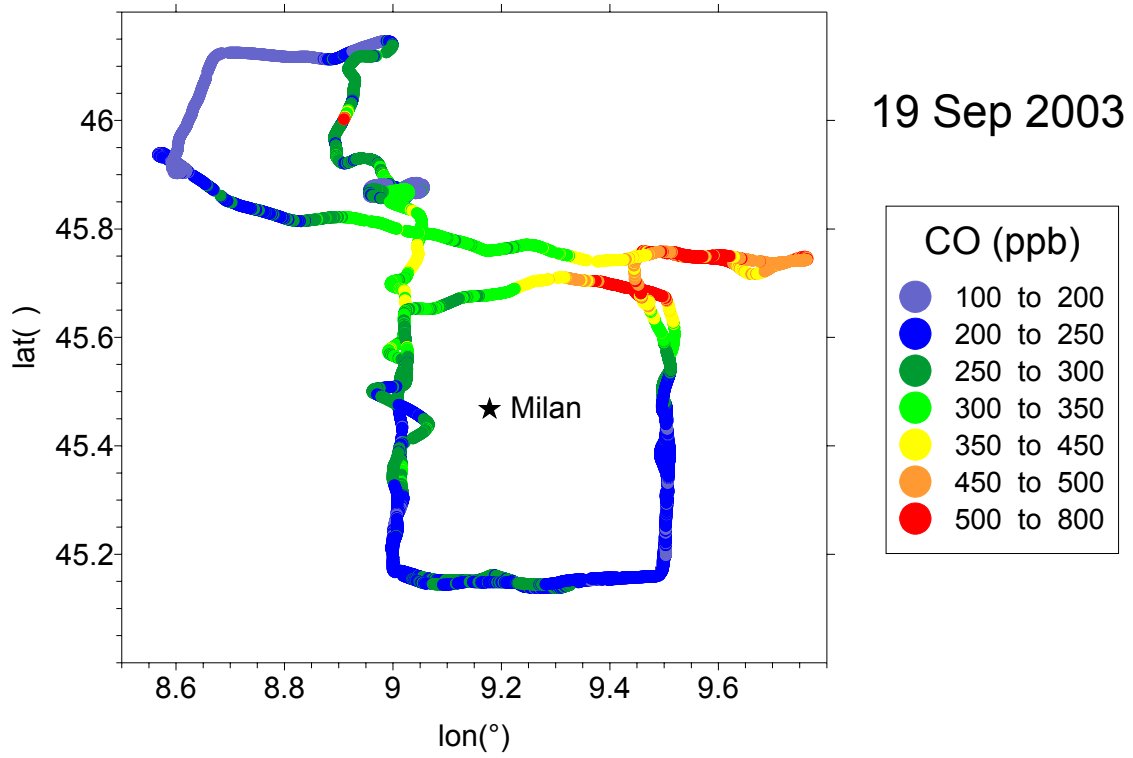


Figure 6.3200.8 c: CO concentrations measured during an afternoon flight on 19 Sep 2003.

## 6. Vehicle emission factors and secondary production of HCHO derived from open path FTIR measurements

### Vehicle emission factors

In addition to HCHO, continuous 5-minute averages of CO, CO<sub>2</sub>, NO, CH<sub>4</sub>, and alkane mass were measured with a 1km open path Whitecell FTIR in Bresso 2003. CO is a good tracer compound for combustion sources, and vehicle emissions were the dominant source in Milano. By correlating the measured compounds to CO for evening rush hour periods after sunset (19:30-00:00), fuel based primary emission factors could be derived, as presented in Table 6.3200.4. Table 6.3200.5 summarizes the mass emission factors with relation to CO, along with their standard deviation and number of readings. Emission factors for alkenes and aromatics (BTEX) have been calculated based on the VOC characterization in Bresso by JRC, applying mass fraction factors relative to alkanes, to the alkane mass reading obtained with the open path FTIR (CTH). For the studied evening rush hours there were 27 GC-MS samples taken by JRC, showing a VOC mass fraction of 47% alkanes, 20% alkenes and 33% aromatics.

Table 6.3200.4. Fuel based primary emission factors from vehicles.

	Emission g/g fuel	Emission g/l avg fuel <sup>a)</sup>
CO	$3.5 \cdot 10^{-2}$	$2.7 \cdot 10^1$
CO <sub>2</sub>	3.1	$2.3 \cdot 10^3$
H <sub>2</sub> CO	$9.5 \cdot 10^{-5}$	$7.2 \cdot 10^{-2}$
NO	$3.4 \cdot 10^{-3}$	2.6
CH <sub>4</sub>	$6.7 \cdot 10^{-3}$	5.0
Alkanes	$3.6 \cdot 10^{-3}$	2.7
Alkenes <sup>b)</sup>	$1.5 \cdot 10^{-3}$	1.1
BTEX <sup>b)</sup>	$2.5 \cdot 10^{-3}$	1.9

<sup>a)</sup> Assumes a fuel consumption of 23% diesel and 77% gasoline, and fuel densities as  $\rho_{\text{citydiesel}} = 817 \text{ kgm}^{-3}$  and  $\rho_{\text{gasoline}} = 738 \text{ kgm}^{-3}$  (Shell Sweden 2003).

<sup>b)</sup> Calculated from the alkane emission factor and the VOC fractionation among alkanes, alkenes and BTEX by JRC.

Table 6.3200.5. Mass emission factors obtained by open path FTIR at Bresso.

Mass emission factors	CO:CO <sub>2</sub>	H <sub>2</sub> CO:CO	NO:CO	CH <sub>4</sub> :CO	Alkanes <sup>a)</sup> : CO	Alkenes: CO <sup>b)</sup>	BTEX:CO <sup>b)</sup>
Average	$1.1 \cdot 10^{-2}$	$3.27 \cdot 10^{-3}$	$9.6 \cdot 10^{-2}$	$1.9 \cdot 10^{-1}$	$1.1 \cdot 10^{-1}$	$4.5 \cdot 10^{-2}$	$7.8 \cdot 10^{-2}$
STD	$6.4 \cdot 10^{-4}$	$6.4 \cdot 10^{-4}$	$3.2 \cdot 10^{-2}$	$1.1 \cdot 10^{-2}$	$2.0 \cdot 10^{-2}$		
No. of days	8	10	10	4	11		
R <sup>2</sup>	0.75-0.9	0.51-0.95	0.72-0.97	0.62-0.63	0.85-0.99		

<sup>a)</sup> Adjusted for 12.8% overestimation by the FTIR reading compared to the GC-MS speciation by JRC.

<sup>b)</sup> Calculated using alkane to CO mass emission ratio and the VOC fractionation among alkanes, alkenes and aromatics by JRC.

Compared to the on road emission factors for HCHO of 0.0023 (ppb HCHO/ppb CO) for light duty vehicles and 0.0074 for heavy duty vehicles reported by PSI, the FTIR open path measurements in Bresso give a vehicle fleet average emission factor of 0.0025 (ppb HCHO/ppb CO). This is well in agreement also with the downtown Milano HCHO/CO ratio of 0.0029 ppb/ppb obtained by PSI.

The obtained results are included in the manuscript [Samuelsson et. al., in prep., planned for submission to *Atm. Chem. Phys.* in 2005].

### Secondary production of formaldehyde

Using the emission factor for HCHO/CO of 0.0025 (ppb/ppb) derived from dark rush hour measurements in Bresso, a rough estimate of the secondary + background fraction of total formaldehyde can be calculated, as in Equation 1. This assumes that all CO above background is related to formaldehyde by the emission factor. The observed excess HCHO is then either due to secondary formation or background advection. Since formaldehyde has a lifetime of only a few hours during sun light hours, this would be a lower estimate of the secondary + background HCHO fraction.

$$\frac{\text{HCHO}_{\text{Secondary+Background}}}{\text{HCHO}_{\text{total}}} = 1 - 0.0025 \frac{(\text{CO} - \text{CO}_{\text{background}})}{\text{HCHO}_{\text{total}}}$$

(Equation 1)

Major sources of CO with another emission factor for HCHO than the observed, or strong primary sources of HCHO would complicate the picture a lot. However, no such strong sources were evident in the concentration time series, and the HCHO to CO correlation during rush hours were fairly strong. [Figure 6.3200.9](#) shows the estimated secondary + background fraction of the total formaldehyde, as observed by ground level (CTH) and flight (PSI) measurements. A CO background of 170 ppb has been used. The sensitivity of the secondary + background fraction estimate to CO background level in the afternoon is fairly low. During sunny days the formaldehyde present in the afternoon was estimated to origin by around 90% from secondary production (including background advection).

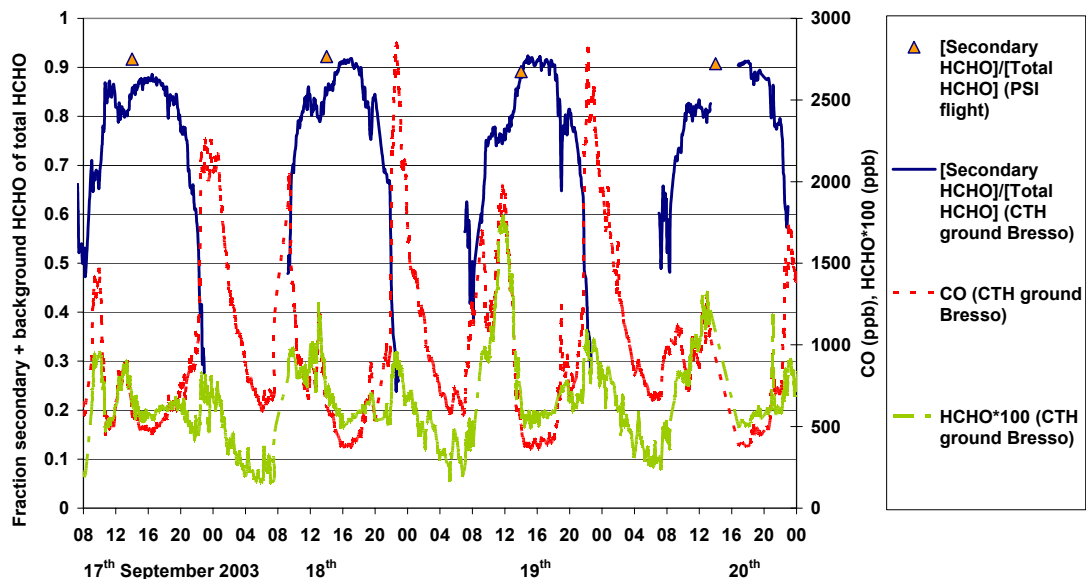
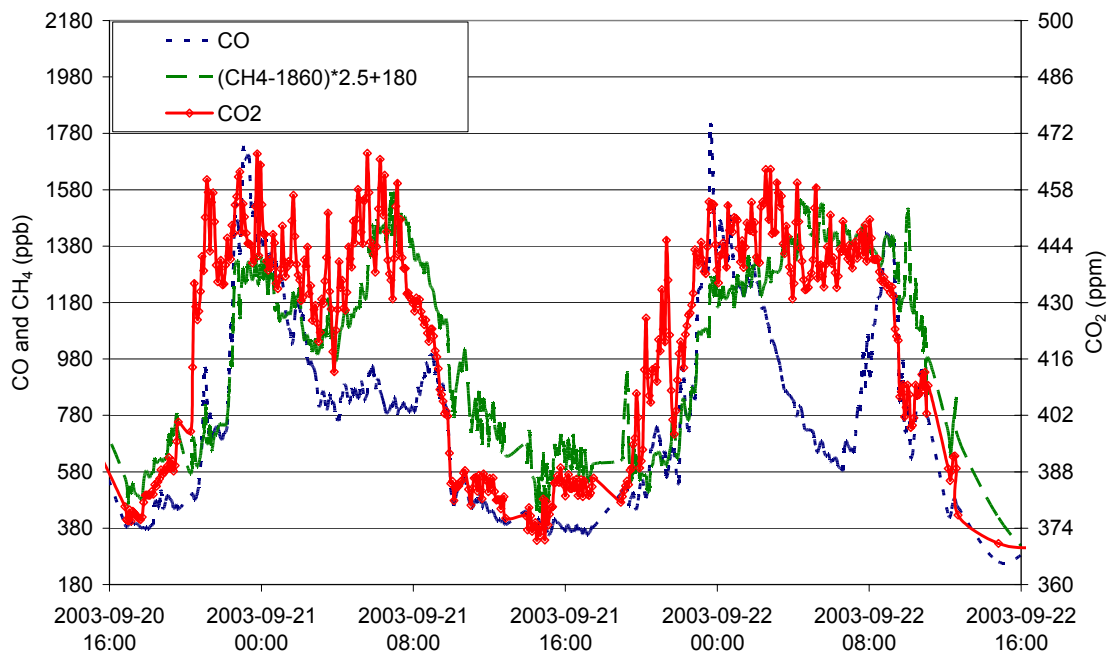


Figure 6.3200.9. Fraction of secondary produced HCHO (including background advection) to total HCHO, as observed by ground level measurements and flight measurements.

### Additional observations

In addition to vehicle emissions, a strong source of  $\text{CO}_2$  and  $\text{CH}_4$  was observed during the FTIR measurements in Bresso 2003. Figure 6.3200.10 shows a two-day time series of  $\text{CO}$ ,  $\text{CO}_2$  and  $\text{CH}_4$ . Parts of the emissions correlate with combustion sources as traced by  $\text{CO}$ . During nighttime continuously elevated concentrations of  $\text{CO}_2$  and  $\text{CH}_4$  were observed, although  $\text{CO}$  was cleaned out by advection and reduced emissions. The suggested source might be landfills located within Milano, supplying fresh emissions into the nighttime boundary layer. Close to the measurement site in Bresso there are old landfills areas, covered with soil and grass in which a large part of the landfill methane is likely to be oxidized to  $\text{CO}_2$  by microbial activity, explaining the relatively strong  $\text{CO}_2$  signal. This source complicated the vehicle emission factor calculation for  $\text{CO}_2$  and  $\text{CH}_4$ , as morning and evening boundary layer height changes sometimes coincided with the rush hour.



*Figure 6.3200.10. Two-day time series of the CO, CO<sub>2</sub> and CH<sub>4</sub> concentrations measured by FTIR at Bresso. Note the apparent CO<sub>2</sub> and CH<sub>4</sub> source obvious during nighttime, when combustion related emissions are cleaned out but methane and carbon dioxide remain high.*

## References

Samuelsson, J., Mellqvist, J., Galle, B., Ordóñez, C., Prévôt, A.S.H., Astorga, C., Larsen, B., Junkermann, W., Hak, C., Neininger, B. Primary and secondary formaldehyde and fuel based emission factors in Milano obtained by long path FTIR, on-road and flight measurements 2002-2003, in prep., for ACP.

## 7. Analysis of the HCHO variability in the context of the VOC measurements

The main source of secondary HCHO is the oxidation of VOCs. Therefore, the HCHO variability might be approximated by the average VOC and OH radical content of the air, under the condition that the NO availability is not an important limiting factor.

VOC measurements from the Dimona aircraft during two field campaigns – PIPAPO 1998 and FORMAT 2003 – were used to explain the temporal and spatial variability in the afternoon HCHO concentrations both around the Milano metropolitan area and within the Po valley. The flight altitude was around 600 - 700 m a.s.l. most of the time and only data below 1000 m a.s.l. were used in the analysis. Different predictor variables dealing with formaldehyde production were used to explain the HCHO variability.

The sum of OH reactivities of a mixture of 10 VOCs including isoprene ( $R_{\text{voc}}$ ), given by their respective concentrations multiplied by their OH reaction rates, explains 45% of the observed HCHO variance during PIPAPO 1998 (Figure 6.3200.11 a). The varying availability of the OH radicals must also be considered. Since ozone photolysis is the major source of OH radicals in the afternoon, the reactivity is multiplied by the ozone concentration in a second step. This term explains 58% of the variance in the HCHO concentrations (Figure 6.3200.11 b). The orange markers denote data points from a flight on 13 May 1998, a day with particularly low humidity but high ozone concentrations. These data points are not in line with those from other days. The reactivity weighted VOCs multiplied by the ozone concentration and specific humidity gives then a measure of the VOCs oxidised with the available OH radical concentration. In addition,  $J(\text{O}^1\text{D})$  should be included in the analysis. However,  $J(\text{O}^1\text{D})$  is more or less proportional to  $J(\text{HCHO})$ , which is an important sink of HCHO. This might be the reason why the radiation does not need to be taken into account for the approximation of HCHO. The data points in Figure 6.3200.11 c fall more closely onto a line than in Figures 3.7.1 a, b. The term seems to be an appropriate predictor for the observed HCHO variability, explaining 65% of the variance. The remaining variance might be due to unconsidered sources like primarily emitted HCHO, VOCs not included in the analysis or possible errors in the measurements.

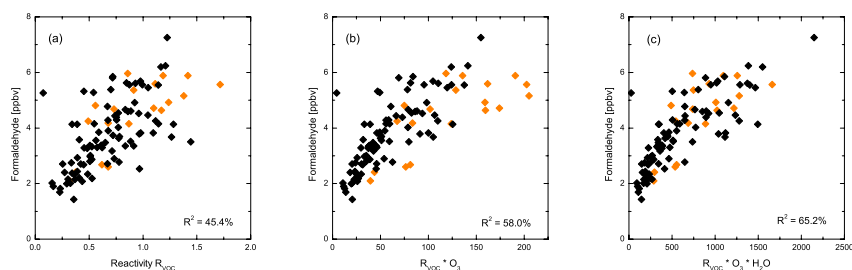


Figure 6.3200.11. Scatterplots of the measured HCHO concentrations vs. (a) OH-reactivity weighted VOCs ( $R_{\text{voc}}$ ), (b)  $R_{\text{voc}} \cdot [\text{O}_3]$  and (c)  $R_{\text{voc}} \cdot [\text{O}_3] \cdot [\text{H}_2\text{O}]$ .

The linear orthogonal regression parameters derived from Figure 6.3200.11c are used to estimate the HCHO concentrations:

$$HCHO_{est} = 1.99 + 0.002964 \cdot react$$

where

$$react = R_{VOC} \cdot [O_3] \cdot [H_2O]$$

The time series of estimated and measured HCHO concentrations is shown in [Figure 6.3200.12](#). The differences between measured and predicted HCHO concentrations vary depending on the flight altitude, the time of day or the measurement region. The largest deviations were found for air samples taken around the region of Locarno. In the region of study (around Milano) the estimated values deviated up to around 15-20% from the measured ones.

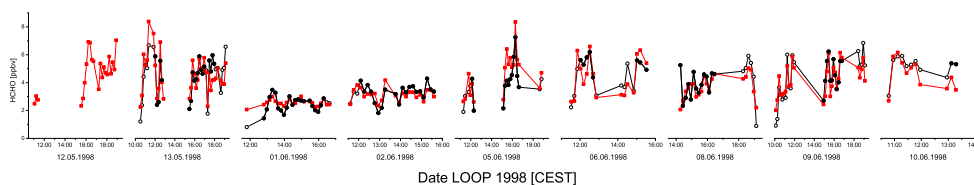


*Figure 6.3200.12. Time series of measured (black) and predicted (red) HCHO concentrations from aircraft measurements during the PIPAPO campaign in 1998. The symbols representing the measurements are empty if the conditions of the analysis – time between 12-17 CEST and flight altitude < 1000 m – are not met.*

The same analysis was done for aircraft measurements from the FORMAT 2003 campaign. The term  $R_{VOC}$  accounts for 63% of the HCHO variability, while more than 77% of the variance is explained by weighting with the  $O_3$  concentration. However, weighting by specific humidity did not improve the results. The linear orthogonal regression gives the relationship:

$$HCHO_{est} = 2.11 + 0.006843 \cdot react$$

Overall, the measured HCHO concentrations are reproduced very well ([Figure 6.3200.13](#)). There is some underestimation during the first part of the flight on 18 September, while values are slightly overestimated on the following day. The largest deviations from the measured concentrations are observed for high flight altitudes. On average, the deviations were within  $\pm 10\%$  for the first 6 flights. During the last 3 flights, with much lower HCHO concentrations, a 30% deviation from the measured values is found. [Figure 6.3200.14](#) shows that we have found a good way of explaining the spatial distribution of HCHO. It obviously depends on the amount of VOCs,  $O_3$  and water vapour in the air. The open question that remains is why we find a different slope for the data in 1998 and 2003.

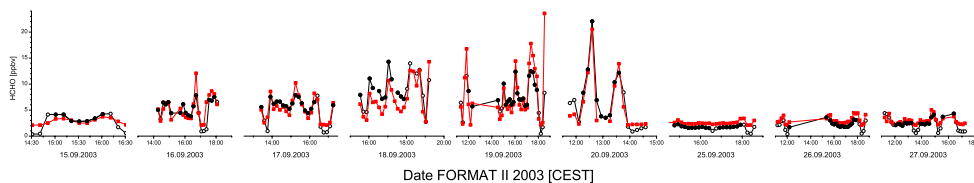


*Figure 6.3200.13. Same as [Figure 6.3200.12](#) but for the FORMAT campaign in 2003.*

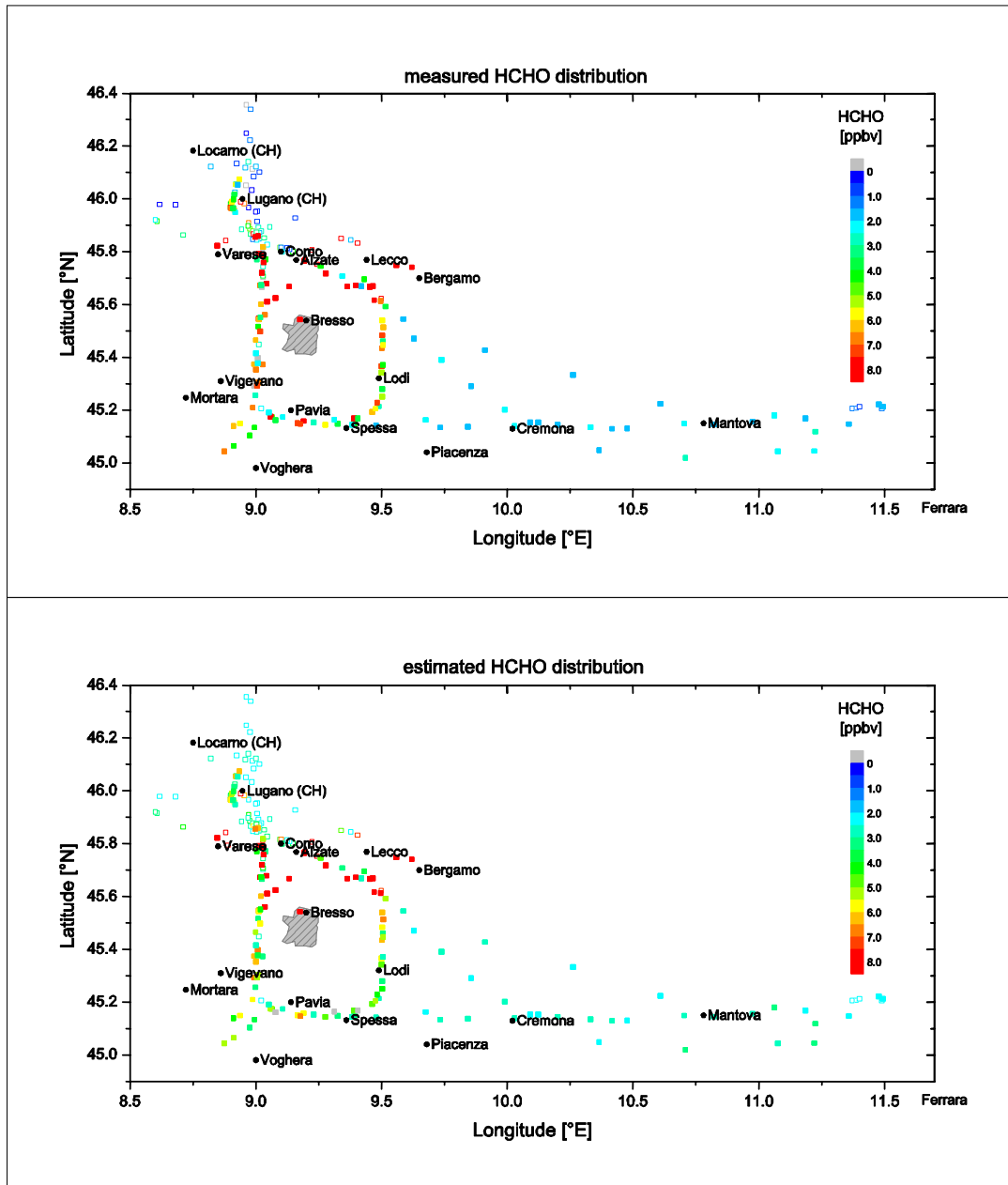


Figure 6.3200.14. Spatial variability of measured (top) and estimated (bottom) HCHO during the flights performed in the 2003 FORMAT campaign. The grey hatched area represents Milano.

## 8. Comparison of NO<sub>2</sub> data from GOME with ground-based measurements

Tropospheric NO<sub>2</sub> vertical column densities (VCDs) retrieved from measurements of the GOME (Global Ozone Monitoring Experiment) spectrometer [Burrows *et al.*, 1999] for the period 1996–2002 were compared with in situ measurements of NO<sub>2</sub> at around 100 ground stations in the Lombardy region. The ground stations were first grouped into 5 categories according to their pollution levels: clean (1), slightly polluted (2), average polluted (3), polluted (4) and heavily polluted (5). The tropospheric NO<sub>2</sub> VCDs were reasonably well correlated with the near surface measurements under cloud free conditions (cloud fraction lower than 0.2). However, the slope of the tropospheric VCDs versus ground measurements was higher in autumn-winter than in spring-summer (Figure 6.3200.15, left panel). This is a consequence of the interferences of conventional NO<sub>x</sub> analyzers – equipped with molybdenum converter – towards peroxyacetyl nitrate (PAN) and nitric acid (HNO<sub>3</sub>), which leads to an overestimation of the NO<sub>2</sub> ground-based measurements, especially when measuring photochemically aged air masses during the warm months [e.g. Winer *et al.*, 1974; Grosjean and Harrison, 1985]. This effect was clearly reduced when those interferences were estimated and taken into account (Figure 3.8.1, right panel).

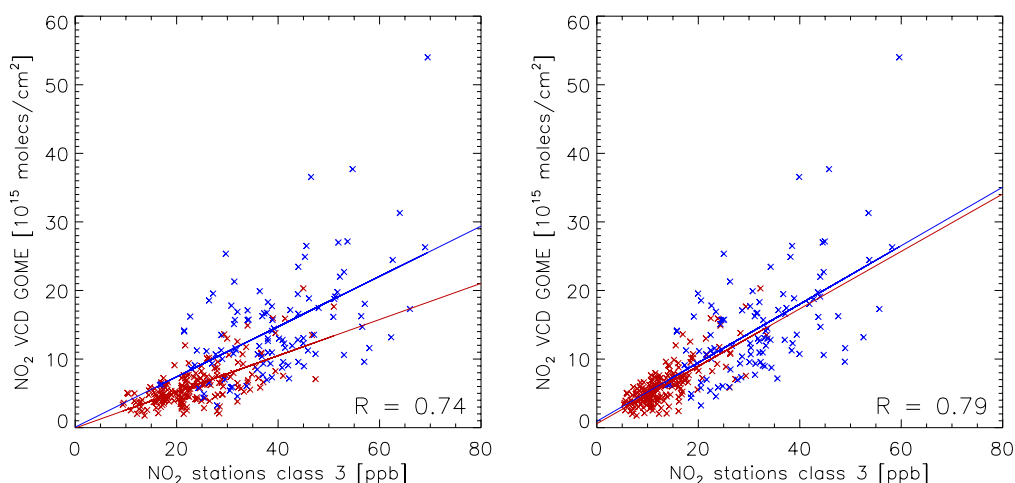


Figure 6.3200.15. Left panel: Tropospheric NO<sub>2</sub> VCDs from GOME vs. the median of the NO<sub>2</sub> mixing ratios from uncorrected in situ measurements at a group of 33 average polluted stations, for days with cloud fraction lower than 0.2. Data during winter-autumn are depicted in blue while red color is used for the spring-summer months. Right panel: Same as left panel after correcting the ground-based NO<sub>2</sub> measurements for the interference of conventional NO<sub>x</sub> analyzers towards PAN, HNO<sub>3</sub> and other interfering species.

For a more quantitative intercomparison, the NO<sub>2</sub> ground measurements were rescaled to tropospheric VCDs using a seasonal NO<sub>2</sub> vertical profile over Northern Italy calculated by a MOZART-2 (Model of Ozone And Related Tracers) run [Horowitz *et al.*, 2003]. The tropospheric VCDs retrieved from satellite and those determined from ground measurements agree well, with a correlation coefficient  $R = 0.78$  and a slope close to 1 for slightly polluted stations (Figure 6.3200.16). GOME cannot reproduce the high NO<sub>2</sub> amounts over the most polluted stations, mainly due to the large spatial variability in the distribution of pollution within the large GOME footprint (320 km x 40 km). The yearly (Figure 6.3200.17) and weekly (Figure 6.3200.18) cycles of the tropospheric NO<sub>2</sub> VCDs were similar for both data sets, with significantly lower values in the summer months and on Sundays, respectively.

Section 6: Detailed report related to overall project duration

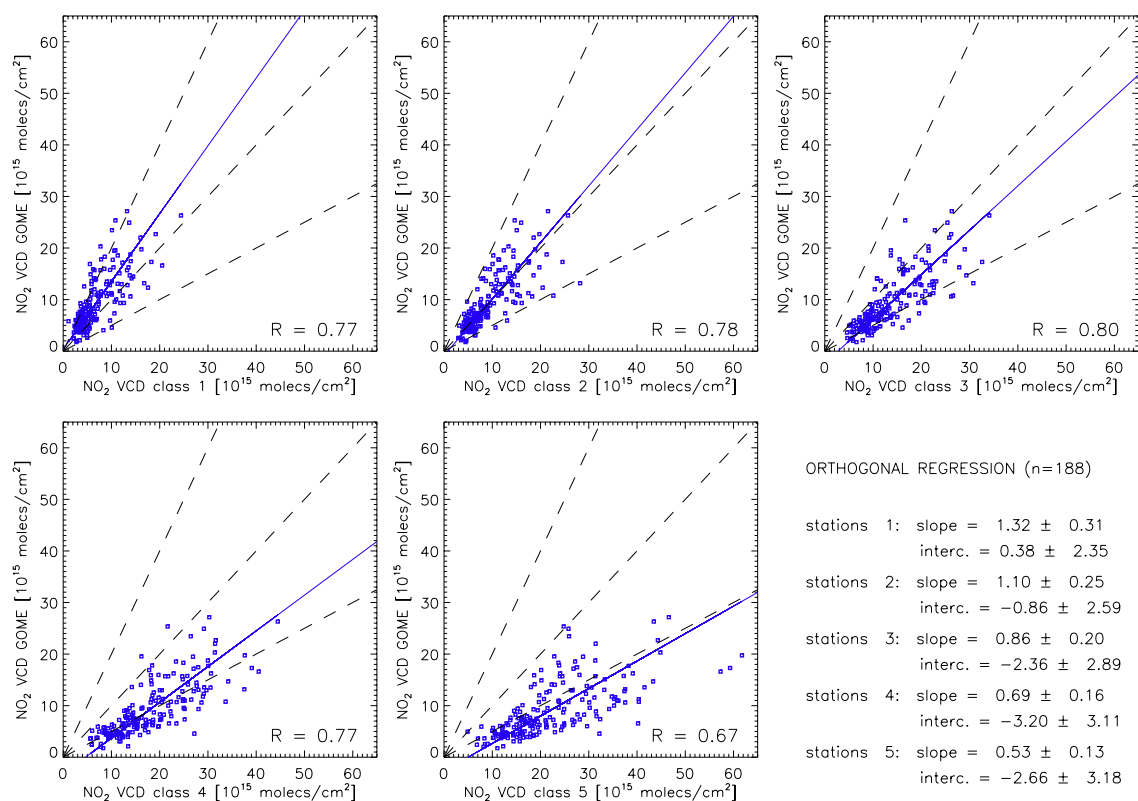


Figure 6.3200.16. Tropospheric  $\text{NO}_2$  VCD from GOME vs. tropospheric  $\text{NO}_2$  VCD from near-surface measurements at the 5 groups of stations (see text) for 188 days under cloud free conditions (cloud fraction lower than 0.1) during 1996-2002. Dashed lines represent the 1:2, 1:1 and 2:1 lines. The slopes and intercepts of the orthogonal regression lines are given together with their 95% confidence intervals.

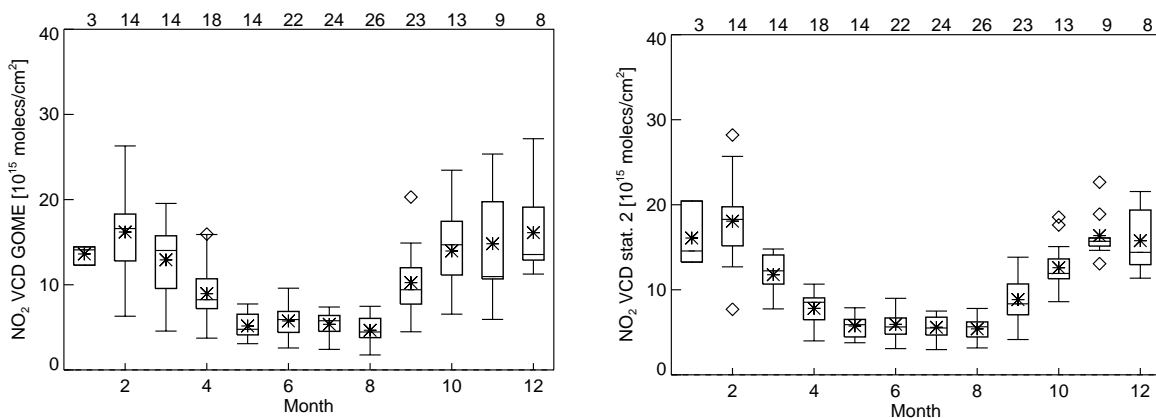
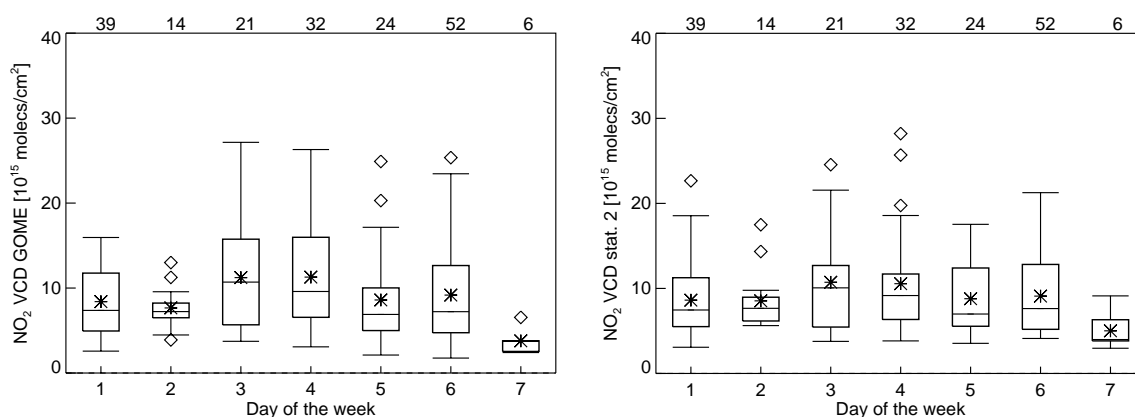


Figure 6.3200.17. Yearly evolution of (a) tropospheric  $\text{NO}_2$  VCD from GOME and (b) tropospheric  $\text{NO}_2$  VCD from near-surface measurements at the 2<sup>nd</sup> group of stations (slightly polluted) under cloud free conditions – cloud fraction lower than 0.1 – for days with GOME overpass over Lombardy during 1996-2002. Each box depicts the central half of the data between the lower quartile ( $q_{0.25}$ ) and the upper quartile ( $q_{0.75}$ ). The line across the box displays the median value ( $q_{0.5}$ ) and the star represents the mean. The whiskers extend from the top and the bottom of the box to depict the extent of the main body of the data. Extreme data values are plotted with rhombuses. The numbers in the upper part of the plots refer to the number of cloud free days considered for each month in the whole period.

## Section 6: Detailed report related to overall project duration



*Figure 6.3200.18. Weekly evolution of (a) tropospheric NO<sub>2</sub> VCD from GOME and (b) tropospheric NO<sub>2</sub> VCD from near-surface measurements at the 2<sup>nd</sup> group of stations under cloud free conditions – cloud fraction lower than 0.1 – for days with GOME overpass over Lombardy during 1996-2002. Same symbols as in Figure 6.3200.17.*

Considering the pollution level including high aerosol concentrations of this region the agreement found in this intercomparison study is surprisingly good. A more detailed description of the methodology used as well as the discussion of the uncertainties of both satellite and ground-based NO<sub>2</sub> data can be found in [Ordóñez *et al.*, 2005, submitted to JGR].

### References.

- Burrows, J. P., M. Weber, M. Buchwitz, V. Rozanov, A. Ladstetter-Weienmayer, A. Richter, R. De Beek, R. Hoogen, K. Bramstedt, K. U. Eichmann, M. Eisinger, and D. Perner: The Global Ozone Monitoring Experiment (GOME): Mission concept and first scientific results, *J. Atmos. Sci.*, *56*, 151–175, 1999.
- Grosjean, D., and J. Harrison: Response of Chemiluminescence NO<sub>x</sub> Analyzers and Ultraviolet Ozone Analyzers to Organic Air Pollutants, *Environ. Sci. Technol.*, *Vol. 19*, No. 9, 862-865, 1985.
- Horowitz, L. W., S. Walters, D. L. Mauzerall, L. K. Emmons, et al.: A global simulation of tropospheric ozone and related tracers: Description and evaluation of MOZART, version 2, *J. Geophys. Res.*, *108* (D24), 4784, doi:10.1029/2002JD002853, 2003.
- Ordóñez, C., Richter, A., Steinbacher, M., Zellweger, C., Nüß, H., Burrows, J. P., and Prévôt, A. S. H.: Comparison between 7 years of satellite-borne and ground-based tropospheric NO<sub>2</sub> measurements around Milano, Italy. Submitted to *J. Geophys. Res.*, 2005.
- Winer, A. M., J. W. Peters, J. P. Smith, and J. N. Pitts, Jr.: Response of Commercial Chemiluminescence NO-NO<sub>2</sub> Analyzers to Other Nitrogen-Containing Compounds, *Environ. Sci. Technol.*, *Vol. 8*, No. 13, 1118-1121, 1974.

## 9. Measurements of NO<sub>2</sub>, O<sub>4</sub>, and the AOD with MAX-DOAS at Alzate

The Bremen MAX-DOAS instrument was operated at the measurement site Alzate from 20 July to 18 August 2002 (1<sup>st</sup> campaign) and from 10 September to 5 October 2003 (2<sup>nd</sup> campaign). There were a few interruptions in the measurements during this time period due to power failures. A description of the instrument and more detailed information on retrieval algorithms is given in WP 1200.

### *Data analysis and results*

Nitrogen dioxide as well as the oxygen dimer O<sub>4</sub> has been analysed in a wavelength window between 350 to 370 nm using the well-known DOAS algorithm. Figure 6.3200.19 shows a clear distinction between the slant column densities of NO<sub>2</sub> for the different viewing directions even when there were cloudy sky conditions (only data from 2002 are shown, the 2003 campaign yields similar results). This indicates the presence of large amounts of NO<sub>2</sub> in the boundary layer. Also a difference between weekdays and weekends can be observed as was the case in several previous studies based on in situ and satellite measurements (see also chapter 8 of this work package).

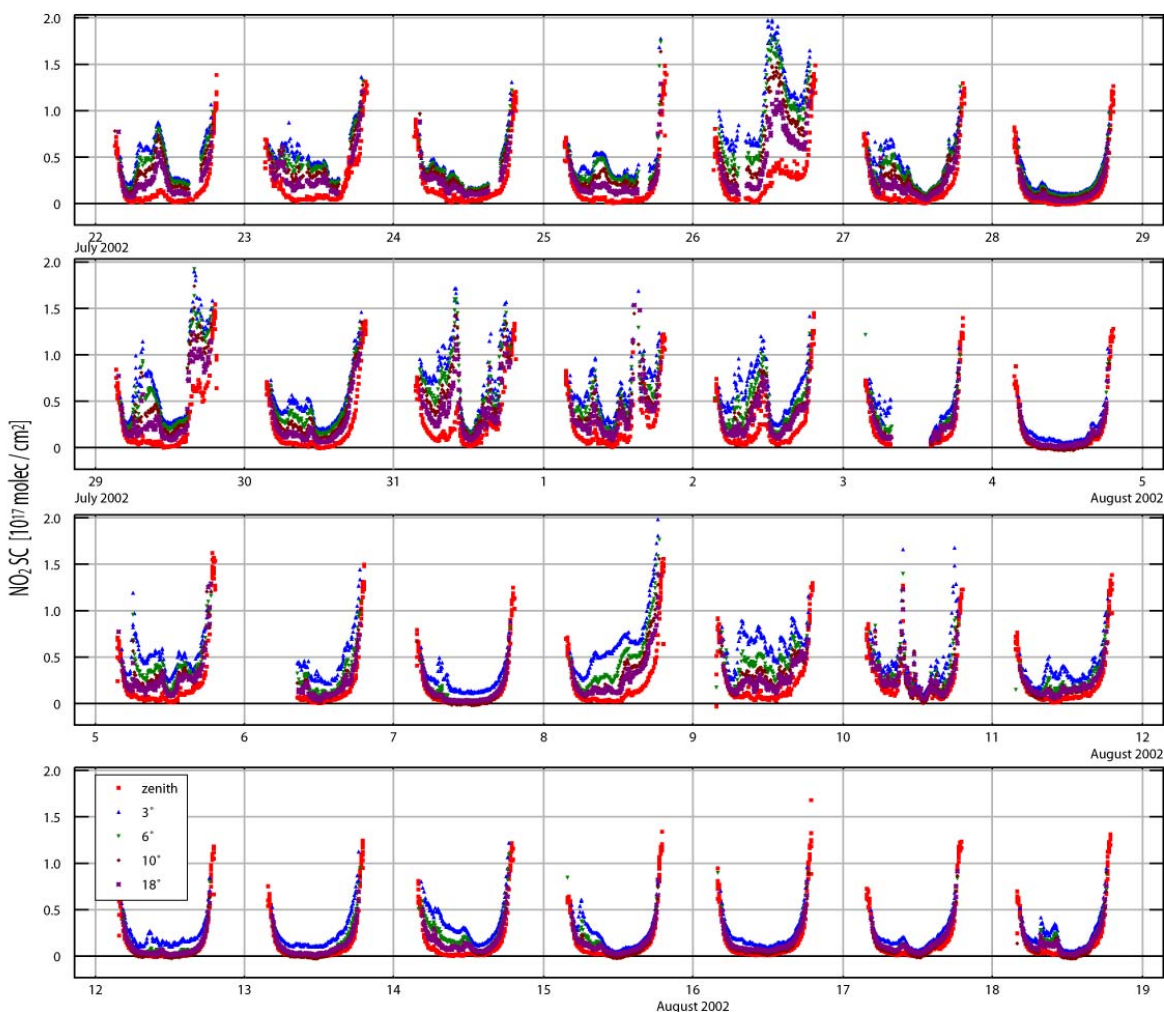


*Figure 6.3200.19. Time series of NO<sub>2</sub> slant column measurements taken by the Bremen MAX-DOAS instrument. The NO<sub>2</sub> columns of the horizon viewing directions are larger as the light path through the boundary layer is much enhanced in this measurement geometry.*

For comparison with in situ measurements and for satellite/model validation tropospheric columns and/or profiles of  $\text{NO}_2$  are needed. The approach developed in WP 1200 for the analysis of HCHO (D1220.3) data has been adapted to  $\text{NO}_2$ . Using optimal estimation according to [Rodgers, 1990] profiles can be retrieved by comparing the measured slant columns with the output from a radiative transfer model. Here the model SCIATRAN [Roazanov *et al.*, 2001] is used. The aerosol loading of the atmosphere is determined directly from the measurements of the oxygen dimer  $\text{O}_2\text{-O}_2$  (or  $\text{O}_4$ ) itself. An example for the evolution of such a retrieved profile during the course of a day is shown in Figure 6.3200.20 for August 14, 2002. The profile peaks close to the surface and a maximum mixing ratio of about 6 ppb was detected on that particular day. Such a profile retrieval yields best results for non-cloudy conditions.

Profiles for each day of the campaign have been uploaded to NILU database together with additional information on surface mixing ratio, aerosol optical depth (AOD) and quality parameters of the retrieval algorithm. In order to illustrate the efficiency of the retrieval algorithm Figure 6.3200.21 shows the time series of the  $\text{NO}_2$  mixing ratio near the surface derived from different instruments at Alzate during the 1<sup>st</sup> campaign in 2002. Figure 6.3200.22 shows the tropospheric  $\text{NO}_2$  columns measured by the Bremen MAX-DOAS instrument during both campaigns. Very high values (e.g. on July 26) are related to thunderstorms. The seasonal variation is in good agreement with the findings of other studies (see e.g. chapter 8 of this work package).

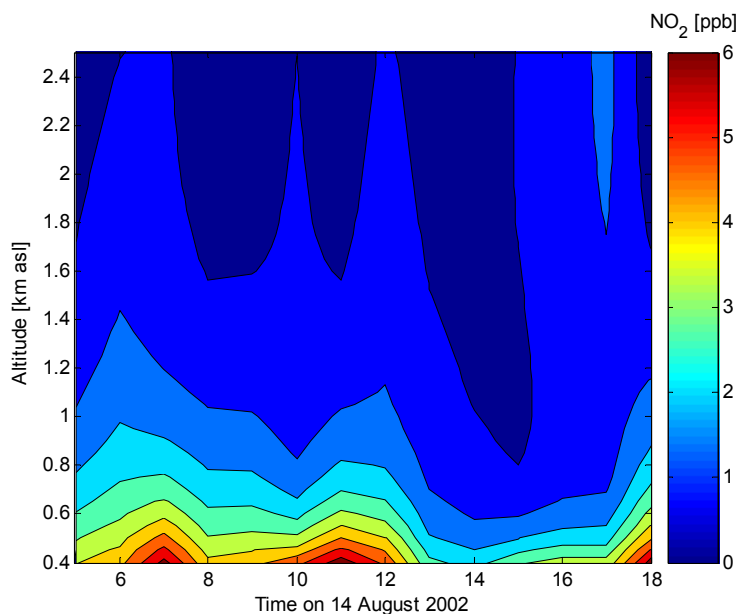


Figure 6.3200.20. Vertical  $\text{NO}_2$  profiles above Alzate retrieved from the measurements of the Bremen MAX-DOAS instrument on August 14, 2002. In contrast to HCHO (see WP 1200) the  $\text{NO}_2$  shows a strong gradient to higher values towards the surface for most of the measurement days during both campaigns.

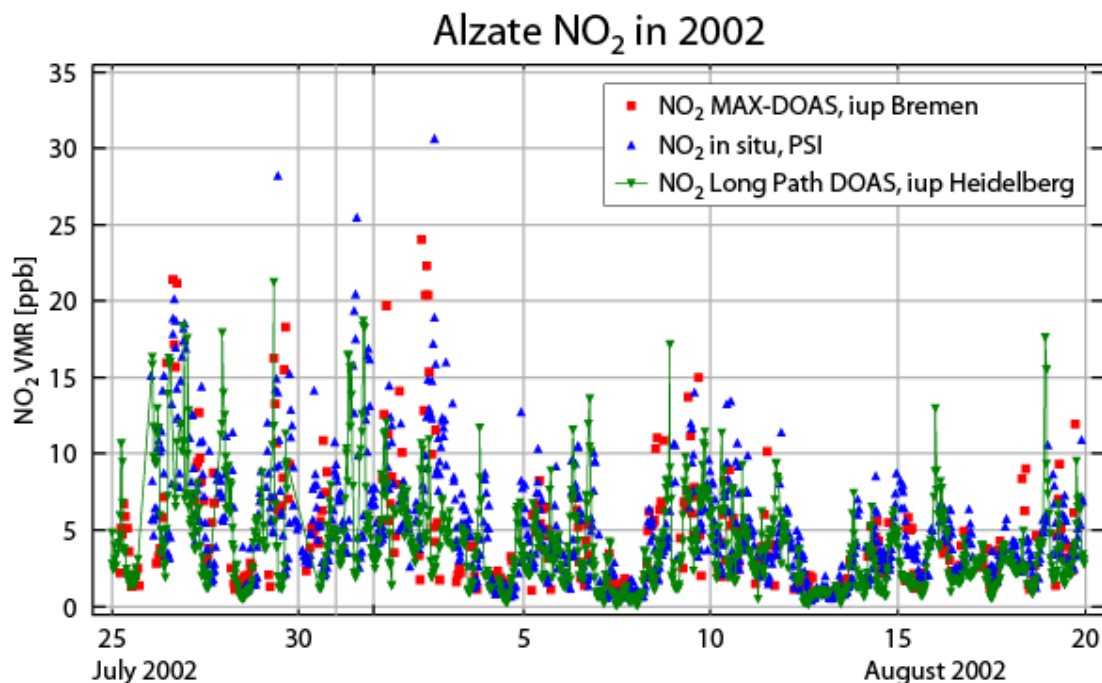


Figure 6.3200.21.  $\text{NO}_2$  mixing ratios near the surface measured by the Bremen MAX-DOAS instrument compared to in situ and LongPath measurements. The sampling of the MAX-DOAS (1 hour) is lower than that of the other instruments (half-hourly averages in this plot).

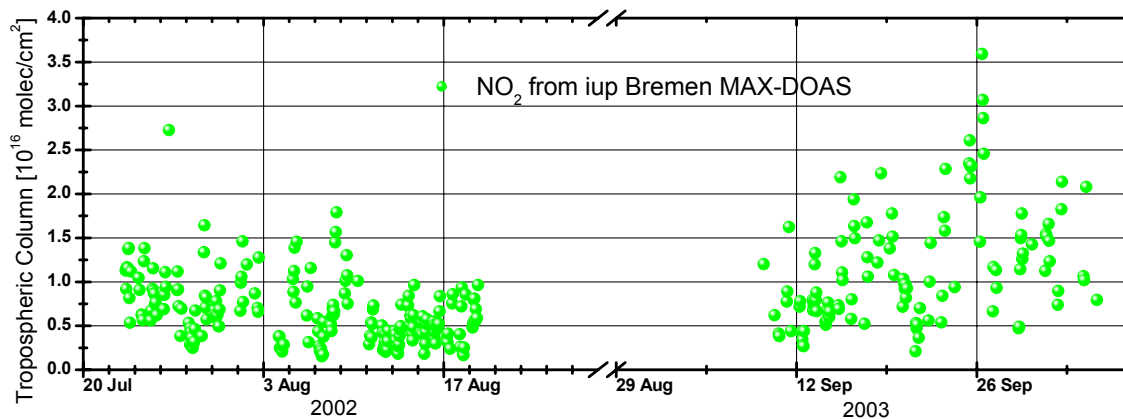


Figure 6.3200.22. Tropospheric  $\text{NO}_2$  columns measured by the Bremen MAX-DOAS instrument during the field campaigns FORMAT 2002 and FORMAT 2003.

## References

Rodgers, C. D. Characterization and error analysis of profiles retrieved from remote sounding measurements, *J. Geophys. Res.*, 95, D5, 5587-5595, 1990.

Rozanov, A., Rozanov, V. V., and Burrows, J. P.: A numerical radiative transfer model for a spherical planetary atmosphere: combined differential-integral approach involving the Picard

iterative approximation, *Journal of Quantitative Spectroscopy and Radiative Transfer*, 69, 491, 2001.

## **WP 4000 Atmospheric chemistry modelling and intercomparison with observations**

### **WP 4100: Collection and preparation of existing measurement data**

A literature review of atmospheric formaldehyde measurements have been carried out and presented in a separate note to the consortium. This includes a systematic overview of campaigns and other programs since the first part of the 1980s where formaldehyde has been measured in different regions in the world. A tabulation of the various campaigns, monitoring equipment and concentration level has been given. An overview of addresses or web links where monitoring data are available has also been included to ease to access of such data for e.g. modellers. Data from the most extensive regular monitoring programme so far, viz. EMEP, is already publicly available from the web. Data from various other programs (such as previous EU projects like TACIA, MAXOX etc.) are also accessible from Partner 1, NILU, on request.

### **WP 4200: Regional modeling**

#### **1. NILU regional CTM model**

The Regional CTM (Chemistry Transport Model) is driven by meteorological data from a NWP (Numerical Weather Prediction) model using global meteorological analyses and forecasts from ECMWF (European Centre for Medium Range Weather Forecasts) as initial and boundary conditions. The model is self-nesting and was used on the two domains shown in Figure 3.4.2.1(below) with grid resolutions 50 and 15 km. In the vertical, 18 and 30 unequally spaced levels with a model top at 100 hPa were used. An additional grid with 150km/10 levels was used to deliver boundary values to the 50km grid. The employed model version includes full tropospheric O<sub>3</sub>, NO<sub>x</sub>, CO and VOC chemistry and simplified SO<sub>2</sub> chemistry. Emissions from CITY-DELTA (<http://rea.ei.jrc.it/netshare/thunis/citydelta>) for the Milan region were employed for the 15 km grid, emissions from EMEP for 2000 were used on the 50 km grid and on the 150 km domain data from EDGAR [Van Aardenne et al.; 2001] for 1995 were used. The NILU CTM is documented in Flatøy et al. (1995) and Flatøy and Hov (1996a; b).

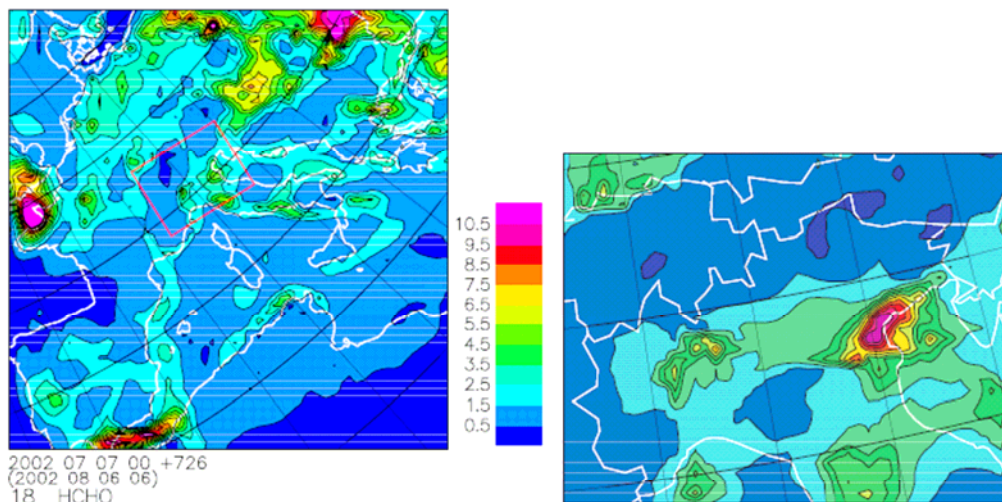


*Figure 3.4.2.1. Snapshot of HCHO concentration (ppb) at ~45 m height at 06 UT on August 6, 2002. The position of the 15 km domain nested within the 50 km domain is outlined.*

Figure 3.4.2.1 shows the HCHO concentration in the lowest model level (~45m) at 06 UT on August 6, 2002. The finer 15 km resolution domain has more details due to higher resolution emissions, more detailed topography and meteorological input where local scale phenomena's are better resolved. Forecasts with the CTM were produced each day during the campaign period and the forecast products made available on a web server. The fine scale emission inventory was only available the last days of the campaign reducing the forecast quality. The regularity of the forecasts was good and available from when the campaign started. Further information about forecast setup and employed methods can be found in Flatøy et al. (2000) A rerun was made when ECMWF analyses were available and the results used to evaluate the model performance during the campaign period. Complete results are available on: <http://tre.i.uib.no/climate/rerun.html> .

## **2. Model results and measurements from two surface sites (2002 and 2003 campaign)**

During 2002 campaign, a variation of measurement techniques was applied for HCHO measurements. All the data available from different instruments have been used to validate the model results. Figure 6.4200.2 shows model results from 15km resolution model and measurements for Alzate, Figure 6.4200.3 for Bresso.

Model simulated ozone levels and time variation agree well with measurements in most of the days at Alzate, the model shows good agreements during the daytime, and slightly underestimated the ozone levels during the nighttime, which may be caused by overestimated dry deposition close to the surface. Some of the dominant spikes in NO<sub>x</sub> and CO can be caused by point sources not resolved on the model grid. The modelled late peaks of CO and NO<sub>2</sub> show the model captured the arrived plume from south, but the transport from north in the morning is not that strong in reality. For three identified North Foehn days, model gives good agreements with measurements.

At the Bresso, model results agree better with observations during the daytime. Measured HCHO, CO and NO<sub>2</sub> show the strong influence from local emissions. During the night, modeled ozone is much lower and modeled NO<sub>2</sub> is much higher. This can only be explained by a too low mixing height in the model trapping emission during the night and causing significant ozone loss from dry deposition.

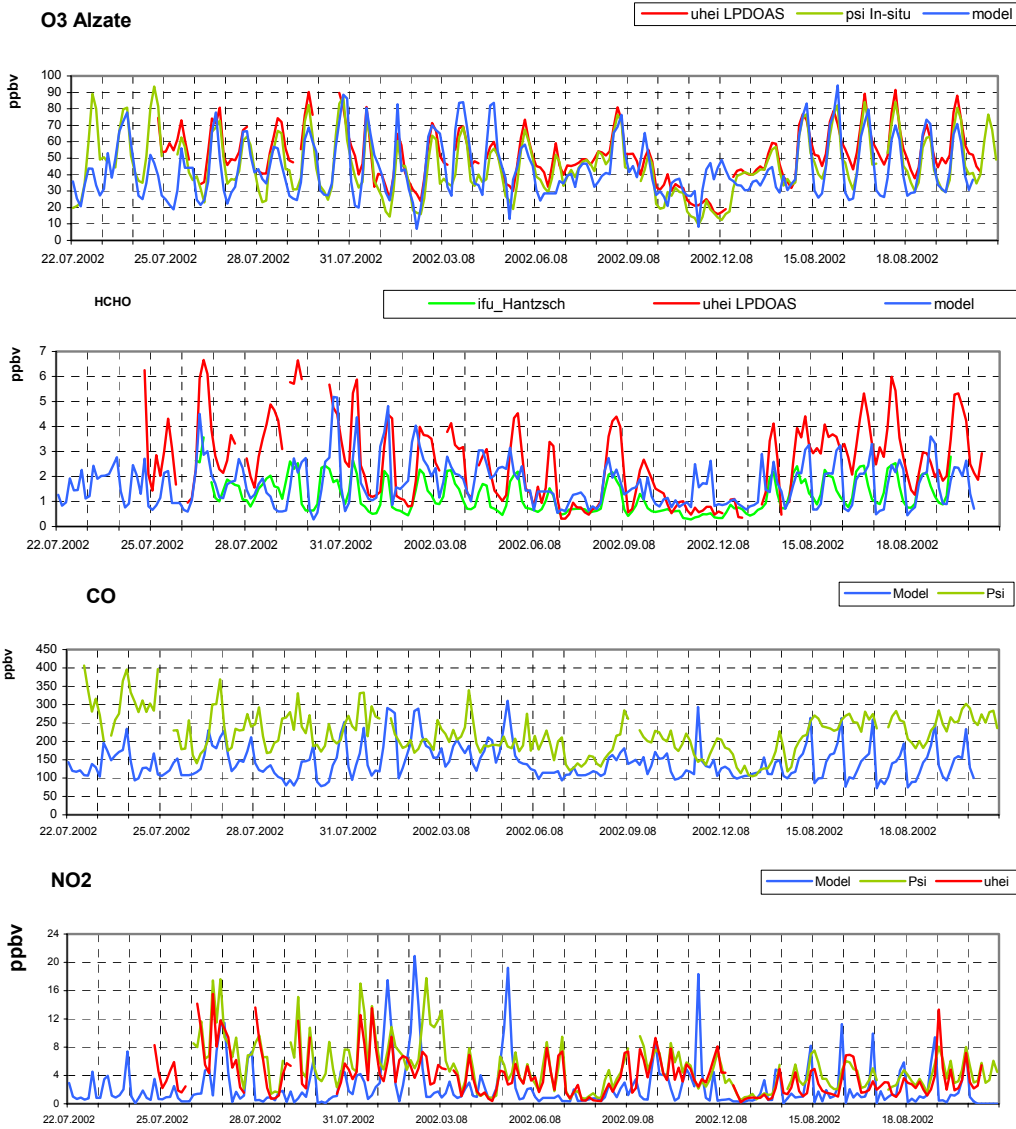


**Figure 6.4200.2.** Time series of measured (red) and modelled (blue; 15 km model, green 50 km model) concentrations at Alzate during the 2002 campaign.

Modelled HCHO at Alzate has been compared with measurements both from in-situ (Hantsch) and remote (LP DOAS) instruments. Because the light path of LP DOAS at Alzate crossed over the forest, HCHO were quickly converted from isoprene emitted from forest. LP DOAS gives doubled values when experienced the strong radiation and high temperature, which can be identified during the fair weather periods. The model results show better agreements with in-situ measurements, since the model results represent the general information in model grid. Figure 6.4200.4 shows the correlation of HCHO and O<sub>3</sub>\*water between modeled and measured air mass from in-situ instruments, the slopes are 1.67 and 1.96 respectively. Meanwhile, the measurements from remote instrument (LP DOAS) have the slope as 4.65, shows the conditions from the different air mass.

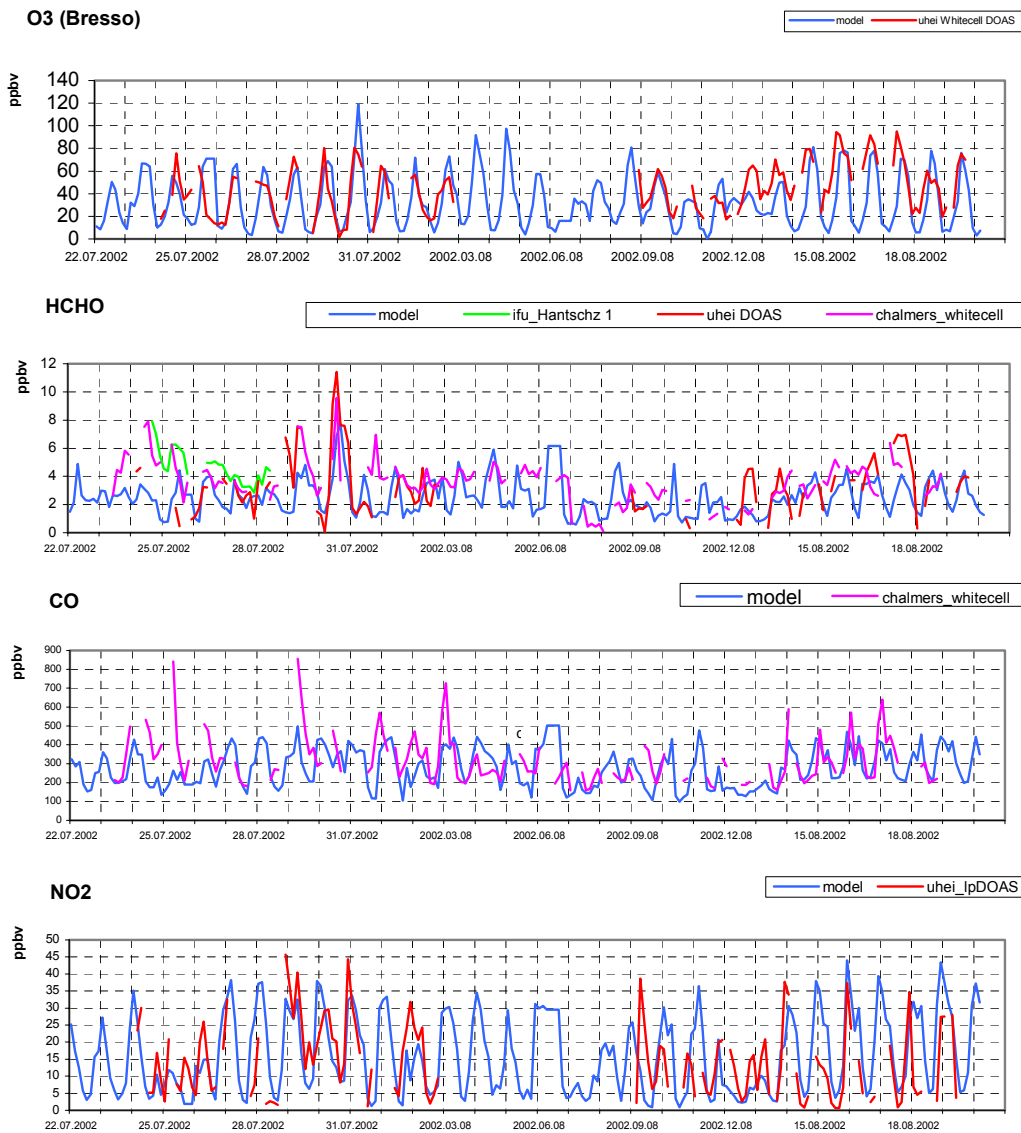


Figure 6.4200.3. Time series of measured (red) and modelled (blue; 15 km model, green 50 km model) concentrations at Bresso during the 2002 campaign.

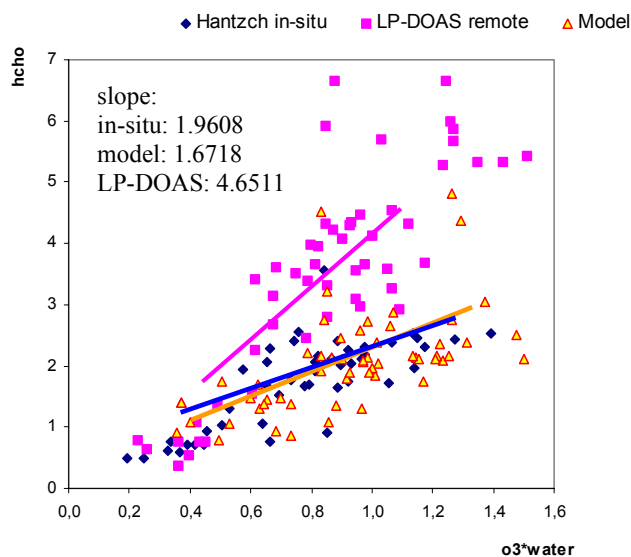


Figure 6.4200.4. The scatter plot between HCHO levels and O<sub>3</sub>\*water content at Alzate (2002), both for model and measured values

Figure 6.4200.5 shows comparison between model results from 15km resolution model and measurements from Bresso, Figure 6.4200.6 for Alzate during 2003 FORMAT campaign. The model has been rerun for 2003 campaign, and has included HCHO as primary emission. The HCHO emission used default speciation of VOC emission from EMEP.

The model gives good results for most of the days at Bresso. Simulated ozone agrees well with measurements both for levels and diurnal variation. Because of lacking information, all the HCHO primary sources were assumed from transport, HCHO levels show the newly added primary HCHO emission is more suitable for urban area, more detailed information about HCHO emissions and land use are needed for future work. Model results for NO<sub>2</sub> are generally good, some peaks observed maybe due to local emissions. At Alzate, the modeled ozone captured the peaks and variation during the daytime, and shows the same low values during the night, especially for the days with fair weather with clear sky, because of the strong dry deposition in the model. During the fair weather period, both CO and HCHO are overestimated during the daytime and underestimated during the nighttime. Because of the strong advection in the model, the clean air from North during the night and polluted air from South during late afternoon or evening.

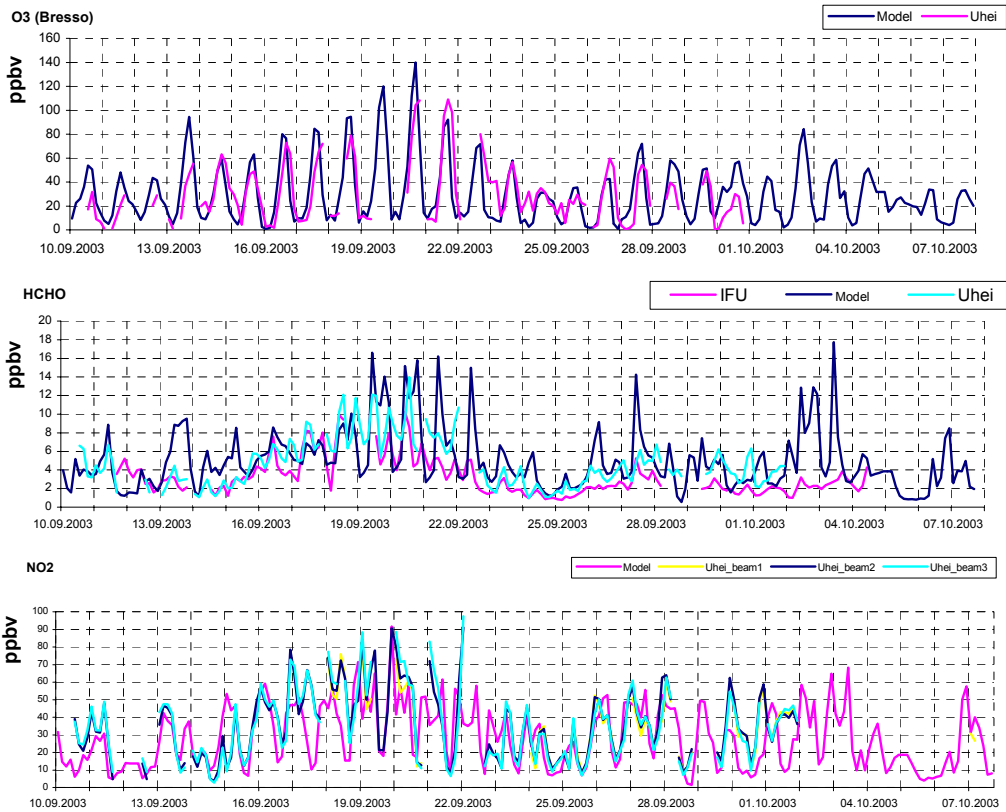
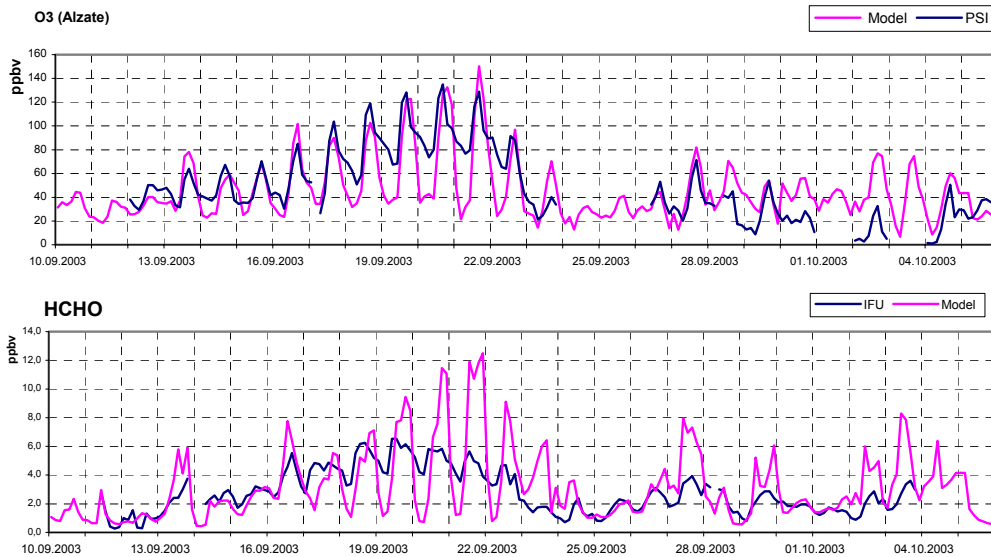


Figure 6.4200.5. Time series of measured and modelled (15 km model resolution) concentrations at Bresso during the 2003 campaign.



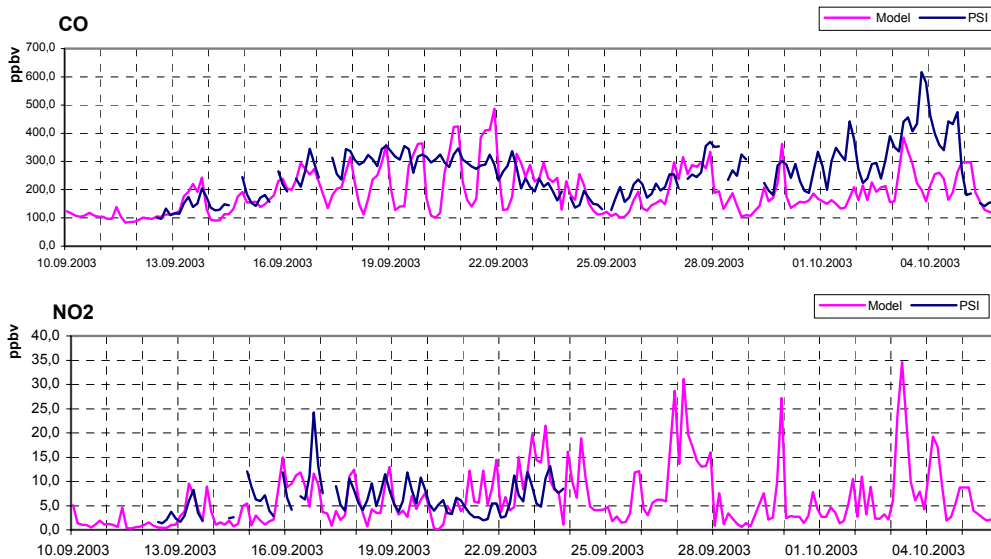


Figure 6.4200.6. Time series of measured and modeled (15 km resolution) concentrations at Alzate during the 2003 campaign.

### 3. Model results and measurement from Lombardy area

Figure 6.4200.7 is comparison made between modeled and measured Ox from Lombardy area. Around Milan city, 5 areas have been separated. Milan ( $9.15^{\circ}\text{E} \sim 9.25^{\circ}\text{E}$  and  $45.4^{\circ}\text{N} \sim 45.5^{\circ}\text{N}$ ), south (south of  $45.4^{\circ}\text{N}$ ), North (north of  $45.5^{\circ}\text{N}$ , between  $9.15^{\circ}\text{E} \sim 9.25^{\circ}\text{E}$ ), Northeast (north of  $45.5^{\circ}\text{N}$ ; east of  $9.25^{\circ}\text{E}$ ), and Northwest (north of  $45.5^{\circ}\text{N}$ ; west of  $9.15^{\circ}\text{E}$ ) of Milan. The correlations of measurements and model results were given for fair weather period. For total 49 stations, model gives good agreements. The discrepancies found for stations located at south of Milan, where model underestimated the model, model also overestimated ozone levels at Northwest of Milan, where is high levels ozone produced at the downwind of Milan city. These discrepancies can be explained by wind field and model resolution, and show that the model results are highly controlled by meteorological conditions.

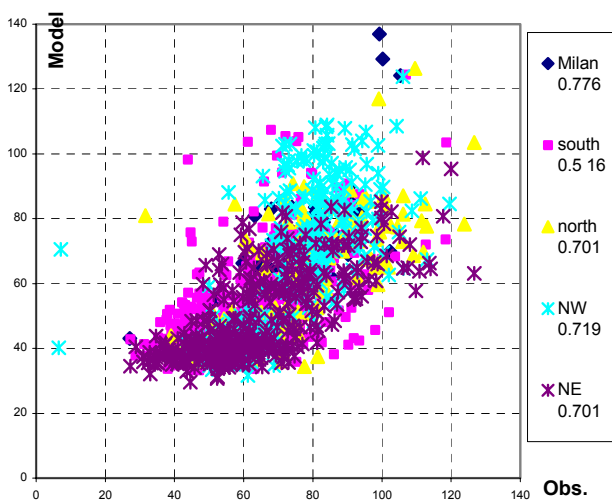


Figure 3.4.2.7. Modelled and measured Ox from Lombardy region during 2002 campaign. Data from 48 stations, afternoon value during the fair weather periods.

#### 4. Flight tracks and model results

Figure 6.4200.8 gives the model results along the flight tracks. The model results agree well for both O<sub>3</sub> and HCHO along the flight track, there are some peaks model does not able to capture, can be caused by local emissions and plume. Flights capture the plumes for couple of the days, the highest level of ozone 125.3ppbv were found on 17 August (Figure 6.4200.9), at the flight height about 300m, where the HCHO is about 5ppbv at the same time. The model also shows the similar levels and spatial distribution for the same day, gives 120ppbv ozone levels on the same level, but the plume is located few kilometers south of real plume. Because of the large gradient between inside and outside of the plume, more explicit simulation of plume are depending on improved meteorological data and model resolution.

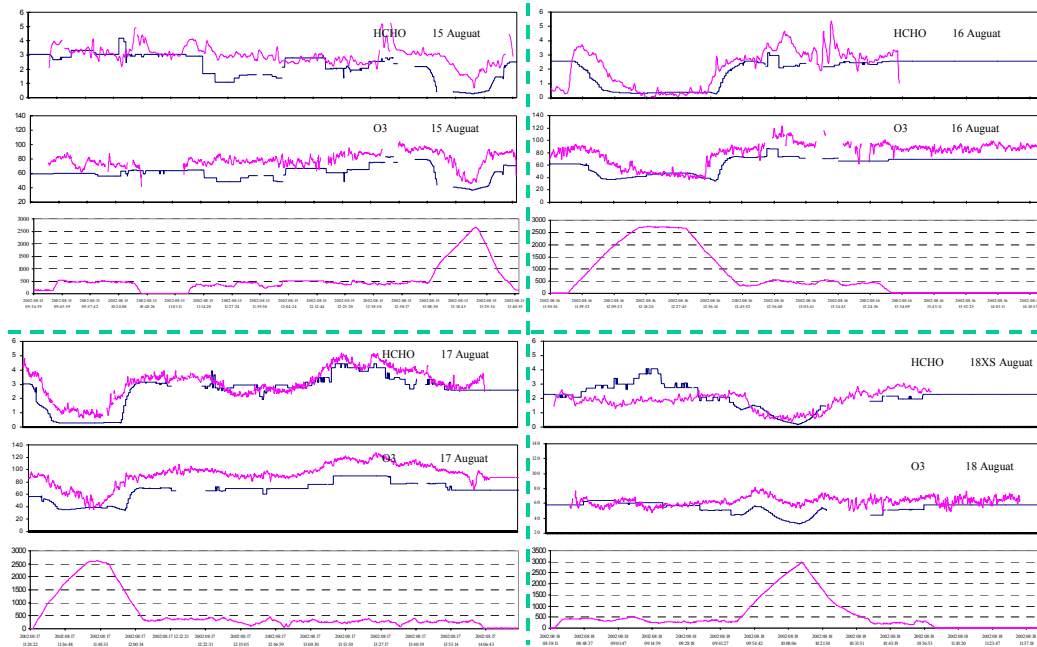


Figure 3.4.2.8. Aircraft measurement for Ozone and HCHO (red), and model simulation along the flight track (Blue); the bottom panel were altitude of flight

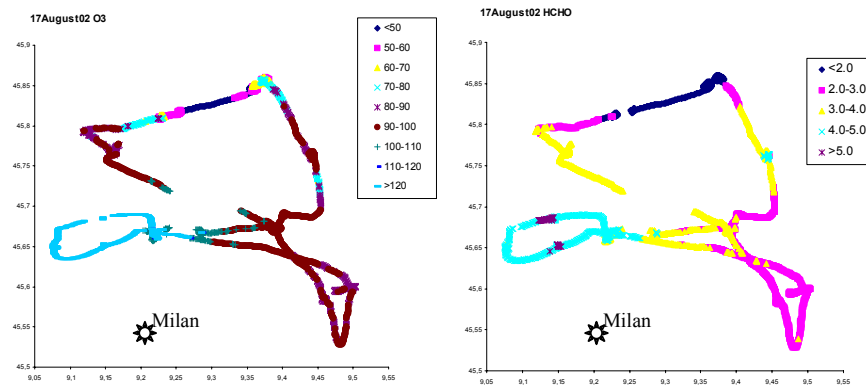


Figure 6.4200.9. Ozone and HCHO measured during the flight on 17<sup>th</sup> August, flight time from 11:00 ~ 14:00.

## References:

Flatøy, F., Ø. Hov, and H. Smit, Three-dimensional model studies of exchange processes of ozone in the troposphere over Europe, *J. Geophys. Res.*, 100, 11465-11481, 1995.

Flatøy, F., and Ø. Hov, 3-D model studies of the effect of NO<sub>x</sub> emissions from aircraft on ozone in the upper troposphere over Europe and the North Atlantic, *J. Geophys. Res.*, 101, 1401-1422, 1996.

Flatøy, F., Ø. Hov, C. Gerbig, and S. J. Oltmans, Model Studies of the Meteorology and Chemical Composition of the Troposphere over the North Atlantic During August 18-30, 1993, *J. Geophys. Res.* 101, 29,317-29,334, 1996.

Flatøy, F., Ø. Hov and H. Schlager, Chemical forecasts used for measurement flight planning during POLINAT 2, *Geophys. Res. Lett.*, 27, 951-954, 2000.

Van Aardenne, J.A., Dentener, F.J., Olivier, J.G.J., Klein Goldewijk, C.G.M. and J. Lelieveld, A 1 x 1 degree resolution dataset of historical anthropogenic trace gas emissions for the period 1890-1990. *Global Biogeochemical Cycles*, 15(4), 909-928, 2001.

## **WP 4300 Global modelling**

### **Model studies of CH<sub>2</sub>O using OsloCTM2**

Contribution to FORMAT final report

Authors: Tore F. Berglen, Ivar S.A. Isaksen & Stig B. Dalsøren

## **Introduction**

Formaldehyde, CH<sub>2</sub>O, is a key component in the atmospheric hydrocarbon cycle. It is both emitted as a primary gas and it is a product in the oxidation of hydrocarbons (CH<sub>4</sub> and higher-order HC). Biomass burning is a large source of CH<sub>2</sub>O. In this study we will focus primarily on CH<sub>2</sub>O, trying to quantify the impact of biomass burning on both CH<sub>2</sub>O and the atmospheric chemistry cycle. In addition we will focus on the production of hydrogen (H<sub>2</sub>) since this is an important gas that will receive much attention in the future.

## **Background**

Biomass burning largely influence the levels of CH<sub>2</sub>O, at least regionally if not globally. The emissions vary from year to year. 1997 was a year with huge biomass burning episodes both in South America and in S-E Asia. Emission estimates for 1997 are listed in table 6.4300.1. In 1997 biomass burning accounted for over ¾ of the direct emissions of CH<sub>2</sub>O.

<b>Code</b>	<b>Category</b>	<b>Total mass emitted</b>
BTO	Total biofuel	0,526 Tg(CH <sub>2</sub> O) / year
F51	Transport road	0,338 Tg(CH <sub>2</sub> O) / year
FOT	Other fossil fuel	0,073 Tg(CH <sub>2</sub> O) / year
L41*	Biomass burning deforestation	2,243 Tg(CH <sub>2</sub> O) / year
L42*	Biomass burning savannas	0,717 Tg(CH <sub>2</sub> O) / year
L43*	Agricultural waste burning	0,258 Tg(CH <sub>2</sub> O) / year
* these categories are excluded in the model runs without biomass burning emissions		

Table 6.4300.1: Emissions of CH<sub>2</sub>O for 1997 used in the model.

Biomass burning also influences the concentration of CH<sub>2</sub>O through emissions of CH<sub>4</sub> and higher-order hydrocarbons which in turn are oxidized to CH<sub>2</sub>O, and further on to CO<sub>2</sub>. The main oxidation pathway is listed in table 6.4300.2 (example of CH<sub>4</sub>, but other HC follow the same oxidation). Reactions R1, R4, R5, R6 and R8 are part of the odd-hydrogen cycle, which rapidly cycles H, OH and HO<sub>2</sub> and is hence important for the atmospheric oxidation capacity. Reaction R7 gives H<sub>2</sub>, a gas that is important for the atmospheric oxidation and that will be more and more important in the future as reservoirs of fossil fuel are exhausted and a hydrogen economy will arise.

CH <sub>4</sub> + OH	→	CH <sub>3</sub> + H <sub>2</sub> O	R1
CH <sub>3</sub> + O <sub>2</sub> + M	→	CH <sub>3</sub> O <sub>2</sub> + M	R2
In NO <sub>x</sub> -rich environment (NO > 10 ppt):			
CH <sub>3</sub> O <sub>2</sub> + NO	→	CH <sub>3</sub> O + NO <sub>2</sub>	R3
CH <sub>3</sub> O + O <sub>2</sub>	→	CH <sub>2</sub> O + HO <sub>2</sub>	R4
Concerning CH <sub>2</sub> O there are three possibilities:			
CH <sub>2</sub> O + hv	→	H + CHO (hv ≤ 338 nm)	R5
CH <sub>2</sub> O + OH	→	CHO + H <sub>2</sub> O	R6
CH <sub>2</sub> O + hv	→	CO + H <sub>2</sub> (hv ≤ 360 nm)	R7
H, OH and HO <sub>2</sub> are also cycled by:			
CO + OH	→	CO <sub>2</sub> + H	R8
NO <sub>x</sub> leads to O <sub>3</sub> production through:			
NO + HO <sub>2</sub>	→	NO <sub>2</sub> + OH	
NO <sub>2</sub> + hv	→	NO + O	
O + O <sub>2</sub> + M	→	O <sub>3</sub> + M	

Table 6.4300.2: Important chemical reactions in the hydrocarbon - CH<sub>2</sub>O - NO<sub>x</sub> - O<sub>3</sub> scheme used in the model.

### Model description and experimental setup

The tropospheric version of the OsloCTM2 model with (e.g. Berglen et al, 2004) is used for this study. It was run in both T21 horizontal resolution (5,6°×5,6°) with 19 vertical layers and T42 horizontal resolution (2,8°×2,8°) with 40 vertical layers in σ-hybrid coordinates. Advection is solved using the Second Order Moment (Prather, 1986). Eddy diffusion coefficients from Holtslag et al. (1990) are used for boundary layer mixing. The method by Isaksen and Rodhe (1978) is used for dry deposition, wet deposition in convective and large scale clouds are treated separately (Berglen et al., 2004). The QSSA solver (Hesstvedt et al., 1978) is used in the chemistry scheme comprising 51 components in the tropospheric O<sub>3</sub>-NO<sub>x</sub>-VOC cycle. Meteorological input data are elaborated by the IFS model at the ECMWF, giving very detailed and internally consistent weather data (mass fluxes, cloud properties, T, p, humidity, etc.). The input data are updated every 3hrs. The T21L19 version used meteorological data representing 1996 while T42L40 version used the year 1997. Time step is five minutes for chemistry and 60 minutes for transport.

For this study two sets of model runs were performed; one with biomass burning emissions included and one without. To analyze our results monthly average concentrations were diagnosed,

in addition a budget for the production of H and H<sub>2</sub> is made, and total columns of CH<sub>2</sub>O and NO<sub>2</sub> are also diagnosed.

## Results

The emissions from biomass burning show a very strong seasonal variation with the strongest emissions in August – November. From table 6.4300.1 we see that the largest source within the biomass burning category is L41 Biomass burning deforestation with a 1997 source strength of 2,243 Tg(CH<sub>2</sub>O) / year. Over ¾ of L41 (1,694 Tg) is emitted during this four-month period (Aug 0,386, Sep 0,582, Oct 0,522, Nov 0,204 Tg(CH<sub>2</sub>O) / month).

To present our result we have chosen to emphasize the month of October since it is one of the months with the strongest emissions. Showing e.g. annual means would easily disguise our results as the September-October peaks would be leveled out.

■ Figure 6.4300.1 shows tropospheric column of CH<sub>2</sub>O for October with and without biomass burning emissions. In regions with the largest emissions (S America and S-E Asia) biomass burning increase CH<sub>2</sub>O with a factor 4-5 due to these exceptional episodes. Also Africa and Russia experience some increase, although not that large and more from savanna burning (L42) and agricultural waste burning (L43), which is to a large degree an annual event.

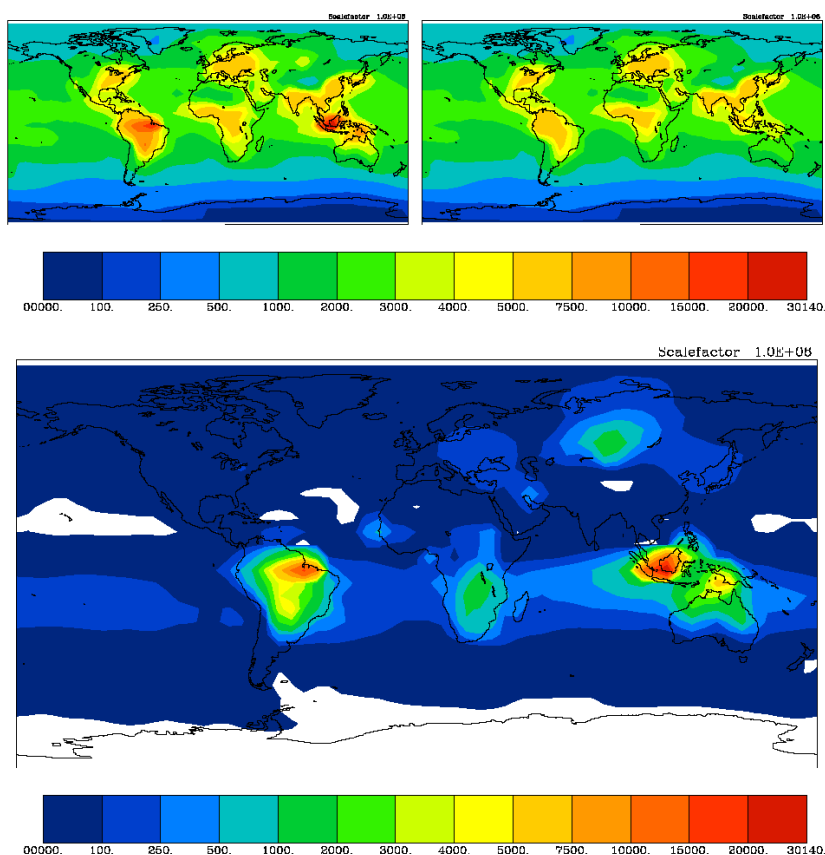


Figure 6.4300.1: Tropospheric column of CH<sub>2</sub>O for October, run with biomass burning emissions (upper left), run without biomass burning emissions (upper right), with=without (lower). Unit: µg(CH<sub>2</sub>O)/m<sup>2</sup>.

■ The levels of  $\text{NO}_x$  are also affected by these large emissions of hydrocarbons (figure 6.4300.2). This will in turn affect  $\text{O}_3$  production through reactions (see table 6.4300.2). Large biomass burning events episodes like October 1997 can increase  $\text{NO}_2$  by nearly a factor 7 in some regions.

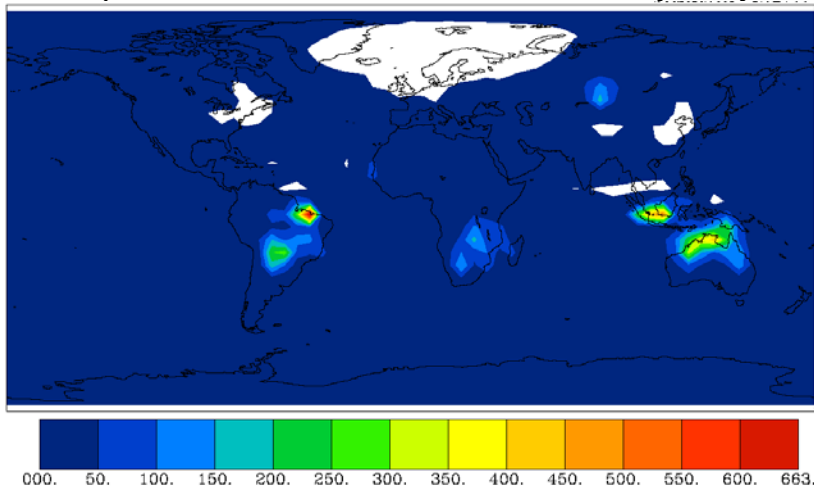


Figure 6.4300.2: Percentage change (increase) in tropospheric column of  $\text{NO}_2$  for October due to biomass burning  $100 \times (\text{with} - \text{without}) / \text{without}$ . Areas in white experience a small decrease.

#### ■ Production of $\text{H}_2$

As seen from table 6.4300.2  $\text{H}_2$  is produced by reaction R7. We have investigated the changes in  $\text{H}_2$  chemical production due to biomass burning emission. Schultz et al. (2003) estimate a total source strength of 77 (+/- 16) Tg  $\text{H}_2$  / year and that between 5 and 25 Tg  $\text{H}_2$  / year originates from fossil fuel combustion. In our calculations we found that the increased emissions of hydrocarbons from biomass burning increased the mass of  $\text{H}_2$  by 6,6% (global annual mean). In figure 6.4300.3 we show the results for October with over a factor 2 increase in the areas most affected by biomass burning.

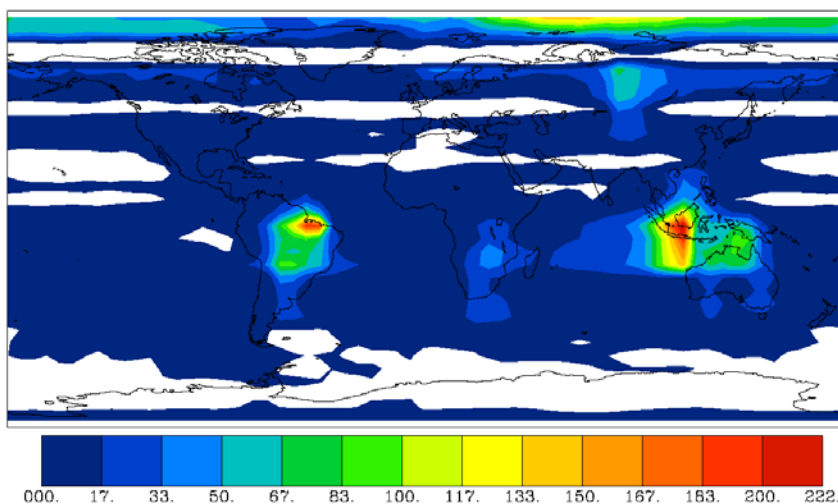


Figure 6.4300.3: Percentage change (increase) in  $\text{H}_2$  abundance for October due to biomass burning. Areas in white experience a small decrease.

#### References:

Berglen, Tore F.; Berntsen, Terje K.; Isaksen, Ivar S. A.; Sundet, Jostein K., A global model of the coupled sulfur/oxidant chemistry in the troposphere: The sulfur cycle  
J. Geophys. Res., Vol. 109, No. D19, D19310

Hesstvedt, E., Ø. Hov and, I.S.A. Isaksen, Quasi steady-state approximation in air pollution modelling: Comparison of two numerical schemes for oxidant prediction, Int. J. Chem. Kinet., X, 971-978, 1978.

Holtslag, A.A.M., E.I.F. DeBruijn, and H.L. Pan, A high resolution air mass transformation model for short-range weather forecasting, Mon. Wea. Rev., 118, 1561-1575, 1990.

Isaksen, I.S.A., and H. Rodhe, A two-dimensional model for the global distribution of gases and aerosol particles in the troposphere, Report AC-47, Dept. of Meteorology, Univ. of Stockholm, 1978.

Prather M.J., Numerical advection by conservation of 2nd order moments, J. Geophys. Res. 91 (D6): 6671-6681 MAY 20 1986

Schultz, M., Diehl, T., Brasseur, G.P. and Zittel, W., Air Pollution and Climate-Forcing Impacts of a Global Hydrogen Economy, Science, vol. 302, Issue 5645, 624-627, 2003.

## **WP 5000 Analysis and validation of GOME and SCIAMACHY data**

### **WP 5100: Algorithm improvements for HCHO retrieval from GOME and SCIAMACHY**

An algorithm to derive HCHO slant columns from earth irradiance spectra measured by GOME has been developed and improved in the first year of the project (see first annual report). Different sets of fitting parameters within the well-known DOAS algorithm have been compared. Finally a spectral fitting window of 337.5 - 357 nm was selected. In the fit the absorption cross-sections of HCHO (Meller and Moortgaat), BrO (Wahner), O<sub>4</sub> (Grennblatt), NO<sub>2</sub> and O<sub>3</sub> (both at two different temperatures, Burrows) have been used together with a synthetic Ring spectrum (calculated with the radiation transport model Sciatran, Vountas et al.) compensating the effect of Raman scattering in the atmosphere. As background for the DOAS fit actual solar irradiance spectra were used. (D5100.1).

The algorithm development for SCIAMACHY spectra has been finished in the last year of the project. Finally a spectral fitting window of 335 to 347 nm was selected. In the fit the absorption cross-sections of HCHO (Meller and Moortgaat), BrO (Wahner), NO<sub>2</sub> and O<sub>3</sub> (both at two different temperatures, Bogumil et al.) have been used together with a synthetic Ring spectrum (calculated with the radiation transport model Sciatran, Vountas et al.) compensating the effect of Raman scattering in the atmosphere. As background for the DOAS fit actual solar irradiance spectra were used. (D5100.2) The UV-shifted fitting window (compared to D5100.1) leads to higher sensitivity on ozone absorption. Therefore this algorithm is limited to scenarios with solar zenith angles less than 70° having weak ozone absorption.

The total error for the retrieved slant columns from the SCIAMACHY instrument is between 40 and 150% for weak absorptions (SCD about  $2 \cdot 10^{16}$  molec/cm<sup>2</sup>) and between 20 and 50% for strong absorptions (about  $5 \cdot 10^{16}$  molec/cm<sup>2</sup>) for single pixel. (D5100.3) A more detailed description on error analysis and retrieval parameters one can find in Wittrock, 2005.

## **WP 5200: Airmass factor calculations for HCHO retrieval from GOME and SCIAMACHY**

Airmass factors (AMF) are needed to convert the slant column (retrieved by the means of the DOAS algorithm, WP 5100) to vertical columns. The tropospheric slant columns depend on many factors such as viewing geometry, solar position, vertical distribution of the absorber, orography, surface albedo, aerosol optical depth, aerosol type and aerosol vertical distribution. Clouds also have a large impact on the sensitivity of the measurements.

To convert the measured slant columns in vertical columns which are independent of all the above quantities, appropriate airmass factors have to be computed with a radiative transfer model. Here three radiative transport models (SCIATRAN, AMFTRAC, LibRadtran) were applied. They have been described in the last annual report. All packages have been benchmarked during a model comparison, which was done in association with the EU project QUILT. A report on the model comparison is available at (<http://nadir.nilu.no/quilt>) and in Hendrick et al., 2005.

While AMFs can easily be computed by the RTMs with high accuracy, it is not obvious what to use for the input parameters such as absorber profile and albedo, and thus the error budget of the HCHO columns is dominated by the uncertainties of the AMFs. In the following we report on studies from the IUP Bremen group.

### **Vertical Absorber Profile**

The sensitivity of nadir measurements in the UV/visible spectral domain decreases strongly towards the surface. To compensate for this, the vertical distribution of the absorber must be known, a piece of information which cannot be derived from the satellite measurements themselves. It is important to realize, that only the shape of the profile needs to be known, whereas the absolute amount has no impact on the airmass factor within a very large concentration range.

From the measurements during the two FORMAT campaigns and from literature four different types of HCHO profiles have been identified: background, biogenic, biomass burning and urban. These profiles have been used to calculate AMFs for numerous meteorological conditions (see below).

Another possible source of estimates for vertical absorber profiles are tropospheric chemical transport models, that based on emissions, transport and chemistry predict trace gas concentrations at a number of altitude levels on global grids.

### **Surface Elevation**

Surface elevation plays a role in airmass factor calculation as the height dependence of the sensitivity makes satellites more sensitive to HCHO from say Mexico City than from a city on sea level. Thus, the surface elevation is taken into account in the AMF calculations.

### **Surface Albedo**

The sensitivity of satellites to the lower troposphere depends strongly on the surface albedo, at least in situations where the aerosol optical depth is not too large. Therefore, a good estimate is needed for surface albedo at the wavelengths used for the retrieval as a function of location and season. Such a data base has been derived from GOME data by Koelemeijer et al., 2001 and from TOMS by Tanskanen et al., 2004. Both data sets are used in the AMF calculations for HCHO.

As in the case of model profiles, the use of an albedo climatology will improve the accuracy of the HCHO columns on average. However, for individual measurements quite large errors can be introduced if the actual surface albedo differs from the one in the climatology as a result of snow

coverage, land use change or variations in albedo below the resolution of the data base ( $1^\circ \times 1^\circ$ ).

### **Aerosols**

The effect of aerosols on HCHO columns measured by satellite is twofold: HCHO within or below an aerosol layer will be seen with reduced sensitivity. HCHO situated above a reflecting aerosol will be seen with enhanced sensitivity. It therefore is necessary to know the vertical distribution of aerosols and also the composition, as absorbing and reflecting aerosols will have different effects on the radiative transfer.

Unfortunately, there is very little information available on the distribution of aerosols, and the large variability in space and time makes this input particularly difficult to assess. Therefore, for the HCHO data products presented in WP 5400 a simple approach was selected based on the aerosol parameterisation of the LOWTRAN model (Shettle and Fenn, 1976). Three types of aerosols were distinguished: a maritime aerosol over the oceans, an urban aerosol over industrialised regions and a rural aerosol elsewhere (for all 70% relative humidity has been assumed). Complementary data have been used to distinguish between four different visibilities: 5, 10, 23 and 50 km.

This simplified treatment of aerosols introduced significant errors into the global HCHO data product. In particular, HCHO from biomass burning regions e.g. above Indonesia will be underestimated. Sensitivity studies show, that for an urban aerosol with 2 km visibility the sensitivity of GOME and SCIAMACHY to HCHO in the lowest km is close to zero.

### **Clouds (D5200.5)**

The effect of clouds on the HCHO retrieval is similar to that of aerosols, only much stronger: clouds effectively shield the atmosphere below them from view and strongly enhance the sensitivity to any absorption above them, in particular close to the cloud top. There also is some enhancement in sensitivity to absorption within the upper part of the cloud.

Two different approaches can be used to account for the impact of clouds: either a simple cloud screening algorithm can be used to select only data below a certain cloud threshold or the impact of clouds can be modelled in detail based on measurements of cloud fraction and cloud top height and assumptions on the amount of HCHO below the cloud. Here a simple threshold technique was used based on the FRESCO cloud cover product. A rather large maximum cloud cover of 30% has been chosen to avoid large data gaps in the Northern Hemisphere in winter and spring. The remaining error on the retrieved vertical column has been estimated to less than 30% for most scenarios.

The following figure shows one example for the sensitivity of HCHO weighting functions on clouds.

## Weightingfunction HCHO

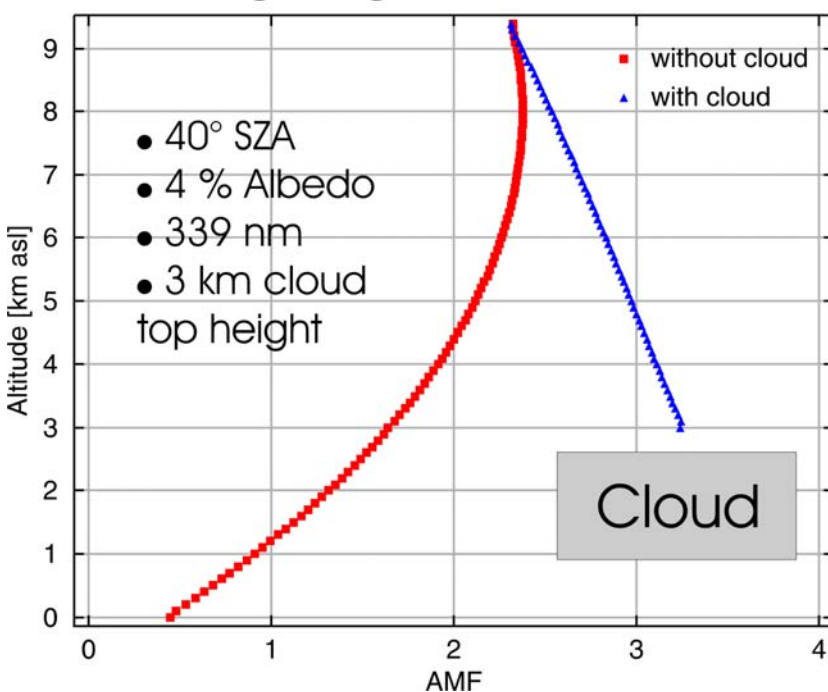


Figure 6.5200.3: Dependence of HCHO AMF on cloud.

### Implementation

In order to provide global data sets of HCHO from GOME and SCIAMACHY around 15.000 sets of AMF depending on SZA have been calculated with the Bremian radiation transfer model SCIATRAN (Rozañov et al., 2001) and stored in an AMF lookup table (see Table 6.5200.1 for a description of the parameters). For every measurement, the elevation, aerosol type, visibility, profile shape and surface albedo values are retrieved from the data bases, and the SZA from the measurement time and location. Using these input data, the appropriate AMF are retrieved from the lookup table and applied to the slant column to get an appropriate vertical column.

Table 6.5200.1. Description of parameters

Parameter	Source	Values	Interpolation
Albedo	<i>Koelemeijer et al., Tanskanen et al.</i>	0.01, 0.03, 0.05, 0.10, 0.15, 0.20, 0.30, 0.40, 0.50, 0.60, 0.70, 0.80, 1.00	linear
SZA		5, 15, 25, 35, 45, 55, 65, 70, 75, 80, 85	linear
Surface Height	TerrainBase Global DTM Version 1.0	0 - 6000m, 500 m layers	nearest neighbour
Aerosol	LOWTRAN Aeronet GADC FORMAT campaign	1° x 1°, urban, rural, maritime Visibility: 5, 10, 23, 50 km Season: winter and summer	nearest neighbour
Vertical Profile Shape	FORMAT campaign, Other profile data from literature, e.g. Arlander et al.	Background, biogenic, urban, biomass burning	Akima interpolation
Latitude /		1° x 1°	linear

Longitude			
Time		Month	nearest neighbour

NILU has also performed several sensitivity studies of air mass factors in order to improve retrieval of formaldehyde columns satellite measurements using the 1D pseudo-spherical discrete-ordinates model libRadtran ([www.libradtran.org](http://www.libradtran.org)) (see WP2400). Air mass factors are sensitive to atmospheric composition and surface reflection, as well as observation and sun geometry. We used formaldehyde profiles simulated by both regional and global CTMs (Chemistry Transport Models). For example, the regional 3D NILU-CTM produced 6-hourly profiles over Milan throughout the FORMAT 2 campaign (7 Sept. – 14. Oct. 2003). Simulations based on all these profiles for a nadir looking satellite instrument at solar zenith angles of 40 degrees for a 336 nm wavelength resulted in air mass factors of  $0.89 \pm 0.36$  ( $2\sigma = 40\%$ ) (D5200.1, D5200.2, D5200.4). We found that air mass factors can vary between 0.06 and 2.45. The mean constitutes the recommended air mass factor when no a priori knowledge on formaldehyde profiles is available.

Air mass factors are highly sensitive to surface albedo. For a nadir looking satellite instrument, the air mass factor can vary between 0.9 for no surface reflection to 4.5 for an albedo of unity. There is a slight solar zenith angle dependency with a maximum at around 65 degrees.

Air mass factors are quite sensitive to variations in HCHO profiles – about 30-40% uncertainty. Large errors exist for extreme cases, up to 200%.

The vertical column retrieval can be greatly enhanced by application of a priori profiles from of CTM supplemented by surface albedo and aerosol optical depth measurements, or alternatively simultaneous retrievals of formaldehyde columns, profiles, aerosol loadings and surface albedo within the multi-axis DOAS algorithm. This has been successfully shown by the IUP Bremen group in WPs 5300 and 5400.

**WP 5300: Validation of GOME and SCIAMACHY measurements**

HCHO slant columns above the Milano region have been calculated from SCIAMACHY and GOME spectra using the algorithms described in WP 5100 (D5100.1 and D5200.2). Applying AMF using the lookup table described in WP 5200 vertical columns of HCHO have been derived and validated with results from WP 1200 (D1210.1 and D1220.1).

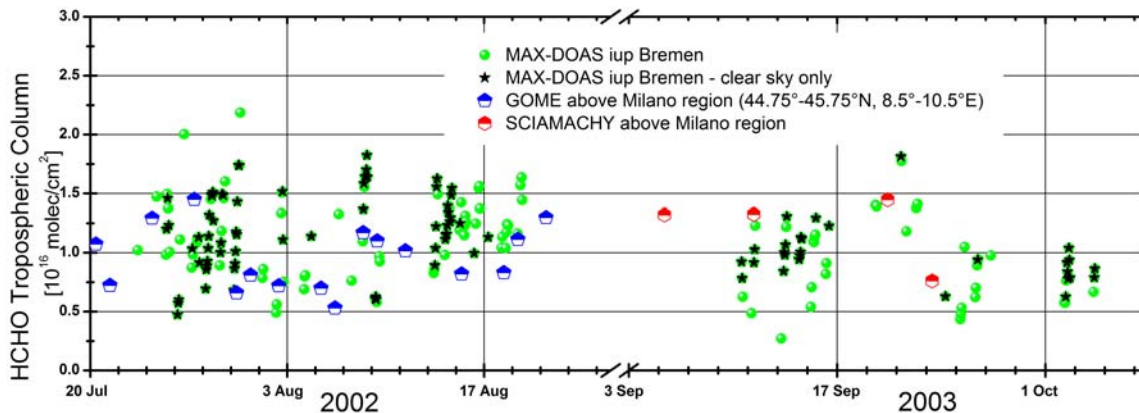


Figure 6.5300.1: Vertical columns of HCHO derived from MAX-DOAS and satellite observations for both campaigns (D5300.1 and D5300.2).

In order to have better statistics it was necessary to average satellite data for the whole Milano region (44.75°-45.75°N, 8.5°-10.5°E). Therefore one should expect, that satellite observations yield lower values than from the ground. The relative error for the satellite values is about 20 %. In 2003 there are no GOME data, because the ERS-2 tape recorder became permanently unavailable due to a technical failure. The ERS-2 Low Rate mission is continued within the visibility of ESA ground stations over Europe, North Atlantic, the Arctic and western North America.

Longer time series from SCIAMACHY have been compared to long-term observations from several BREDOM (Bremian DOAS network for atmospheric measurements) stations. Because of the reduced spatial coverage of SCIAMACHY data compared to GOME measurements, half the data sets are devoted to limb measurements but lost for nadir observations, only monthly averages have been compared. Both the seasonal variation and the absolute values agree quite well. More details are given in Wittrock et al., 2005.

#### WP 5400: Global data set of HCHO from GOME and SCIAMACHY

In the last year of the project SCIAMACHY and GOME spectra have been analysed on a global scale with the algorithms described in WP 5100. The AMF from WP 5200 have been used to produce monthly averages of HCHO vertical columns. In order to pick out an appropriate AMF complementary data sets were used: e.g. AERONET and GADC data for aerosol, ATSR data to identify biomass burning regions. For GOME all data, where a full global coverage is available (July 1995 to February 2003) have been analysed. In the case of SCIAMACHY data from January 2003 to March 2005 were derived.

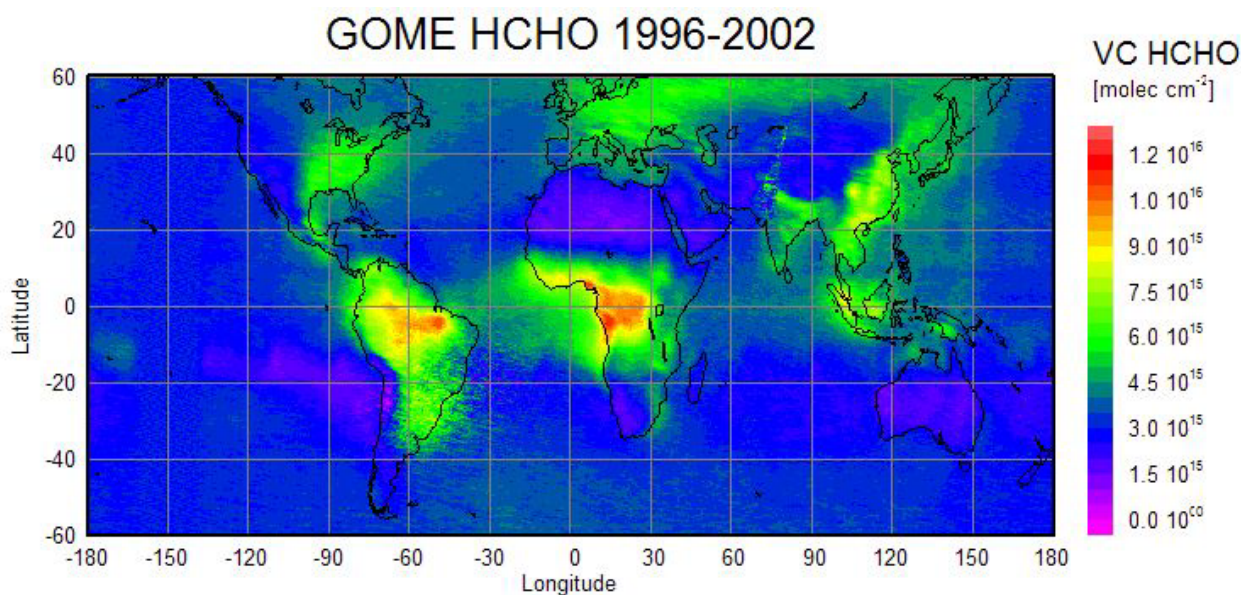


Figure 6.5400.1: Composite of all GOME measurements of HCHO from 1996 to 2002.

All data are available for public on the [IUP Bremen website](#) and from the NILU database. Further comparison of these data sets with CTMs will be available soon as part of the European RETRO project.

## WP 6000 Benefits and recommendations

### WP 6100 Assessment of benefits

Deliverable D6100.1 *Report on changes of VOCs emissions in Europe for the last 40 years and the costs invested and used in obtaining these changes, as well as the impacts on these costs on the employment in the EU region, available on request from partner 1.*

#### Changes of VOCs emissions

Emission of VOCs in Europe was still increasing in years 1960-1990 (*Van Aardenne et al., 2001*). In west Europe the highest increase was associated with fossil fuel production and industrial processes. According to EMEP (2004) total European emission decreased in years 1990-2002 from 25.6 to 16.4 million tonnes per year.

Emission from central and east Europe decreased by 31% and emission from former USRR by 43%, mainly associated with collapse of industry. Emissions from EEA area decreased by 38% in connection with implementation of legislation: EU directives concerning emission from motor vehicles, storage of petrol and use of organic solvents and Geneva Protocol to LRTAP Convention. Increase of emissions happened in Turkey, Norway and Portugal.

#### COSTS OF IMPLEMENTATION OF DIRECTIVES

According to EC (2000) implementation of Solvents Directive 1999/13/EC should cause the total capital costs to 2010 estimated to be 757 million euro and annual average operating costs: 29

million euro in the period 1999-2006 and 84 million euro per year in the period 2007-2010. EC (2002) assessed costs and benefits of Directive 2004/42/EC for the use organic solvents in paints between 108 and 157 million Euro per annum in 2010. Costs of National Emission Ceilings Directive 2001/81/EC implementation for NOx/VOC will be equal 23 billion Euro of capital costs and 1.8 billion Euro per year of operating costs.

Annualized tangible employment linked to Directive 1999/13/EC was estimated to be 1700 FTE (full time equivalent).

Deliverable D6100.2 *Report on „policy correction factor” on the basis of failures in policy implementation in the past 40 years, available on request from partner 1.*

#### **PAST REGULATION**

Directive 70/220/EEC was the first regulation in the European Economic Community concerning emissions of unburnt hydrocarbons. In next years many amendments of this directive were implemented with last Directive 2001/100/EC.

The 1991 Geneva Protocol concerning the Control of Emissions of VOCs or their Transboundary Fluxes to LRTAP Convention was the first international regulation. Protocol was signed or later accessed by 23 European countries and the European Community, which declared to reduce annual VOCs emissions by at least 30% by the year 1999.

Directive 94/63/EC laid down requirements for storage of petrol and its distribution from terminals to service stations. Directive 1999/13/EC laid down limit values for VOCs emissions due to the use of organic solvents in long list of activities. Directive 2004/42/CE prolonged limits for the use of organic solvents in next activities: for paints, varnishes and vehicle refinishing products.

Directive 2001/81/EC of the European Parliament and of the Council established ceilings for annual national emissions of VOCs. Accession treaty from 2003 completed assignation by limits for 10 new EU countries.

#### *Effects of regulation*

According to EEA (2005a) VOCs emission from road transport was decreasing from 1987-89 in Austria, France and Sweden, from 1990 in Denmark, Germany and the United Kingdom and from 1992 in Portugal and Spain. In Germany reported emission decreased by 85%. The lowest decrease happened in Portugal.

In 1999 only half European countries carried out LRTAP Geneva Protocol requirements. Denmark and Finland carried out their targets in next two years. Belgium, Italy and Luxembourg decreased their emissions by less than 30%. However in Norway and Spain emission in 1999 was bigger in relation to 1988. Also Greece and Portugal did not carry out their declaration but they did not ratify Protocol until now.

In effect of Directive 94/63/EC implementation emissions from distribution of oil products decreased more than by 50% in Austria, Denmark, France and the United Kingdom. In Portugal and Spain emission in 2002 were similar to emission in 1994.

In period 1999-2002 significant VOCs emission reduction from industry (expected effect of Directive 1999/13/EC) happened only in Ireland.

### *Policy correction factor*

Delay of meeting the emission reduction targets due to smaller than assumed progress of air protection is called „policy correction factor”.

Targets of Geneva Protocol to LRTAP Convention were carried out in year 1999 in 12 from 21 European countries. Denmark achieved goal in one-year delay and Finland in year 2001. According to projections (EMEP, 2004) next 5 countries should achieve target before 2010 (Belgium, Greece, Italy, Luxembourg and Spain), Norway – before year 2020. Only projections for Portugal (which not ratified VOCs Protocol) are pessimistic. Effects of implementation of Directive 94/63/EC did not happen in Portugal and Spain.

Effects of implementation of more restrictive limit values for motor vehicles are softened by increase of car numbers in EU countries with bigger GDP growth.

Deliverable D6100.3 *Report on future scenarios of policy implementation with and without „policy correction factor”*, available on request from partner 1.

### **SCENARIO WITH „POLICY CORRECTION FACTOR”**

According to IIASA (2005) baseline scenario 4 countries: Belgium, Germany, Netherlands and Spain will not carry out national emission ceilings (NEC Directive 2001/81/EC) in year 2010. In case of Portugal NEC Directive target for 2010 is soften than LRTAP target for 1999. Expected policy correction factor will be equal about three years in case of Germany and more than 10 years for Belgium, Netherlands and Spain.

Reduction of 3310 Gg VOC per year to 2010 in EU-25 is expected, with main measures in 15 old EU Member States. To 2020 reduction of emission by 79% from roads is expected. In case of solvent use in industry implementation of directives should cause 32% reduction.

#### *Scenario without „policy correction factor”*

In this scenario additional control measures in industry are used to not exceed VOC national emission ceilings in Belgium, Germany, Netherlands and Spain. Also Portugal will obtain declared but not ratified LRTAP target. Total reduction of 3540 Gg/year is expected. Emission in 2010 can be lower than total EU emission ceiling by 1365 Gg/year.

Additional reduction of 230 Gg/year in five countries is necessary to carry out all European and international legislation in 2010.

*Table 6.6100.1. Projections of total VOC emission in scenarios for European Union, Gg/year,*

Group of countries	Emission in 2002	NEC Directive target for 2010	Emission in 2010 for scenario:	
			with policy correction factor	without policy correction factor
EU-15	9 037	6 510	6 114	5 883
New 10 EU	1 285	1 640	902	902

members				
<b>EU-25</b>	<b>10 322</b>	<b>8 150</b>	<b>7 016</b>	<b>6 785</b>

Deliverable D6100.4 Report on applicability of current assessment tools, deficiencies in current understanding of policy response, and research priorities for future improvement of the assessment tools

Existing datasets are insufficient for proper assessment of past policy implementation successes. Additional data about emissions of VOCs and PAHs from road transportation in EU countries are necessary. For assessment of directives 1999/13/EC and 2004/42/EC (concerning the use of organic solvents) data about VOCs emission from detail industry activities are necessary.

Besides it data about concentration of VOCs in Europe are important to check emission data and VOCs modelling.

#### References:

1. EC 2000, *Study on investment and employment related to EU Policy on Air, Water and Waste. Final Report*, European Commission Directorate General – Environment, September 2000,
2. EC 2002, *Proposal for a Directive of the European Parliament and the Council on the limitation of emissions of volatile organic compounds due to the use of organic solvents in decorative paints and varnishes and vehicle refinishing products and amending Directive 1999/13/EC*, COM(2002) 750 final, Commission of the European Communities, Brussels, December 2002,
3. EEA 2005a, *Applications. Trends in emissions of ozone precursors (NFR02 format). Raw data and trend*, on based CLRTAP/EMEP dataset, <http://dataservice.eea.eu.int/dataservice/available2.asp?type=findkeyword&theme=air%20emissios>
4. EMEP 2004, *Emission Inventory Review*, EMEP, [http://www.emep.int/index\\_data.html](http://www.emep.int/index_data.html),
5. IIASA 2005, *Baseline Scenarios for the Clean Air for Europe (CAFE) Programme. Final Report*, corrected version February 2005, IIASA, Laxenburg, [http://www.iiasa.ac.at/rains/CAFE\\_files/CAFE-baseline-full.pdf](http://www.iiasa.ac.at/rains/CAFE_files/CAFE-baseline-full.pdf), Van Aardenne, J.A., Dentener, F.J., Olivier, J.G.J., Klein Goldewijk, C.G.M. and J. Lelieveld 2001, A 1 x 1 degree resolution dataset of historical anthropogenic trace gas emissions for the period 1890-1990. *Global Biogeochemical Cycles*, 15(4), 909-928, [http://www.mnp.nl/edgar/model/100\\_year\\_emissions/edgar-hyde-1.3/](http://www.mnp.nl/edgar/model/100_year_emissions/edgar-hyde-1.3/)
6. Van Aardenne, J.A., Dentener, F.J., Olivier, J.G.J., Klein Goldewijk, C.G.M. and J. Lelieveld 2001, A 1 x 1 degree resolution dataset of historical anthropogenic trace gas emissions for the period 1890-1990. *Global Biogeochemical Cycles*, 15(4), 909-928, [http://www.mnp.nl/edgar/model/100\\_year\\_emissions/edgar-hyde-1.3/](http://www.mnp.nl/edgar/model/100_year_emissions/edgar-hyde-1.3/),

## 6.4 Conclusions including socio-economic relevance, strategic aspects and policy implications

Two measurement campaigns at different times and with formaldehyde levels have been completed successfully. Formaldehyde has been measured with different type of instrumentations, and the different techniques have been intercompared. The understanding of the formation processes of formaldehyde has been improved.

The Hantzsch results agree generally well with the results of the spectroscopic techniques. With three independent techniques (DOAS, FTIR, and Hantzsch) applying 20 completely different ways of determining the formaldehyde concentration, results within 15% were obtained. Previously observed significant differences in mixing ratios obtained by Hantzsch monitors and the DOAS technique could not be observed in this study. No systematic difference between DOAS and Hantzsch was found under the conditions present during 25 comparison measurements. It is assumed that the improvement is due to the employment of multi-reflection setups in the spectroscopic techniques which ensured that all instruments sampled essentially the same air volume. Previously reported differences between DOAS and Hantzsch techniques seem to be larger than the uncertainties in CH<sub>2</sub>O measurements as characterised in this study, and thus may have been caused by spatial (vertical) gradients of CH<sub>2</sub>O concentrations.

Longpath DOAS instruments from University of Heidelberg and NILU was intercompared. The agreement is best for SO<sub>2</sub> and NO<sub>2</sub> and worse for HCHO. NILU's HCHO values are most of the time overestimated.

#### *WP 2000 Airborne measurements of HCHO and intercomparison*

After the two campaigns a large amount of data is now available: Hantzsch in situ data of about 30 aircraft flights (including Dimona and Microlight), and AMAXDOAS slant column data of about 20 aircraft flights. SOF measurements were performed almost every day during the second campaign. In addition continuous MAX-DOAS measurements were performed at two stations during the first campaign and at three stations during the second campaign. Spectral analysis algorithms and vertical inversion techniques have been developed and optimized for MAX- and AMAXDOAS measurements, and it was possible to derive vertical profiles of HCHO with both techniques. The agreement between profiles obtained with the different techniques is excellent and within 0.5-1 ppbv (or 15%) in most cases. The profiles from the Microlight Hantzsch, the AMAX and the MAX-DOAS agree very well, whereas data points obtained at the ground with the long path DOAS are up to 3 ppbv (or 45%) higher than the Microlight data and 1.5 ppbv higher than the ground based Hantzsch instrument. The difference of 2 ppbv between the ground Hantzsch and the Long path DOAS on the same day suggests that there were small scale spatial variations (over some tens to hundreds of meters), which could be the reason for the discrepancy of all three instruments. However, the excellent agreement between the other instruments suggests that the 3D data can be used as input for model studies or satellite validation without any further data correction.

#### *WP 3000 Assessment of additional species during the field campaigns*

The additional measurements have helped investigate the role of HCHO in the ozone production or generally how secondary aerosols are formed. The spatially and temporally resolved ozone and nitrogen dioxide measurements are relevant by themselves because they are important toxic gases and surpass in many countries of Europe the national ceilings. The measurements will be used to evaluate photochemical models that are also used to predict the pollution levels in the future.

The first and second field campaigns were successfully performed. The weather was much more stable during the 2003 campaign than in the 2002 campaign. This yielded higher ozone and formaldehyde levels in 2003.

The analyses of the ground data on additional species constitute the basis to put the measurements of HCHO into perspective. Very good three-dimensional data, covering both important emission areas and the rural surroundings, have been gathered from ground-based and aircraft-borne measurements in this work package. These data can be used for the evaluation of photochemical models and for further process studies. With the help of these data, we have also evaluated the contribution of primary and secondary HCHO to the total concentrations measured in the area of analysis. In most areas the contribution of secondary HCHO dominates during the afternoon.

The successful intercomparison of satellite derived nitrogen dioxide (NO<sub>2</sub>) columns with ground-based NO<sub>2</sub> measurements in Lombardy is an additional outcome of this work package.

#### *WP 4000 Atmospheric chemistry modelling and intercomparison with observations*

The regional model results agree in general well for both O<sub>3</sub> and HCHO along the flight tracks. There are some peaks model does not able to capture, can be caused by local emissions and plume. Because of the large gradient between inside and outside of plumes, more explicit simulation of plumes are depending on improved meteorological data and model resolution.

The emissions from biomass burning vary strongly over the season with the strongest emissions in August – November. The largest source within the biomass burning category is biomass burning deforestation with a 1997 source strength of 2,243 Tg(CH<sub>2</sub>O) / year. 1,694 Tg is emitted during this four-month period (Aug 0,386, Sep 0,582, Oct 0,522, Nov 0,204 Tg(CH<sub>2</sub>O) / month).

In regions with the largest emissions (S America and S-E Asia) biomass burning increase CH<sub>2</sub>O with a factor 4-5 due to these exceptional episodes. Also Africa and Russia experience some increase, although not that large and more from savanna burning (L42) and agricultural waste burning (L43), which is to a large degree an annual event.

The levels of NO<sub>x</sub> are also affected by these large emissions of hydrocarbons. This will in turn affect O<sub>3</sub> production through reactions. Large biomass burning events episodes like October 1997 can increase NO<sub>2</sub> by nearly a factor 7 in some regions.

H<sub>2</sub> is produced by reaction R7. We have investigated the changes in H<sub>2</sub> chemical production due to biomass burning emission. Emissions of hydrocarbons from biomass burning increased the mass of H<sub>2</sub> by 6,6% (global annual mean). In October a factor 2 increase is observed in the areas of heavy biomass burning.

#### *WP 5000 Analysis and validation of GOME and SCIAMACHY data*

It has been shown, that satellite measurements give the opportunity to obtain a better knowledge of the global distribution and role of HCHO as a tracer of fossil fuel, biomass burning and biogenic emissions.

The formaldehyde satellite retrieval algorithms for the GOME and SCIAMACHY has been improved. Satellite observations for the for the whole Milano region yield lower values than from the ground. The relative error for the satellite values is about 20 %. Longer time series from SCIAMACHY have been compared to long-term observations from several BREDOM (Bremian DOAS network for atmospheric measurements) stations. Both the seasonal variation and the absolute values agree quite well.

Vertical profiles of HCHO and the atmospheric composition of the atmosphere has been shown to have a significant impact on air mass factors, and thus the HCHO retrieval from satellites.

### *WP 6000 Benefits and recommendations*

Emission of VOCs in Europe increased in years 1960-1990, but has decreased after that. According to EMEP (2004) total European emission decreased in years 1990-2002 from 25.6 to 16.4 million tonnes per year. Emission from central and east Europe decreased by 31% and emission from former USRR by 43%, mainly associated with collapse of industry. Emissions from EEA area decreased by 38% in connection with implementation of legislation. The effect of legislation and directives are quite substantial for the countries where such measures have been implemented.

Projections of total VOC emission in scenarios for European Union in year 2010 implies an effect of policy implementation at around 4%.

Existing datasets are insufficient for proper assessment of past policy implementation successes. Additional data about emissions of VOCs and PAHs from road transportation in EU countries are necessary.

## **6.5 Dissemination and exploitation of results**

### 6.5.1 Dissemination

Most experimental data are located at NADIR data centre at NILU ([zardoz.nilu.no](http://zardoz.nilu.no)). Access to the database must be requested by the system administrator. A CD ROM is available on request.

The FORMAT project has a Web site <http://www.nilu.no/format>

Results published in peer-reviewed publications and presented at conferences (see section 6.6 for details)

A perl script to compute air mass factors in terms of various atmospheric compositions and surface reflections, as well as observation and sun geometries, can be run at the server [zardoz.nilu.no/home/olaeng/software/libradtran-1.0-beta/tools/airmass-v1.2](http://zardoz.nilu.no/home/olaeng/software/libradtran-1.0-beta/tools/airmass-v1.2) Access to this script requires a user account on the [zardoz.nilu.no](http://zardoz.nilu.no) server, with restricted availability (must contact the NILU IT administration). The script was accessible to all FORMAT participants. Air mass factors can also be computed on the Internet on the web page <http://zardoz.nilu.no/~olaeng/AMF/AirMassFactors.html>

The AMF lookup table calculated by the IUP Bremen team has been stored together with the satellite data (WP 5400) on the Zardoz server.

### **6.5.2 End users of data**

In FORMAT several groups of users are identified and mechanisms have been set up to provide the results from FORMAT in a form which allows direct exploitation for the users purposes. These mechanisms range from an active involvement of FORMAT partners in the technical underpinning of environmental policy definition on the international, national, regional, local and sectoral level, to assessments of scientific knowledge on specific environmental issues, to scientific partnerships internationally, nationally and regionally.

### **6.5.2.1 Environmental policy at the EU user level**

The Community Directive on national emission ceilings (NEC) and the new ozone Directive (COM (99)125) are likely to be adopted in 2001. One objective is to reduce long-term ground-level ozone Economic development and S and T prospects 88 Modified description of work of Sept. 2004 (ecosystem damage). The EU legal framework also includes air quality legislation, and in the proposed ozone daughter ozone target values are defined. The target values are a politically visible environmental goal against which progress of control strategies have to be monitored. All existing and proposed EU legislation on air quality as well as the NEC proposal share a common requirement for revision by 2004.

The technical underpinning of the preparations for revision takes place through the Clean Air for Europe (CAFE) initiative in DG Environment, and is supported by the member countries and European Environment Agency (EEA) through its Topic Centre on Air Quality, Air Emissions and Climate Change (ETC-ACC), where the FORMAT partner NILU is a core member. One objective of ETCACC is to provide support to EU policy and legislative frameworks, with a focus on the EU-ECCP (European Climate Change Programme) and CAFE (Clean Air for Europe), related legislation such as the Monitoring Mechanism and the Air Quality Framework Directive and international conventions (UNFCCC and CLRTAP). Another objective of ETC-ACC is to implement data collection and information systems to deliver quality assured information and indicators for support to policy and legislation. A third objective is to contribute to EEA main reports through assessments on the issues of air pollution and climate change, in description of past trends, current state and prospective development.

The exploitation of FORMAT results (for specification see the lists of deliverables in the WPs) in CAFE and in EEA is taken care of by NILU as an ETC-ACC core member, and by each individual FORMAT partner through their roles as advisers to national and regional governments, and by all partners as they play active roles in workshops and technical meetings.

### **6.5.2.2 Environmental policy at the United Nations' user level**

The European Community has signed the Kyoto Protocol (KP), under the Framework Convention on Climate Change (UNFCCC). Major efforts will be required to reduce emissions according to the KP and beyond. Because these efforts can be very costly it will be important to assess the (cost-) effectiveness of implemented and/or proposed policies and measures. To assess the most cost-effective contributions that the various sectors could be making to emission reductions the Commission has set up the European Climate Change Programme (ECCP). The FORMAT proposal is relevant here because changes in free tropospheric ozone on the regional level contributes to changes in radiative forcing. FORMAT results will be exploited in the IPCC process and in the ECCP process as the partners advise their national governments, and through NILU's membership in the ETC-ACC, which has such support in its mandate.

Tropospheric ozone and precursors are evaluated in the WMO/UNEP ozone assessments in support of the Montreal Protocol. FORMAT results will be exploited in this way by FORMAT partners that contribute actively to these assessments.

Tropospheric ozone and nitrogen oxides is addressed under the Convention on Long Range Transboundary Air Pollution (CLRTAP), to which the Community and most European countries are Parties. The most recent multi-pollutant, multi-effect Protocol (1999) was negotiated to minimize effects by the most cost-effective measures using extensive integrated assessment modelling. This led to national ceilings for 2010 for all European countries for emissions of nitrogen and sulphur

oxides, volatile organic compounds and for the first time for ammonia. The 1999 CLRTAP Protocol will be reviewed in 2004. The technical underpinning takes place through the European Monitoring and Evaluation Programme (EMEP) where all European countries including the CEC are members, and where the FORMAT partner NILU is one of three core technical institutions. In this capacity NILU will ensure that FORMAT results are exploited in EMEP. The FORMAT partners will additionally contribute FORMAT results to the CLRTAP through the Task Force on Measurements and Modelling, FORMAT recently established in EMEP to help review existing Protocols, and to which all European countries belong.

Other user groups are related to ICAO (International Civil Aviation Organisation (ICAO) and the Convention for the protection of the Mediterranean Sea against Pollution (The Barcelona Convention) which has a very broad scope and where the results from FORMAT are marginal.

#### **6.5.2.3 Environmental policy, users at the national, regional and local levels, and in sectors of society**

Industrialists, often involved in policy development (e.g. fossil fuel producers, motor manufacturers) will have access to the results from FORMAT. In some cases, members of the FORMAT consortium are directly involved with advising industrial partners on environmental issues allowing industry to be proactive in dealing with them, and such partnerships ensures that FORMAT results are communicated in a customer oriented way. Some of the partners in FORMAT are advisers to their national and regional governments, and also in many cases to local authorities. FORMAT results will be exploited in the preparation of assessments and methodology to manage air quality and to forecast ozone concentrations for their region.

#### **6.5.2.4 Users in the scientific community**

The scientific community organized in the International Geosphere Biosphere Programme (IGBP) and its sub-projects International Global Atmosphere Chemistry Programme (IGAC) and the new Intercontinental Transport and Chemical Transformation (ITCT) project is intimately linked to FORMAT, as a user of the results from FORMAT through the involvement in IGAC and ITCT by several of the FORMAT partners. Some of the sub-projects in EUROTRAC-2, such as TROPOSAT, and the North American research activities under NARSTO are also user groups for FORMAT results, and the communication and exploitation of FORMAT results is taken care by the active involvement of several FORMAT partners in these research activities.

#### **6.5.2.5 The general public**

The general public will be kept informed via communication with the press and via the FORMAT web site at NILU. There will be both background information explaining this environmental problem and there will be updated results based on the measurements to be carried out.

## **6.6 Main literature produced**

### Peer reviewed articles

- Bruns, M., S. Bühler, J. P. Burrows, K.-P. Heue, U. Platt, I. Pundt, A. Richter, A. Rozanov, T. Wagner, P. Wang, Retrieval of Profile Information from Airborne Multi Axis UV/visible Skylight Absorption Measurements, *Applied Optics*, 43 (22), 4415-4426, 2004
- Hak, C., I. Pundt, S. Trick, C. Kern, U. Platt, J. Dommen, C. Ordóñez, A. S. H. Prévôt, W. Junkermann, C. Astorga-Lloréns, B. R. Larsen, J. Mellqvist, A. Strandberg, Y. Yu, B. Galle, J. Kleffmann, J. Loerzer, G. O. Braathen, and R. Volkamer; Intercomparison of four different in-situ techniques for ambient formaldehyde measurements in urban air, *Atmos. Chem. Phys. Discuss.*, 5, 2897–2945, 2005.
- Heckel, A., A. Richter, T. Tarsu, F. Wittrock, C. Hak, I. Pundt, W. Junkermann, and J. P. Burrows, MAX-DOAS measurements of formaldehyde in the Po-Valley, *Atmos. Chem. Phys.*, 5, 909-918, 2005.
- Heue, K.-P., A. Richter, M. Bruns, J. P. Burrows, C. v. Friedeburg, U. Platt, I. Pundt, P. Wang and T. Wagner, Validation of SCIAMACHY tropospheric NO<sub>2</sub>-columns with AMAXDOAS measurements, *Atmos. Chem. Phys.*, 5, 1039-1051, 2005. Junkermann W., and Burger, J.M., A new portable instrument for continuous measurement of formaldehyde in ambient air, JOAT, in print July 5. 2005
- Junkermann W., and Burger, J.M., A new portable instrument for continuous measurement of formaldehyde in ambient air, JOAT, in print July 5. 2005
- Kononov, I. B., M. Beekmann, R. Vautard, J. P. Burrows, A. Richter, H. Nüß, N. Elansky, Comparison and evaluation of modelled and GOME measurement derived tropospheric NO<sub>2</sub> columns over Western and Eastern Europe, *Atmos. Chem. Phys.*, 5, 169-190, 2005
- Kunhikrishnan, T., M. G. Lawrence, R. von Kuhlmann, A. Richter, A. Ladstätter-Weissenmayer, and J. P. Burrows, Analysis of Tropospheric NO<sub>x</sub> Over Asia Using the Model of Atmospheric Transport and Chemistry (MATCH-MPIC) and GOME-Satellite Observations, *Atmospheric Environment*, 38 (4), 581-596, 2004
- Ladstätter-Weissenmayer, A., Meyer-Arnek, J., Richter, A., Wittrock, F., Burrows, J. P., Tropospheric O<sub>3</sub> over Indonesia during biomass burning events measured with GOME (Global Ozone Monitoring Experiment) and compared with trajectory analysis, *Atmospheric Chemistry and Physics Discussions*, 5, 3105-3130, 2005
- Ladstätter-Weissenmayer, A., J. Heland, R. Kormann, R. v. Kuhlmann, M. G. Lawrence, J. Meyer-Arnek, A. Richter, F. Wittrock, H. Ziereis, and J. P. Burrows, Transport and build-up of tropospheric trace gases during the MINOS campaign: Comparison of GOME, in situ aircraft measurements and MATCH-MPIC-data, *Atmos. Chem. Phys.*, 3, 1887–1902, 2003
- Petritoli, A., P. Bonasoni, G. Giovanelli, F. Ravegnani, I. Kostadinov, D. Bortoli, A. Weiss, D. Schaub, A. Richter, and F. Fortezza, First Comparison Between ground-based and Satellite-borne Measurements of Tropospheric Nitrogen Dioxide in the Po Basin, *J. Geophys. Res.*, 109, D15307, doi:10.1029/2004JD004547, 2004
- Pundt, I. and K. U. Mettendorf, Multibeam long-path differential absorption spectroscopy instrument: a device for simultaneous measurements along multiple light paths, *Appl. Opt.*, 44, 23, 4985-4994, 2005.
- Richter, V. Eyring, J. P. Burrows, H. Bovensmann, A. Lauer, B. Sierk, and P. J. Crutzen, Satellite Measurements of NO<sub>2</sub> from International Shipping Emissions, *Geophys. Res. Lett.*, 31, L23110, doi:10.1029/2004GL020822., 2004
- Richter, A. and J.P. Burrows, Retrieval of Tropospheric NO<sub>2</sub> from GOME Measurements, *Adv. Space Res.*, 29(11), 1673-1683, 2002.
- Savage, N. H., K. S. Law, J. A. Pyle, A. Richter, H. Nüß, J. P. Burrows, Using GOME NO<sub>2</sub> satellite data to examine regional differences in TOMCAT model performance, *Atmos. Chem. Phys.*, 4, 1895-1912, 2004
- Spichtinger, N., Damoah, R., Eckhardt, S., Forster, C., James, P., Beirle, S., Marbach, T., Wagner, T., Novelli, P. and Stohl, A., Boreal forest fires in 1997 and 1998: a seasonal comparison using transport model simulations and measurement data, *Atm. Chem. Phys.*, 4, 1857-1868, 2004.
- Steinbacher, M., J. Dommen, C. Ordóñez, S. Reimann, F. C. Grübler, J. Staehelin, S. Andreaani-Aksoyoglu, and A. S. H. Prévôt, Volatile organic compounds in the Po Basin. Part A: anthropogenic VOCs. *J. Atmos. Chem.* 51:271-291, 2005.
- Steinbacher, M., J. Dommen, C. Ordóñez, S. Reimann, F. C. Grübler, J. Staehelin, S. Andreaani-Aksoyoglu, and A. S. H. Prévôt, Volatile organic compounds in the Po Basin. Part B: biogenic VOCs. *J. Atmos. Chem.*, 51:293-315, 2005.
- Vountas, M., A. Richter, F. Wittrock, and J. P. Burrows, Inelastic scattering in ocean water and its impact on trace gas retrievals from satellite data, *Atmos. Chem. Phys.*, 3, 1365-1375, 2003
- Vandaele, A.C., C. Fayt, F. Hendrick, C. Hermans, F. Humbled, M. Van Roozendaal, M. Gil, M. Navarro, O. Puentedura, M. Yela, G. Braathen, K. Stebel, K. Tørnkvist, P. Johnston, K. Kreher, F. Goutail, A. Mieville, J.-P. Pommereau, S. Khaikine, A. Richter, H. Oetjen, F. Wittrock, S. Bugarski, U. Frieß, K. Pfeilsticker, R. Sinreich, T. Wagner, G. Corlett, and R. Leigh, An intercomparison campaign of ground-based UV-visible measurements of NO<sub>2</sub>, BrO, and OClO slant columns: Methods of analysis and results for NO<sub>2</sub>, *J. Geophys. Res.*, 110, doi:10.1029/2004JD005423, 2005
- Wagner, T., B. Dix, C.v. Friedeburg, U. Frieß, S. Sanghavi, R. Sinreich, and U. Platt, MAX-DOAS O<sub>4</sub> measurements - a new technique to derive information on atmospheric aerosols. (I) Principles and information content, *J. Geophys. Res.*, in press, 2005.

- Wang, P., A. Richter, M. Bruns, J. P. Burrows, W. Junkermann, K.-P. Heue, T. Wagner, U. Platt, and I. Pundt, Airborne multi-axis DOAS measurements of tropospheric SO<sub>2</sub> plumes in the Po-valley, Italy, *Atmos. Chem. Phys. Discuss.*, 5, 2017-2045, 2005.
- Wang, P., A. Richter, M. Bruns, V. Rozanov, J. Burrows, K.-P. Heue, T. Wagner, I. Pundt, and U. Platt, Measurements of tropospheric NO<sub>2</sub> with an airborne multi-axis DOAS instrument, *Atmos. Chem. Phys.*, 5, 337-343, 2005.
- Wittrock, F., H. Oetjen, A. Richter, S. Fietkau, T. Medeke, A. Rozanov, J. P. Burrows MAX-DOAS measurements of atmospheric trace gases in Ny-Ålesund - Radiative transfer studies and their application, *Atmos. Chem. Phys.*, 4, 955-966, 2004

**Planning of peer reviewed articles:**

- Bruns, M., S. A. Buehler, J. P. Burrows, A. Richter, A. Rozanov, P. Wang, K.-P. Heue, U. Platt, I. Pundt, and T. Wagner, NO<sub>2</sub> Profile Retrieval using airborne multi axis UV-visible skylight absorption measurements over central Europe, paper in preparation, 2005.
- Engelsen O., F. Flatoý and A. Kylling, Sensitivity of air mass factors to atmospheric profiles of formaldehyde, In preparation.
- Hak, C., J. Dommen, A.S.H. Prévôt, et al. "On the spatial and temporal variability of formaldehyde in the Po Basin. An approach based on VOC reactivities". To be submitted for publication in a peer-reviewed journal by the end of 2005.
- Hendrick, F., M. Van Roozendaal, A. Kylling, A. Petritoli, S. Sanghavi, R. Schofield, C. von Friedeburg, F. Wittrock, and M. De Mazière, Interpretation of ground-based zenith-sky and multi-axis DOAS observations: Intercomparison exercise between different radiative transfer models, *Submitted to Atmospheric Chemistry and Physics Discussions (ACPD)*.
- Junkermann, W. The 3D-distribution of HCHO in the Milano area during FORMAT campaigns 2002 and 2003.
- Liu, L., Assessment of performance of a regional CTM during the 2002 FORMAT campaign, in preparation. Will be submitted to *Atmospheric Chemistry and Physics*.
- Marbach, T., S. Beirle, J. Hollwedel, F. Khokhar, U. Platt and T. Wagner, Influence of the Vegetation Type on formaldehyde (HCHO) and Nitrogen oxide (NO<sub>2</sub>) Tropospheric Emissions during Biomass Burning: Synergistic use of Satellite Observations, submitted to ASR, 2005.
- Ordóñez, C., A. Richter, M. Steinbacher, C. Zellweger, H. Nüß, J.P. Burrows, and A. S. H. Prévôt, Comparison between 7 years of satellite-borne and ground-based tropospheric NO<sub>2</sub> measurements around Milan, Italy, *J. Geophys. Res.* (submitted), 2005.
- Pundt, I., K.-P. Heue, U. Platt, B.-C. Song, T. Wagner, M. Bruns, J.P. Burrows, A. Richter, P. Wang Airborne Tomographic Measurements of NO<sub>2</sub> Plumes from Point sources using the AMAXDOAS instrument, *submitted to J. Geophys. Res.*, 2005.
- Pundt, I., K.-P. Heue, T. Laepple, A. Richter, P. Wang, J.P. Burrows, T. Wagner, C. v. Friedeburg, B.-C. Song, M. Bruns, and U. Platt, Airborne Multi-Axis-DOAS measurements of formaldehyde of the photochemical plume of Milano city, *paper in preparation*. 2005
- Pundt, I., DOAS tomography for the localisation and quantification of anthropogenic air pollution, submitted to *J. Anal. Bioanal. Chem.*, 2005.
- F. Wittrock et al., Retrieval of trace gas profiles from MAX-DOAS observations
- Wittrock, F., A. Richter and J.P. Burrows, Formaldehyde – the global view, manuscript in preparation for ACPD.

**Theses**

- Bäuerle, A., Messung von Spurenstoffverteilungen in Mailand mit Hilfe eines Multistrahl-Langpfad Teleskops, Staatsexamensarbeit, University of Heidelberg, 2004.
- M. Bruns: NO<sub>2</sub> Profile Retrieval using Airborne Multiaxis Differential Optical Absorption Spectrometer (AMAXDOAS) data, PhD Thesis, University of Bremen, 2004
- Hak, C., PhD thesis, University of Heidelberg, to be finished end of 2005.
- A. Heckel: Messungen troposphärischer Spurengase mit einem MAXDOAS-Instrument, Diploma-Thesis, University of Bremen, March 2003 (in German)
- Heue, K.-P., PhD thesis, University of Heidelberg, to be finished end of 2005.
- Mettendorf, K. U., PhD thesis, University of Heidelberg, to be finished end of 2005.
- J. H. Nüß: An improved tropospheric NO<sub>2</sub> retrieval for GOME and SCIAMACHY, PhD Thesis, University of Bremen, 2005 (in German)
- von Friedeburg, C., Derivation of Trace Gas Information combining Differential Optical Absorption Spectroscopy with Radiative Transfer Modeling, PhD thesis, University of Heidelberg, 2003.
- F. Wittrock: Global Observations of Formaldehyde, PhD Thesis, University of Bremen, 2005.

## **Non refereed literature**

### **Reports**

- C. Ordóñez, M. Steinbacher, J. Dommen, A.S.H. Prévôt. The FORMAT campaign in summer 2002, PSI-Scientific Report 2002, Volume V, General Energy, p119, ISSN 1423-7342 March 2003
- C. Ordóñez, A.S.H. Prévôt, S. Henne, A. Richter, Intercomparison of satellite and ground based NO<sub>2</sub> measurements in the Lombardy region, PSI-Scientific Report 2003 / Volume V, General Energy, pg. 132, ISSN 1423-7342, , March 2004.
- Damian Panasiuk, Report on changes of VOCs emissions in Europe for the last 40 years and the costs invested and used in obtaining these changes, as well as the impacts on these costs on the employment in the EU region, FORMAT Report D.6100.1, version July 2005
- Damian Panasiuk, Report on „policy correction factor” on the basis of failures in policy implementation in the past 40 years, FORMAT Report D.6100.2, July 2005
- Damian Panasiuk, Report on future scenarios of policy implementation with and without policy correction factor, FORMAT Report D.6100.3, August 2005
- Damian Panasiuk, Report on applicability of current assessment tools, deficiencies in current understanding of policy response, and research priorities for future improvement of the assessment tools, FORMAT Report D.6100.4, July 2005
- A.S.H. Prévôt, R. Richter, C. Ordóñez, W. Junkermann, Early morning concentrations of formaldehyde and carbon monoxide in Milano measured with the mobile pollutant lab, PSI-Scientific Report 2003 / Volume V, General Energy, pg. 131, ISSN 1423-7342, March 2004

### **Proceedings**

- Ordóñez, C., S. Henne, A. S. H. Prévôt, A. Richter, C. Zellweger, and C. Hüglin. Intercomparison of tropospheric NO<sub>2</sub> columns retrieved from GOME with ground based NO<sub>2</sub> measurements in the Lombardy region, Italy. XX Quadrennial Ozone Symposium, Kos, Ed. by Christos. S. Zerefos, Greece, June 2003.
- Wittrock, F., A. Richter, A. Ladstätter-Weissenmayer, and J. P. Burrows, Global Observations of Formaldehyde, in proceedings of the ERS-ENVISAT symposium, Gothenburg October 2000, ESA publication SP-461, 2000